NTNU
Norwegian University of
Science and Technology

Experimental and numerical investigation of oil-water dispersions

Eksperimentell og numerisk analyse av
olje-vann dispersjoner

Karoline Langøy Tresvik

Master of Science in Mechanical Engineering
Submission date: June 2016
Supervisor: Maria Fernandino, EPT
Co-supervisor: Vegard Sørbø, Cameron Systems

Norwegian University of Science and Technology
Department of Energy and Process Engineering

Norwegian University of Science and Technology

Department of Energy and Process Engineering

EPT-M-2016-142

MASTER THESIS

for

Karoline Tresvik
Spring 2016

Experimental and numerical investigation of oil-water dispersions

Eksperimentell og numerisk analyse av olje-vann dispersjoner

Background and objective

Cameron is a global leading provider of flow equipment products, systems, and services to worldwide oil, gas, and process industries. A key product range is separator internals for enhanced oil-water separation. Onshore and offshore production can have increased safety margins through large separation arrangements, but as the industry move towards more compact subsea solutions the need for better knowledge is obvious. The vision is to gain knowledge on oil-water separation in horizontal separators used by the oil and gas industry.

In this thesis batch separation tests with model oil, water and surfactants will be carried out. The goal is to gain knowledge about batch settling, through experimental and numerical investigation. Investigation of relationship between continuous separation behavior and batch settling will be done. The motivation is to find a model fluid system that can be used to simulate crude oil and water emulsions.

The following tasks are to be considered:

1. Literature study on oil-water separation in batch tests, numerical simulation of mixing and relationship between batch settling and continuous settling.
2. Engineering and assembly of batch test rig. Numerical simulation and post processing of mixing in batch test, mixing performance, work conducted etc.
3. Planning of experiment setup and test matrix, perform experiments according to test matrix.
4. Execution of experiments in continuous test rig. Evaluation of result.
5. Analysis of experimental results. Comparison with existing theory.

The Master thesis shall comprise of 30 credits.

A progress plan *(Planned activities and scheduled progress)* shall be submitted to the responsible subject teacher/supervisors for comments within 14 days after the candidate has received the project description.

The work shall be edited as a scientific report, including a table of contents, a summary in Norwegian, conclusion, an index of literature etc. When writing the report, the candidate must emphasise a clearly arranged and well-written text. To facilitate the reading of the report, it is important that references for corresponding text, tables and figures are clearly stated both places.
By the evaluation of the work the following will be greatly emphasised: The results should be thoroughly treated, presented in clearly arranged tables and/or graphics and discussed in detail.

The candidate is responsible for keeping contact with the subject teacher and teaching supervisors.

The candidate shall comply with the working regulations at Cameron Systems and any other orders given by the person in charge. The candidate is not allowed to intervene in the operation of plants, installations etc. without the management's consent.

According to "Utfyllende regler til studieforskriften for teknologistudiet/sivilingeniørstudiet ved NTNU" § 20, the Department of Energy and Process Engineering reserves all rights to use the results in connection with lectures, research and publications.

The report must be submitted to the Department in 3 complete, bound copies. Further, a separate page must be submitted, giving a short summary of the work and stating the author's name and title of the project work. This information will be used in case of the work being referred to in journals, and must not exceed one typed page with double spacing. Additional copies should be given directly to the supervisor(s) involved in the project according to agreement with the supervisor(s).
A CD with a complete copy of the main report in Word-format or similar, shall be submitted to both the subject teacher and the Department of Energy and Process Engineering.

The main report from the project work shall be submitted to the Department of Energy and Process Engineering *within 10 June 2014.*

Olav Bolland
Department Head

Maria Fernandino
Academic Supervisor

Research advisor(s): Vegard Sørbø, Dag Kvamsdal, Fredrik Carlson, Mauritz Talseth.

Acknowledgement

I would like to thank my supervisor Maria Fernandino for help during this semester. A special thanks goes to Cameron System A/S for help, support and advice during this work. I would like to thank Vegard Sørbø, Dag Kvamsdal, Erik Storaas, Fredrik Carlson, Mauritz Talseth, Roger Hansen and Kåre Nordnes.

15.06.2016
Karoline Langøy Tresvik

Abstract

Crude oil in the reservoir is accompanied by formation water. Separating water from oil offshore before transporting it is necessary. This requires compact and robust separators. In order to optimize the design of separators, a good understanding of separation mechanisms and crude oil behavior is essential. Testing separation with batch tests compared to continuous flow tests is less time assuming and less expensive. This work has been dedicated to gain knowledge about batch settling, through experimental and numerical investigation. Separation experiments with Exxsol D60, water and Span 80 have been carried out. Testing with model oil instead of crude oil is beneficial. The ultimate goal is to simulate crude oil and water emulsions using a model fluid systems. Numerical simulations of mixing performance were performed as an optimization study before batch testing. They showed that both rotation and the presence of static baffles improve the mixing significantly. The experimental batch tests was performed with different concentrations of Span 80, different water cuts and different rotations. The result showed that Span 80 can be used as a surfactant to stabilize model oil. Investigation of what affects the stability the most was done. Rotation proved to have the greatest effect. Span 80 concentrations of 0.05-0.2 vol.% showed small changes on the stability. It is suspected that these concentrations are too high, and that Span 80 should be estimated with respect to oil volume instead of total volume. Polderman's model was used to connect batch data with flowing systems. Fluxes based on the batch result were plotted, and showed promising result which indicates that model oil can be used to simulate crude oil. Experiments with the same fluid system were performed in a flowing rig. The purpose was to investigate if these tests provided the same stability result. This resulted in a stable emulsion, which prevented further flow tests. This may be because of a too high Span 80 concentration.

Sammendrag

Reservoar inneholder både råolje og vann. Separasjon av vannet offshore før oljen transporteres er nødvendig. Dette krever kompakte og robuste separatorer. Det er nødvendig med god forståelse for separasjonsmekanismer og karakteristikkene til råoljen, for å optimalisere separatorer. Testing av separasjon med batch er billigere og mindre tidskrevende enn å teste i et strømmende system. Formålet med oppgaven har vært å lære om batch-testing numerisk og eksperimentelt. Eksperimenter med Exxsol D60, vann og surfaktant har blitt utført. Det er fordelaktig å teste med modellolje istedenfor råolje. Det endelige målet med arbeidet er å kunne simulere emulsjoner med råolje og vann ved hjelp av modellolje. Numeriske simuleringer av miksing ble gjort for å optimalisere batchtestene. Disse viste at både rotasjon og statiske bafler forbedrer agitasjonen betraktelig. Eksperimentelle batch tester ble utført med ulike konsentrasjoner av Span 80, ulike vannkutt og ulike rotasjoner. Disse testene viste at Span 80 kan brukes som en surfaktant for å stabilisere modellolje. Hvilke faktorer som påvirket stabiliteten til væsken ble undersøkt. Disse viste at rotasjon hadde størst effekt. Ulike Span 80 konsentrasjoner mellom 0.05-0.2 vol.% endret stabiliteten lite. Disse konsentrasjonene kan være for høye og det spekuleres i om Span 80 burde bli beregnet basert på oljevolumet. Polderman sin modell ble brukt til å relatere batch resultatene til et strømmende system. Fluks basert på batch resultatene ble regnet ut og plottet. Disse viste lovende resultater, noe som en indikasjon påat modellolje kan brukes til å simulare råolje. Eksperimenter med samme fluidsystem ble gjort i et strømmende rig. Formålet var å undersøke om stabiliteten var lik som batch testene. Emulsjonen ble nå for stabil, noe som hindret videre testing. Dette kan være fordi konsentrasjonen av Span 80 var for høy.

Contents

List of Figures

List of Tables

Nomenclature

Roman Symbols

A	Area $[m^2]$
a	Interception constant
b	Slope constant
C_D	Drag coefficient
D	Impeller diameter
d	Droplet diameter $[m]$
E_σ	Surface energy
E_K	Turbulent kinetic energy
F	Force $[N]$
g	Gravity $[m/s^2]$
H	Steady State dispersion band height $[m]$
h	Height [m]
j	Constant
k	Constant
k_b	Batch constant
k_c	Continuous constant
L	Length $[m]$
N	Impeller speed [rev/sec]
P	Pressure
Q	Flow rate $[m^3/s]$
Q	Flow rate
q	Flux $[mm/s]$

R Radius $[m]$

r Constant

Re Reynolds number

t Mean power input per unit mass $[W/kg]$

t Time [s]

u Fluctuation component

V Volume $[m^3]$

v Velocity $[m/s]$

v_t Sedimention velocity $[m/s]$

We Weber number [dimensionless]

x Horizontal length $[m]$

y Vertical length $[m]$

Z Axial length $[m]$

Greek Symbols

$\bar{\bar{\epsilon}}$ Average dispersed hold up fraction

$\bar{\epsilon}$ Mean hold up fraction

Δh Dispersion layer thickness $[m]$

ϵ Hold up fraction

ϵ_F Hold up fraction in feed dispersion

η Grade efficiency

γ Shape factor

κ Viscosity ratio

μ Kinematic viscosity

ν Dynamic viscosity

ϕ Drop diameter

ψ Coalescence rate

ρ Density $[kg/m^3]$

σ Interfacial tension $[N/m]$

τ Coalescence time

θ Phase inversion coefficient

ε Energy dissipation rate

ζ Geometric conversion factor

Subscripts

$()_0$ Initial value

$()_B$ Buoyancy

$()_c$ Coalescence

$()_c$ Continuous phase

$()_d$ Dispersed phase

$()_i$ Interface

$()_o$ Oil phase

$()_p$ Dense-packed

$()_R$ Residence

$()_s$ Sedimentation

$()_w$ Water phase

$()_{max}$ Maximum

Acronyms

BS&W Basic Sediment and Water

DNS Direct Numerical Simulation

DSD Drop Size Distribution

LES Large Eddy Simulation

NIL Normal Interface Level

NLL Normal Liquid Level

RANS Reynolds average Navier-Stoke

wc Water cut

Chapter 1

Introduction

The offshore industry is constantly developing. Deeper and more marginal oil fields are found. Focus on environmental impacts and profitability is increasing. This requires new exploration and better technologies. One of the challenges in oil production is the extensive water amount occupied in the well together with crude oil. As water moves through chokes, valves, pumps and etc., the water droplets break into smaller droplets by the pressure differential across the devices [23]. The result is an oil-water emulsion, where small droplets of water are dispersed in the oil. The emulsion is stabilized by the natural surfactants present in the crude oil [15].

Horizontal gravity vessels are used to separate oil and water. It is beneficial to separate the water from the oil subsea before transporting it onshore. This requires compact and efficient separators. In order to optimize the performance of the separation, a good understanding of separation mechanisms and the characteristics of crude oil is essential.

Continuous settling experiments is used to illustrate industrial settlers. It is advantageous to test with model oil instead of crude oil, but it is important to find a fluid system with similar behavior as crude oil. Continuous tests are both time assuming and expensive. Batch settling tests can be done to test more efficient. The idea of using batch settling tests has always seemed attractive, but the difficulties of transferring unsteady data to a steady state situation complicates things [17]. Several authors have presented models for how to predict the steady state dispersion height based on batch data.

In this thesis batch separation tests with model oil, water and surfactant will be carried out. The goal is to gain knowledge about batch settling, through experimental and numerical investigation. Investigation of relationship between continuous separation behavior and batch settling will be done. The motivation is to find a model fluid system that can be used to simulate crude oil and water emulsions.

1.1 Objectives

Topics that will be covered in this thesis are:

- Numerical analysis of mixing performance in batch tests
- Experimental setup and testing in batch settling rig
- Experimental setup and testing in flowing settling rig

1.2 Scope and limitations

The scope only include information about liquid-liquid separation. To simplify the numerical work, simulation is performed as a one phase liquid, using water properties. ANSYS Fluent is used due to available support and licenses at Cameron System A/S. This thesis does not go into details regarding numerical models.

1.3 Structure of the thesis

This thesis is divided into sicks chapters. Chapter 2 contains the literature study. Theory regarding liquid-liquid separation, batch testing and simulation of mixing is covered. The third chapter includes the numerical setup and simulation of a mixing tank, and evaluation of the mixing performance. Chapter 4 present the batch test setup, and discussion of the result. The batch result is also connected to continuous settling by a separation model. Chapter 5 present the setup and the result of the flowing settling tests. Conclusion is given in chapter 6 and recommendation for further work is discussed in chapter 7.

Chapter 2

Literature review

2.1 Oil and Water separation

Reservoir normally contains both crude oil and water. An oil-water emulsion is created due to shear forces under pumping and transporting through valves and pipelines [25]. Separating water from oil offshore before further transportation has several advantages. Not only will the difference in viscosity make it difficult to pump the emulsion over long distances. The dimensions needed for pipelines will also be reduced, which is economically beneficial. The salinity in the formation water is another important argument for separating before transporting. A high water content in the oil, can result in corrosion of the equipment and in the pipelines. In addition, separation reduces the requirement of chemical inhibitors, and therefore also the discharge of chemicals to the sea [36].

Gravity settlers are the cheapest and simplest technology for separation of oil and water [10]. The principle is that gravitational forces govern the separation, and the phases will settle in separate layers. Water has higher density than oil, and will therefore settle at the bottom. The liquid-liquid mixture is continuously fed at one end and the separated phases are withdrawn from the other [16].

The separation process normally takes place in stages, where the operational pressure is reduced throughout the process. A schematic of this is shown in figure 2.1. The separated gas is transported out at the top of each separator, the produced water at the bottom and the oil phase in the middle continues to the next separator for further separation. The produced water goes through deoilers, here shown as hydrocyclones. They remove small amounts of oil in the water, meeting the requirement of treated water that can be released to the sea [36].

Gravity separators are typically horizontal or vertical. The horizontal gravity separator will be discussed in the following section.

2.1.1 Horizontal Gravity Separators

Oil-water separation by horizontal gravity separators has higher efficiency than with a vertical one, and is therefore considered a better choice [30]. A horizontal gravity separator consist of three sections:

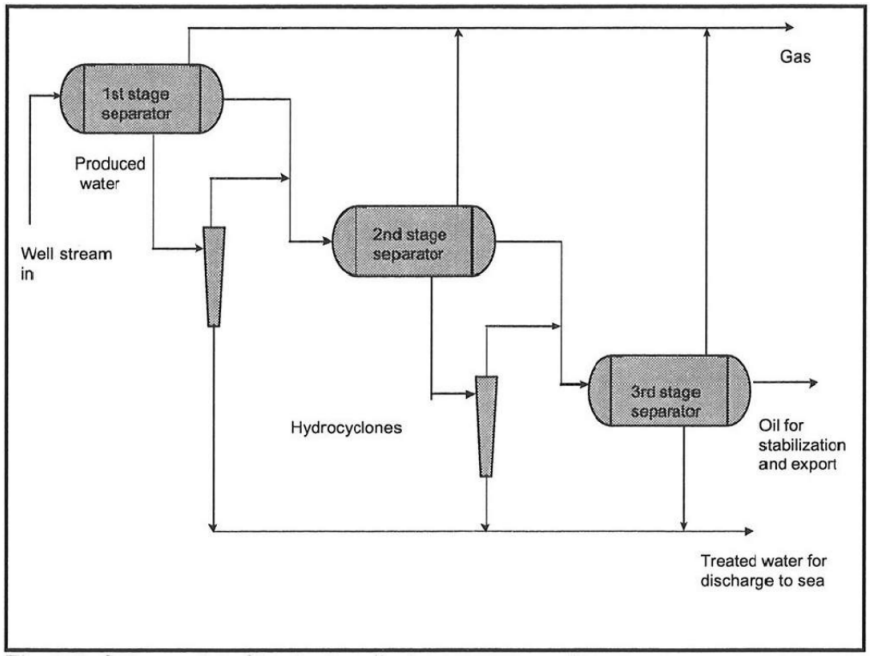

Figure 2.1: Schematic of typical well stream processing [36]

- Inlet section
- Settling section
- Outlet section

These sections are illustrated in figure 2.2. In the inlet section, the momentum of the fluid should be reduced gently to minimize droplet break up. Also, it should redistribute the flow in order to create an even mass flux along the flow direction. This can be done with different inlets, where a momentum breaker is the simplest one. Vanes and cyclones are other examples of inlets that are common to use [5].

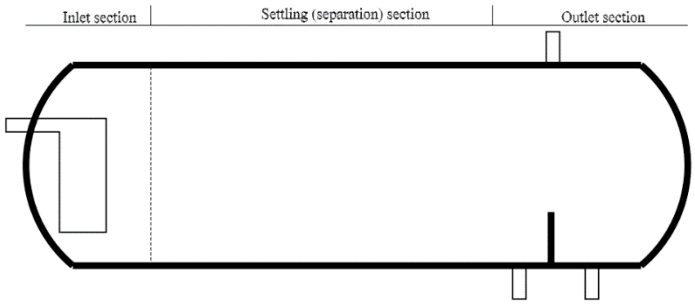

Figure 2.2: Illustration of the three sections in a horizontal separator

After the inlet section, the flow enters the settling section where the separation happens. The difference in density makes the less dense phase rise to the top, while the heavy

phase settles to the bottom. In between these layers, a dispersion band is created, Here, dispersed drops are separated from the continuous phase. In the outlet section, gas exits at the top of the vessel while a weir plate divides the liquids. The weir plate allows the oil to flow over, and holds back water and the dispersion band [28].

The residence time is the retention time of each phase in the settling part of the separator. Residence time means the effective time available for the droplets to be separated from the other phase. It is determined by the inlet volume flow and the volume of the liquid [5]. BS&W (basic sediments and water) is a measurement of the performance of the separation, meaning the percentage of water in the treated crude oil. In order to avoid poor oil quality, oil companies are normally defining a maximum water content in the oil.

2.2 Separation processes

A dispersion consists of two immiscible liquids, where the dispersed phase exist as droplets in the continuous phase. In the case of water in oil, oil will be the continuous phase and water the dispersed phase. This thesis will focus on separation where oil is the continuous phase.

Separation of the dispersion take place in two processes:

- Sedimentation
- Coalescence

2.2.1 Sedimentation

Sedimentation is the mechanical part of the separation, and is due to gravitational forces where droplets from the disperse phase are "falling" through the continuous phase [11]. Generally, three forces are acting on a droplet in a motionless fluid; buoyancy force, viscous resistance and Brownian motion (thermally induced). For a droplet bigger than 1 μm, which is the case in a gravity separator, the Brownian motion is neglected [5]. The buoyancy force F_B and drag force F_D are respectively given in equation 2.1 and 2.2:

$$F_B = (\rho_d - \rho_c)gV_p \tag{2.1}$$

$$F_D = C_D \frac{v_t^2}{2} \rho_c A_p \tag{2.2}$$

where ρ_d and ρ_c are densities to the dispersed phase and continuous phase respectively, g the gravitational coefficient and V_p the volume occupied by a droplet. C_D is the drag coefficient, v_t the sedimentation velocity and A_d the area of a particle projected on plane normal to direction of flow.

The gravitational force is opposed by the drag force. By doing a force balance on a

single, hard sphere, the settling velocity can be derived. This is shown in equation 2.3.

$$v_t = \sqrt{\frac{4}{3}\frac{(\rho_d - \rho_c)gd}{\rho_c C_D}} \tag{2.3}$$

d is the particle diameter. The relation between the drag coefficient and Reynolds number is shown in equation 2.4.

$$C_D = \frac{24}{Re}(1 + 0.1 \cdot Re^{0.75}) \tag{2.4}$$

For low Re numbers ($Re << 1$), equation 2.3 can be reduced to the Stokes law. Then $C_D = 24/Re$.

$$C_D = \frac{24}{Re_d} \tag{2.5}$$

The resulting settling rate v_{stoke} of a single droplet in a motionless fluid is shown in equation 2.6 [29].

$$v_{stoke} = \frac{(\rho_d - \rho_c)gd^2}{18\mu_c} \tag{2.6}$$

Where μ_c is the dynamic viscosity of the continuous phase. Stokes law is only valid for a single sphere suspended in liquid. In reality there is a high concentration of droplets, and the droplets are hindered by each other. Stokes's law is therefore overestimating the sedimentation velocity of the droplets in three phase separators [10]

One can see that if the droplet size is constant and the viscosity increases, the droplet velocity will decrease and the result is a slower separation time.

Stokes law has several limitations and is only applicable for non-interacting spherical droplets at low concentration. Predictions or calculation of settling rates in concentrated emulsions, where other than hydrodynamic factors come to account, are therefore complicated [29]. Several authors have modified Stokes equation to make it more applicable to realistic conditions. A correction that is based on viscosity is given in equation 2.7, which compensates for the internal flow in fluidic particles [5].

$$v_{st,visc} = \frac{(\rho_d - \rho_c)gd^2}{18\mu_c}\frac{\mu_c + \mu_d}{\frac{2}{3}\mu_c + \mu_d} \tag{2.7}$$

Where μ_d is the dynamic viscosity of the dispersed phase. Another modification is Kumar and Hartland's empirical equation (2.8). This equation is for settling in concentrated batch samples, so called hindered settling.

$$v_{KH} = \frac{(\rho_d - \rho_c)gd^2}{18\mu_c}\frac{(1 + \phi_d)^2}{1 + 4.56\phi_d} \tag{2.8}$$

As mentioned, this thesis is focusing on separation where oil is the continuous phase. For

an oil in water situation, water is the continuous phase where oil droplets are dispersed in the oil. In this case, the oil droplets will rise to the top. This phenomena is called creaming. The settling velocity will be significant higher in this case due to oil generally having a higher viscosity than water [30].

Separator cut size is defined as the smallest droplet that will settle or rise in the vessel. Arnold and Steward [30] calculated the cut size from Stokes' settling law and came up with an approximation of the BS&W. This can be seen in figure 2.3. Here the cumulative volume of water in oil is plotted against water droplet size.

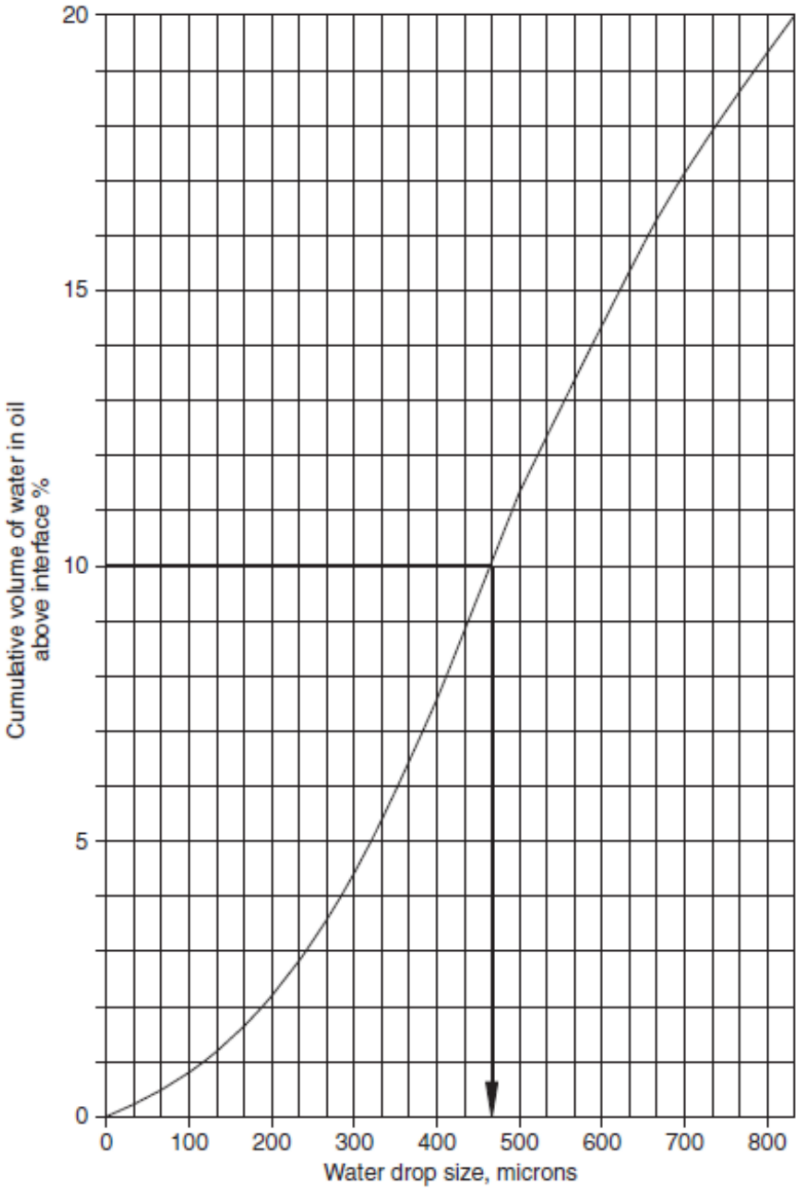

Figure 2.3: Approximation of the BS&W from Stokes law

Since the droplet diameter is squared in Stokes' law (equation 2.6), it is an important parameter for the water settling. The larger the droplet size, the less time it takes for the droplet to settle to the bottom of the vessel. It is important to know the droplet size that

must be separated from the oil to meet the desired BS&W specifications. When sizing a separator, it is necessary to predict the droplet cut size. [30]. Polderman [26] pointed out the influence of droplet size distribution, and stated that the ability of a separator to achieve the required outlet specification depends to a large extent on the droplet size distribution of the feed. Having a high shear element in the upstream production system can create a large proportion of tiny droplets. Droplets too small, slows the coalescence and result in a more stable emulsion [26]. Until recently crude oil emulsion separation has been modeled using Stokes law.

2.2.2 Coalescence

As a general rule, the smaller the dispersed droplets, the more stable the emulsion. To separate the two intimately mixed phases, the dispersed droplets have to grow in size to be able to settle. This process where droplets grow in size is called coalescence, and is the physicochemical part of the separation [11]. Coalescence mechanism can be divided into binary coalescence and interfacial coalescence. Binary coalescence describes the mechanism of when two drops collides and forms a bigger drop. Interfacial coalescence is a case of binary coalescence, where one of the drops has an infinite diameter like when a droplet coalescence with the homophase [25].

When two drops approach each other, a thin film of continuous phase liquid will be trapped between the droplets. An illustration of this is given in figure 2.4. The film needs to be drained in order for coalescence to happen. Generally this determines the necessary time for coalescence. The drainage time decreases with increasing viscosity of the continuous phase [25]. In the case of a highly concentrated water/crude oil emulsion, the drainage rate represents the limiting factor in order to determine the coalescence rate [10].

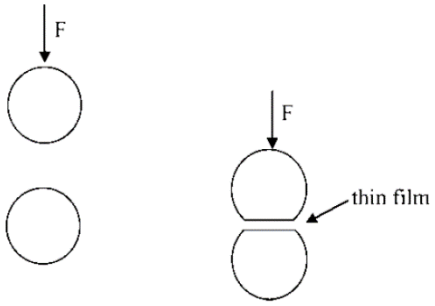

Figure 2.4: Thin film of continuous phase between droplets [10]

2.2.3 Dispersion Layer

At steady-state, drops are entering at the inlet end and will due to sedimentation and throughput flow move both vertically and horizontally in the vessel [16]. The drops will undergo binary coalescence before finally coalescing with the interface. The thickness of the dispersion band will decrease with the length of the settler. [15]. In the water in oil

case, the water droplets settle down trough the oil. It will create a coalescing interface at the bottom of the dispersion and a sedimentation interface at the top of the dispersion.

A water in oil case can be change to a oil in water case by increasing the water concentration. This is called the inversion point, and is the maximum water cut one can have before the continuity changes. Estimations of the inversion point can be done. In crude oil separation, a water-continuous dispersion is generally easier to separate. Understanding and controlling phase inversion is thus important. Phase inversion may occur locally at lower water cuts after choke valves. It is also important from a rheological point of view since the viscosity is reduced when going from a water in oil to a oil in water system. The phase inversion point can be altered by adding chemicals [6].

2.3 Droplet break up

2.3.1 Drop size distribution (DSD)

It is important to know the drop size distribution to understand or predict the separation behaviour [25]. This is because the DSD determine the settling velocity and retention time [3]. The break-up of the dispersed phase is characterized by the upstream turbulence, created by the upstream components [5]. When the break-up ends, the flow will have a DSD with droplet diameters below a maximum droplet diameter. The maximum surviving drop size in the dispersion can be found by determining the critical Weber number, given in equation 2.9. This number is the ratio of the forces acting to destroy the particles (shear force), divided by the forces acting to retain the particle form (surface tension). When the Weber number is large enough, break-up of the dispersion will occur [5]. If the Weber number is below a threshold value the break-up stops and the drops at or below this diameter will survive the shear [28].

$$We = \frac{E_K}{E_\sigma} \tag{2.9}$$

Where E_K and E_σ are the turbulent kinetic energy and surface energy respectively. These are defined in equation 2.10 and 2.11.

$$E_K = \rho_c v_c^{'2}(d) d^3 \tag{2.10}$$

$$E_\sigma = \sigma d^2 \tag{2.11}$$

Where ρ_c is the density of the continuous phase, $v_c^{'2}$ is the turbulent velocity fluctuation, σ is the surface tension, and d is the droplet diameter.

It is shown that the size of the droplet downstream of the choke valve is a function of the interfacial tension between oil and water, the dimensions of the choke and the energy dissipation rate of the flow in the valve. To be able to calculate the force acting on a droplet, the flow around the droplet has to be known. It is therefore necessary to look in detail into the flow occurring in a choke valve [8].

2.3.2 Pressure drop

Choke valves have in common that the fluid flow is forced through a restriction where energy is dissipated and a pressure drop occurs. The flow is accelerated through the restriction and a jet is formed. Due to this acceleration the pressure will decreases and reach a minimum. This position is called the Vena Contracta. Downstream of the Vena Contracta, the fluid decelerates, and part of the pressure is recovered. Still, there will always be a permanent pressure drop [8]. An illustration of the restriction and the Vena Contracta is given in figure 2.5.

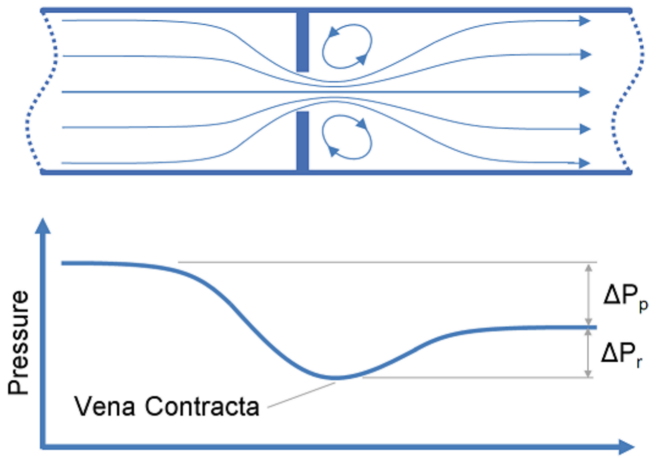

Figure 2.5: Illustration of the restriction of a simple concentric restriction orifice, and the location of a the Vena Contract [8]

2.3.3 Break up due to turbulent motion

The velocity in the jet zone following the restriction, is higher than the mean velocity in the pipe. Because of this, the turbulence here is higher. Droplets can break up due to the increased turbulent intensity at the orifice. In general, droplet break-up due to turbulence can be described using the Weber number. To be able to calculate the disturbing force acting on a droplet, some characteristics of the turbulence have to be known [8]. For a Reynolds number much lower than one, the inertial force is the dominant force causing droplet break-up. In this case the Weber number is given by equation 2.12.

$$We = \frac{\rho_c(\Delta u)^2 d}{\sigma} \tag{2.12}$$

Here Δu is the velocity difference across the droplet and σ the interfacial tension between the liquids.

In the case of homogeneous isotropic turbulence, a relation between Δu and the energy dissipation rate of the flow ε is given by equation 2.13.

$$\Delta u = (\varepsilon d)^{1/3} \tag{2.13}$$

The assumption of homogeneous isotropic turbulence is not valid for the entire flow field in the orifice. However, on the scale of the droplets this assumption can be used. By substituting equation 2.12 and 2.13, and consider droplets to break when $We >> We_{crit}$, the following relation for the maximum stable droplet diameter d_{max} in a turbulent zone of energy dissipation rate ϵ can be derived. This is given in equation 2.14 [8].

$$d_{max} = \left(\frac{\sigma}{\rho_c}\right)^{0.6} \varepsilon^{-0.4} \tag{2.14}$$

However, it is not practical to determine the energy dissipation rate locally. Instead the energy dissipation rate of the entire orifice zone $\bar{\epsilon}$ is used. Van der Zande [32] calculated the mean energy dissipation rate with equation 2.15.

$$\bar{\varepsilon} = \frac{\Delta P U_p}{\rho_c \Delta x} \tag{2.15}$$

Here ΔP is the pressure drop, Δx the length of the orifice and U_p the velocity in the pipe.

2.4 Batch testing

When estimating separation performance and designing separators, a typical approach in the industry today is calculating the theoretical cut size using Stokes law and finding the efficiency from the plotted value in figure 2.3. As mentioned earlier, Stokes law is only valid for unhindered settling, with a negligible dispersed phase concentration, and Re $<<$ 1. This is a simplification. The actual separation takes place in a dispersion band as mentioned above, located between the oil and the water phase [26]. An alternative to Stokes approach is having a macroscopic view and do experiments. The settling characteristic can be studied by performing small-scale batch tests. These tests are the most common tests for determining emulsion stability of water and oil. They involve mixing oil samples with water, and then watch the phases separate. In order to change the properties of the emulsion and control the stability, chemicals can be added [27]. This give an indication of how easy the emulsion separates and the relative effect of chemicals, temperature, mixing conditions etc. Tests like this is an effective way of studying the emulsion due to simple, repeatable and inexpensive experiments [27].

2.4.1 Batch testing studies

Several authors have studied separation mechanisms by using batch tests, and come up with different separation models.

Hartland and his coworkers [17] have published several papers regarding batch testing and prediction of separation behavior. Models have been presented, which relates the drop sedimentation and coalescence in batch and continuous flow separators. These models predicts the steady state behavior from parameters obtained from the batch data. Verification of the models are done with experiment data. The purpose is to simplify the

future design and scale-up of continuous settlers [17]. Models for prediction of separation profiles in batch dispersion has also been presented. The effect of dispersion phase holdup and dispersion height on the separation is experimentally investigated in terms of variations in the heights of the sedimentation and coalescing interfaces with time. These models are also verified with experimental data [15].

Panoussopoulos [25] carried out batch experiments using different crude oils and model oils to simulate the oil-water emulsion formed in offshore oil rigs. The effect of hold-up, settler geometry, temperature, mixing conditions, the concentration of demulsifies and type of oil was investigated. The goal for this work was to determine sedimentation and coalescence rate, and then also separation quality for different oil systems. The experimental study was done in order to establish a basis for selection and design of the separation process of a heavy crude oil field [25].

Shell Research and Technology Center in Amsterdam (SRTCA) performed extensive laboratory tests, and published a design philosophy for vertical separators. The basis of the philosophy is close to Hartland's approach, and looks at the dispersed phase transport through an interface [5]. The theory is developed for settling tanks where the oil is flowing upwards opposing the settling velocity of the dispersed water. The aim of this work was to find guidelines for the design of separators where viscosity were the only stabilising factor. Shell Research team used the settling characteristics to establish an operation window of primary oil/water separators. To study the characteristics of crude oil and water, a model settler was build. By performing experiments in this batch settler, the goal was to establish the relation between nominal settler capacity, crude viscosity and dispersion quality. Polderman and his coworkers [26] published a new philosophy for design of separation tanks and vessels. This is an alternative to Stokes microscopic way. Instead of looking at the sedimentation zone and the dense-packed zone as two separate zones, the authors behind this approach considered them as a whole. Based on the hypothesis that crude oil viscosity and operation temperature are the most influential parameters, the authors performed a series of batch experiments that lead to correlations and figures in order to determine the allowable horizontal flux [26].

Another approach has been launched by TOTAL and IFPEN. It involves a methodology based on determining coalescence parameters from batch-settling experiments. The idea is to match a separator model with experimental data. The parameters can then be used as input data in a steady state model. With this model, which is in 1D, separation efficiency can be calculated. Validation of the model was done by real crude oil experiments in a pilot loop. Similar to Hartland and his coworkers' theory, can this approach also be represented by the time development of the sedimentation interface, the dense-packed zone and the coalescing interface. This batch model can be adapted to batch-settling experiments, like a bottle test [24].

The physical processes of sedimentation and interfacial coalescence leading to the formation of a dense-packed zone occur in both batch and continuous settlers. Therefore, the information obtained from batch tests can be used as a rough indicator, and a first step when designing large continuous gravity settlers [15]. Different approaches have been presented to predict the characteristics of continuous settling dispersion based on

parameters from batch settling tests. In the following sections, a few of these models are discussed.

2.4.2 Hartland's approach

Hartland and his coworkers presented what is called sedimentation-based models. These models are based on sedimentation of droplets and interfacial coalescence. It assume that coalescence only takes place at the lower end of the dense-packed zone at a fixed drop concentration [10]. The size of the drops within the dispersion will therefore be equal although the height of the dispersion decreases with time [19]. Interfacial coalescence is preferred to binary coalescence, because experiments shows relatively constant mean droplet diameter in the sedimentation zone.

Interfacial coalescence

The volume rate of coalescence per unit area ψ_i for both batch and continuous dispersions can be expressed like equation 2.16.

$$\psi_i = 2\gamma_i \epsilon_i \phi_i / 3\tau_i \tag{2.16}$$

Where ϵ_i is the hold-up at the coalescing interface, τ_i is the coalescence time, ϕ_i is the drop diameter at the interface and γ_i is a shape factor. This shape factor is less than unity when the drop is flattened, and this is usually the case [17].

In a batch dispersion of height h and mean holdup $\bar{\epsilon}$, the volume rate of coalescence at the interface is equal to the volume rate of appearance of clear dispersed phase per unit area at the coalescing interface $-dy/dt$. This is also equal to the decrease rate in dispersion volume $-d(\bar{\epsilon})/dt$. In a continuous settler, the volume rate of coalescence at the interface is equal to the volume throughput of dispersion phase per unit area Q_d/A [17].

The coalescence time τ_i for drops with diameter ϕ_i at the coalescence interface can be expressed like equation 2.17.

$$\tau_i = k_i \phi_i^i / h_p^p \tag{2.17}$$

Here h_p is the height of the dense-packed zone. This equation also applies to a steady state continuous dispersion if h_p is replaced by the steady state dispersion height H_p.

The thickness of the dense-packed layer increases with sedimentation, which means the coalescence rate increase too before it reaches its maximum at the inflection point, and then decreases again [15].

Hartland and his coworkers derived equations which relates the behavior of batch and continuous dispersions. With these equations, the variations in steady state height with dispersion throughput can be predicted from batch decay curves. The steady state height

is empirically related to the dispersion throughput in terms of batch separation time. The constants involved must be independently determined for each liquid-liquid system and set of operation conditions used [17]. The authors observed the batch separation by recording the interfaces as a function of time. The batch decay curves are either exponential or sigmoid. The choice of model is dependent of which of these decays the batch settling gives.

Exponential batch decay

Sedimentation and coalescence influences each other and can take place simultaneously. They depend on different factors such as droplet diameter, disperse phase concentration, continuous phase viscosity and presence of surfactants. In order to sediment, the gravity force need to exceed the hydrodynamic force acting on the droplet. Even if sedimentation and coalescence occur at the same time, one of the processes determines the separation rate. If interfacial coalescence is faster than the sedimentation rate, the droplets are removed before the next ones arrives. In this case, the separation rate is completely determined by sedimentation. Figure 2.6 illustrates how a plot of the dispersion height decay with time will look like in this situation.

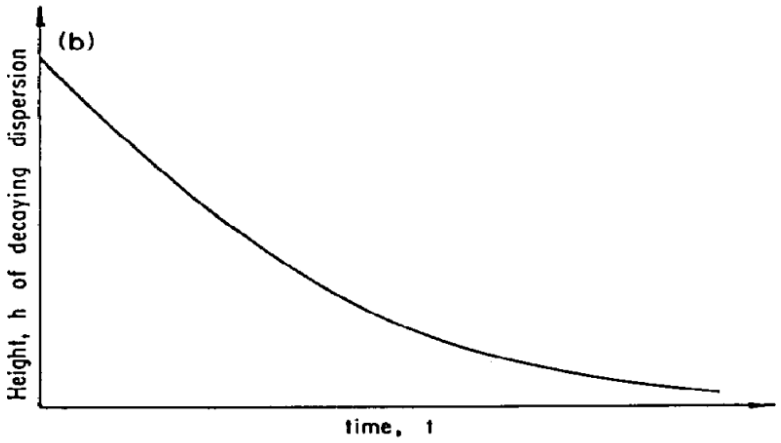

Figure 2.6: Illustration of exponential decay of batch dispersion height h with time t [13]

The interfacial coalescence is finished when the next drop settles at the interface. In this case a dense-packed layer is not created. The interfacial coalescence time τ_i is then a function of the drop diameter ϕ_i and the dispersion height h. One then yields a general equation 2.18.

$$\tau_i = k_i \phi_i^i f(1/h) \tag{2.18}$$

By substituting this into equation 2.16, and writing the function f(1/h)=k+1/h this yields:

$$\psi_i = K_i \psi_i^{1-i} h/(1+kh) \tag{2.19}$$

If ψ_i is independent of the drop diameter ϕ_i at the coalescing interface, then 1 - i = 0. This gives equation 2.20.

$$\psi_i = K_i h/(1 + kh) \tag{2.20}$$

For a batch dispersion, $\psi_i = -dy/dt = -(\bar{\epsilon}h)/dt = -\bar{\epsilon}dh/dt$. With this, one obtain a relationship for the decay of the dispersion layer. This is expressed in equation 2.21.

$$\frac{h}{-dh/dt} = \frac{1}{k_{b1}} + \frac{h}{k_{b2}} \tag{2.21}$$

Where $k_{b1} = K_i\bar{\bar{\epsilon}}$ and $k_{b2} = K_i/\bar{\bar{\epsilon}k}$. These are constants that can be obtained from the batch decay data. $h/(-dh/dt)$ can be considered as the notional residence time of the batch dispersion. Plotting this with respect to h, will give a straight line with intercept $1/k_1$ and slope $1/k_2$. Alternatively, integrating equation 2.21 with the initial conditions $h = h_0$ and $t = 0$ gives equation 2.22.

$$t = \frac{1}{k_1}\ln(\frac{h_0}{h}) + \frac{1}{k_2}(h_0 - h) \tag{2.22}$$

If the drop size, turbulence and coalescence rate are similar in the batch test and the continuous experiment, these constants can be used to predict the steady state behavior [17]. With equal coalescence mechanisms as in continuous settling, h can be replaced by H, which is the steady state dispersion height. -dh/dt can be replaced by the flux Q/A. This yields the relationship for a steady state situation, given in equation 2.23. By using this equation, the authors state that one can predict the variation of H with Q/A. This indicates that the range of the dispersion flux Q/A should correspond to the range of -dh/dt from the batch experiment.

$$\frac{H}{Q/A} = \frac{1}{k_1} + \frac{H}{k_2} \tag{2.23}$$

Sigmoidal batch decay

When the rate of sedimentation is higher than the rate of interfacial coalescence, the droplets will not be removed before the next ones arrives. In this case, a structure of disperse phase droplets will be created. This layer with droplets is called a dense-packed zone [25]. The height of the dense-packed zone will affect the interfacial coalescence rate since the force increases with height. The dense-packed zone will grow by sedimentation until there is a balance between the water settling on top of the dispersion and the water coalescing at the interface. This point is called the inflection point t_i. After the inflection point is reached the dense-packed zone covers the whole dispersion band. Further, the dense-packed height will steadily decrease due to the interfacial coalescence at the bottom of the disperse band [15]. The dispersion height will have a sigmoid, which is illustrated in figure 2.7. When looking at the whole dispersion band, this thickness will grow until the amount of water that coalesce at the interface balances the amount of water that settles on top of the dispersion band.

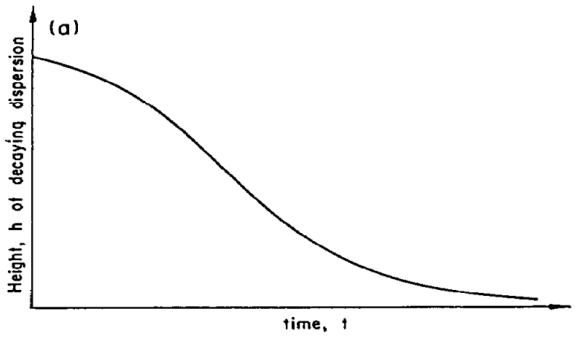

Figure 2.7: Illustration of sigmoidal decay of batch dispersion height h with time t [13]

The authors stated that coalescence only takes place at the lower end of the dense-packed zone. In the next stage the height of the dense-packed zone diminishes. According to the authors, the mean droplet diameter remains relatively constant throughout the experiment. Because of this, coalescence with the interface is the governing mechanism for separation [10]. Figure 2.8 illustrates a situation where there exist both a dense-packed layer and a sedimentation zone.

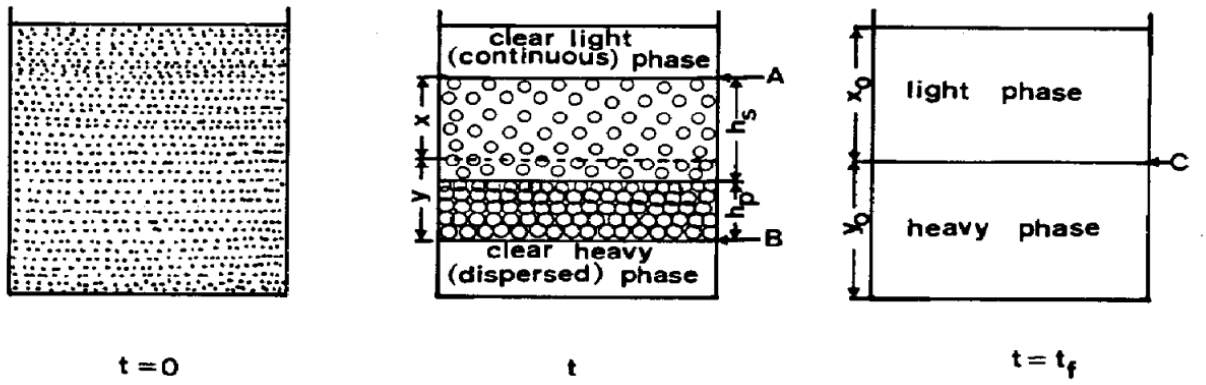

Figure 2.8: Decay of an unsteady-state batch dispersion with time showing development of sedimentation and dense-packed zones [13]

The batch dispersion height h is the sum of the sedimentation height h_s and the dense-packed layer h_p, $h = h_s + h_p$. x and y are the distances from the final undisturbed interface (x + y = h), and these are more practical to measure. Hence, h_s and h_p must be predicted from $-dx/dt$ and $-dy/dt$.

Based on settling velocities, mean droplet diameter and dispersed phase holdup fraction ϕ_s, the authors considered equation 2.24 to determine the height of the sedimentation zone h_s. This is for an unsteady batch settler.

$$-\frac{dx}{dt} = k_s t^{r/s} \tag{2.24}$$

Here $-dx/dt$ is the settling velocity of the drops relative to the continuous phase. The possible values of r and j are given in Table 2.1.

Constant	Laminar	Intermediate	Turbulent
r	2	$0.5 < r < 2$	0.5
j	1	$0.5 < j < 1$	0.5

Table 2.1: Values of sedimentation velocity constants r and j for different flow regimes

After integrating equation 2.24 with the boundary condition $x = x_0$ at t=0, this yields equation 2.25. Taken the logarithm of this equation gives equation 2.26, which is a straight line.

$$x_0 - x = \frac{k_s}{1 + (r/s)} t^{1+r/s} \tag{2.25}$$

$$ln(x_0 - x) = \ln \frac{k_s}{1 + (r/s)} + (1 + \frac{r}{s}) \ln t \tag{2.26}$$

Here $(1 + (r/s))$ gives the slope of the line and $\ln k_s/(1 + (r/s)$ gives the intercept. From this r/s and k_s can be found.

For continuous settler the equivalent velocity is $Q_d/A\epsilon_s$ and the residence time of drops in the sedimentation zone is $t = \epsilon_s H_s A/Q_d$. Equation 2.24 then becomes:

$$\frac{1}{\epsilon_s}\frac{Q_d}{A} = k_s\Big(\frac{\epsilon_s H_s A}{Q_d}\Big)^{r/n} \tag{2.27}$$

Equation 2.27 can be rewritten so that H_s is found [17].

For calculation of the dense-packed thickness, the volume balance for the dispersed phase is considered. This is given in equation 2.28.

$$\bar{\epsilon_s} h_s + \bar{\epsilon_p} h_p = \bar{\epsilon} h \tag{2.28}$$

Where $\bar{\epsilon}$ is the instantaneous average holdup fraction of the dispersed phase for the entire dispersion. The volumes of the the dispersed phase and the clear continuous phase are proportional to y and x, and $\bar{\epsilon} = y/(x+y)$. The volume balance can therefore be written like equation 2.29.

$$\bar{\epsilon_s} h_s + \bar{\epsilon_p} h_p = y \tag{2.29}$$

where $x+y = h$. This yields the expression for the dense-packed thickness h_p in equation 2.30.

$$h_p = (y - \bar{\epsilon_s} h)/(\bar{\epsilon_p} - \bar{\epsilon_s}) \tag{2.30}$$

$\bar{\epsilon_s}$ and $\bar{\epsilon_p}$ are assumed to be constant. This yields equation 2.31, which computes p and k_p when comparing to batch data.

$$-\bar{\epsilon} dh/dt = k_p h^p \tag{2.31}$$

By defining $\psi_i = Q_d/A$ and $h_p = H_p$, this gives the steady state situation in equation 2.32.

$$H = (Q_d/k_p A)^{1/p} \tag{2.32}$$

2.4.3 Polderman's approach

Combined with experimental data and field data, Polderman and his coworker [26] developed a generalised design windows for destabilised crude oils [5]. As mentioned above, the idea is to consider the sedimentation zone and the dense-packed zone as a whole, called the dispersion band. This approach is more pragmatic, since it can be difficult to observe the individual heights of the sedimentation zone and the dense-packed zone.

The top of the dispersion band is determined by the smallest water drops that can settle against the rising oil flow. The bottom of the dispersion band is determined by

the coalescing front where the water drops join the water-phase [26].

The dispersion band is stated to be in equilibrium during steady-state conditions. Both fronts of the dispersion band approach each other with a velocity equal to the superficial velocity of the incoming feed. When the throughput increases, the dispersion height will rise and establish a new equilibrium at a higher separation capacity. This is because an increase in the dispersion expansion height, means less hinder for small droplets, and thus more residence time for coalescence. The relation between throughput, dispersion height and interfacial area can be seen in equation 2.33 [26]. One observe that this equation is the same as what Hartland used for an exponential decay.

$$\frac{Q}{A} = \frac{H}{a + bH} \tag{2.33}$$

Where H is the dispersion band height and A is the interfacial area. The constants a and b depends on feed properties and operating conditions, where crude viscosity is the most important parameter. Equation 2.33 predicts that the separator becomes increasingly sensitive to variations in flow rate with increased throughput [26].

The relationship between batch and continuous settling, is given by the conditions at stationary conditions [26]. As explained, the decay of the dispersion height is equal to the feed rate. This is given in equation 2.34.

$$\frac{dH}{dt}\Big|_H = \frac{Q}{A_i}\Big|_H \tag{2.34}$$

By combining equation 2.33 and 2.34, and plotting $H/(dH/dt)$ as a function of H, the characteristics of a continuous settler can be derived. a being the intercept and b being the slope of the straight line. The result is figure 2.9, which is a design window for horizontal (vessel) and vertical separators (tank) [10].

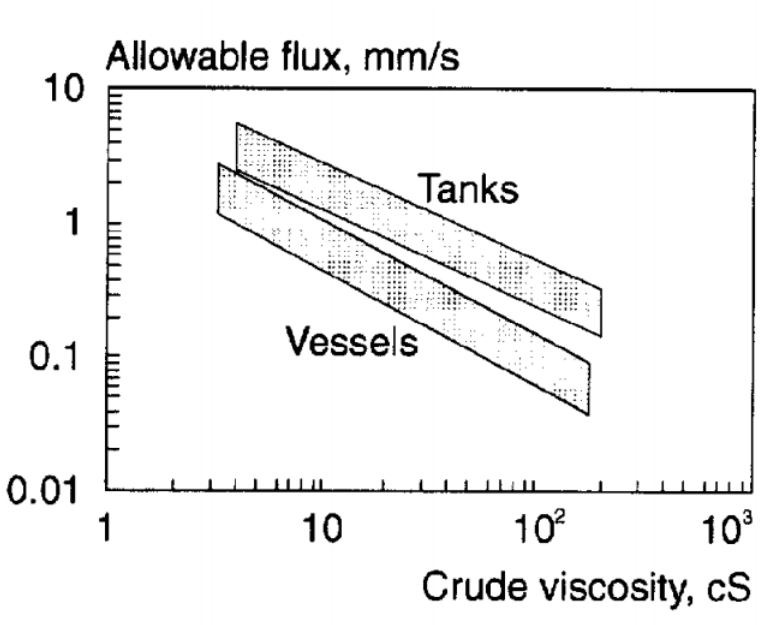

Figure 2.9: Allowable flux in the separator as a function of the viscosity [10]

The slopes in the figure is found for a dispersion height of 0.4 meter. To find the maximum allowable flux for other dispersion heights, a and b are needed. When the mixture is a dispersion, these constants can be defined as functions of viscosity [28]:

$$a = k\nu^l \tag{2.35}$$

$$b = m\nu^n \tag{2.36}$$

By a regression analysis, these equations can be solved to fit the slopes in the figure, which gives equation 2.37.

$$\frac{Q}{A_I} = \frac{H}{0.0512(\nu)^{0.8555} + 0.0328(\nu)^{0.7184} * H} \tag{2.37}$$

By inserting the viscosity and dispersion height, the flux can be computed. Equation 2.37 shows that the fluid viscosity has large influence on the dispersion height. Sizing of a separator can be done after determining the dispersion height variations [26]. Polderman's model is the simplest one for estimating the dispersion thickness in separators. It is therefore widely used in the industry.

2.5 Stability of emulsions

The concepts dispersion and emulsion are often mixed up in the literature. A dispersion is a mixture of pure oil and water that only need gravity to separate, an emulsion is a mixture that contains two mutually immiscible liquids and an emulsifying agent. The emulsifying agent will work as a stabilizer and therefore will an emulsion separate slower. For an emulsion to exist, it also requires sufficient agitation to disperse one liquid in the other [30]. In oil production, the flow from the well contains organic and inorganic

material in addition to oil and water. This is contaminants, that are absorbed at the oil and water interface. Once this happens, they form a rigid film that prevents water droplets from coalescing. The stability of an emulsion is enhanced by increasing the interfacial viscosity. Highly viscous interfacial films slows down the rate of film drainage by providing a mechanical barrier to coalescence [18]. The agitation in oil production happens mainly due to the turbulence caused by pressure drop in the chokes as the fluid flow makes it way from the well [30].

The stability of an emulsion depends on the degree of agitation and the amount of emulsifying agent. From a practical point of view, measurement of stability is an important tests for an emulsion. It determines the ease at which the oil and water separates [18]. Stable emulsions can take weeks or months to separate, while unstable emulsions may separate immediately [30]. The stability of an oil-water emulsion depends on several factors. These are briefly discussed below.

2.5.1 Density

A difference in density affects the settling rate of water droplets through the continuous oil. The greater the density difference is, the faster the droplets will settle. Heavy oil is often more stable since then the water droplets are kept in the continuous oil longer. Light oils allows the water droplets to fall a lot faster [30].

2.5.2 Droplet size

The stability of an emulsion is also affected by the size of the dispersed water droplets. The smaller the droplet is, the slower it will settle through the oil phase. The size of the droplet is as discussed earlier dependent on the degree of the agitation. Flow through pumps, chokes and valves will break up the drops into smaller sizes [30].

2.5.3 Viscosity

Viscosity affects the stability in two ways. When oil viscosity increases, the migration of emulsifying agents to the interface between oil and water is reduced. This leads to larger water droplets dispersed in the oil, which again means a less stable emulsion. A viscous oil require more agitation than a less viscous oil. Second, an increase in viscosity results in an decrease in the rate at which water droplets settle through the the oil. This results in less coalescence. On the other hand, an increase in oil viscosity results in less friction between the droplets as water settle through the oil. This promotes the separation [30]. Coalescence is reduced since the drainage time of fluid between droplets increases [6].

2.5.4 Interfacial Tension

The force that holds the surfaces of immiscible fluids together is called interfacial tension. This force is, among other factors, dependent on the degree of emulsifying agents. When an emulsifying agent is not present, the interfacial tension is high. This results in an easier coalescence between the water droplets. The present of emulsifying agents reduces the interfacial force, and this reduces the coalescence rate.

2.5.5 Water Salinity

The density of water increases with the salinity level, which again increases the difference between the oil and water density. Hence, an increase in salinity result in a more rapid separation. Also, small amounts of salt in the water phase will markedly lower the interfacial tension and thus decrease the difficulty of separation [30]. Water salinity will also reduce stabilization of oil droplets since it allows movement of electrodes [6].

2.5.6 Age of the emulsion

The age of an emulsion also influence the stability. Properties of the flow will change throughout the life of production, and as emulsions age they become more stable. Before an emulsion is created, the emulsifying agents are uniformly dispersed in the oil. When the agitating start, and the water is mixed with the oil, the emulsifying agents start to cluster around the dispersed water droplets. An initial stabilization can happen in only a

few seconds, but after that film developing continues. It may continue for several hours, until a state of equilibrium. At this point the emulsion is said to be aged. The older the emulsion, the more difficult it is to separate the phases [30].

2.5.7 Agitation

The type and degree of agitation on a oil–water mixture determine the water drop size. As mentioned, agitation in oil production is mainly cased by turbulence. The more turbulence and shearing action present in a production system, the smaller the water droplets in the mixture. Small water droplets settle slower, and result in a more stable emulsion [30].

2.5.8 Emulsifying Agents

An emulsifying agent is a material, which has a surface-active behavior that affects the surface tension between the phases. When a surfactant is used in an emulsion, it is called an emulsifier or emulsifying agents. The present of stabilizers can make the emulsion kinetically very stable [22]. A pure oil and water mixture, without an emulsifying agent, will fail to create an emulsion. If the pure oil and water are mixed and placed in a container, they quickly separate. This type of mixture is typically called a true "dispersion" [30]. Figure 2.10 illustrates how a surfactant work to protect the water droplets from coalescing.

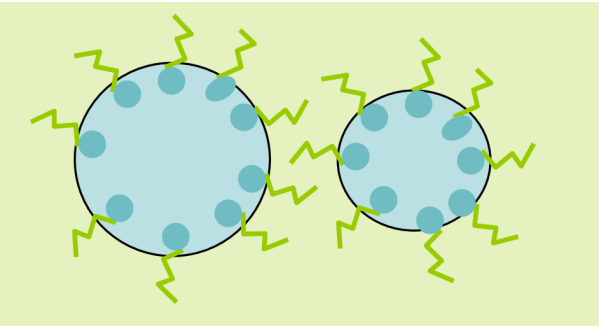

Figure 2.10: Illustration of how a surfactant work on a water droplets and the hydrophobic effect [12]. The blue circles are the water droplets and the green surroundings are the oil

There are several ways emulsifiers cause a dispersion to become an emulsion. It forms a coating on the droplets, which hinders them from coalescing into larger droplets when they collide. Since coalescence is prevented, it take longer for the small droplets, which are caused by agitation in the system, to settle out. Naturally occurring surface-active materials normally found in crude oil serve as emulsifiers. Paraffins, resins, organic acids, metallic salts, colloidal silts and clay, and asphaltenes are common emulsifiers in oil fields. Workover fluids and drilling mud are also sources of emulsifying agents [30]. In this thesis, Span 80 will be used as an emulsifying agent to stabilize the dispersion. When working with real crude oils, the present of surfactants may make the emulsion quite stable. In that case, the emulsion will not separate into pure phases by gravity alone. Then demulsifiers can be added.

2.5.9 Demulsifiers

Water-in-crude oil emulsions occur at many stages during the production and processing of oil. A common method of treating an emulsion is by adding demulsifiers. These chemicals are designed to reduce the stabilizing effect of emulsifying agents. Demulsifiers are surface-active compounds that when added to the emulsion, migrate to the oil/water interface, rupture or weaken the rigid film, and enhance water droplet coalescence. [18]. The required amount of demulsifiers to break up an emulsion depends on several factors. The type and concentration of surfactants at the interface influenced the amount. In addition to the droplet size distribution and the oil flow rate [12].

collision frequency are: the settling of drops, the shear flow, and the turbulence in the flow field [27].

2.6 Computational fluid dynamics - CFD

Agitation in a stirred tank is a common mechanism for a mixing process. However, it represent challenges when it comes to computer simulations. Mixing is typically performed by an impeller mounted on a shaft. Optionally, baffles and other internals can also be included to influence the agitation [20]. Analyzing the flow pattern in stirring vessels and its properties can be an effective tool when designing equipment, or for process scale up and quality control. By simulating turbulent flow in a stirred tank with the use of CFD, useful data can be obtained. Examples are data on flow behavior, circulation patterns, Reynolds stresses and vortex arrangement [31]. The challenges involves the non-isotropic nature of the flow, the complex geometry of the impeller and the imbalance in geometric scales present. Implementation of baffles increases the complexity further. In this thesis, computational simulation will be used to investigate the performance of the mixing.

Computational fluid dynamics is defined as the set of methodologies that enable the computer to numerical simulate fluid flows, heat transfer and phenomena such as chemical reactions [35]. By the use of the governing equations of fluid dynamics; the continuity, momentum and energy equations, problem regarding flows can be analysed and solved.

Computational simulations of stirred tanks are typically done in 2 or 3 dimensions. For asymmetric 2D simulations, the flow field and geometry are assumed to be independent of the angular dimension. This means that approximations are required for elements that are angular dependent, like the impellers and baffles. When simulating in 3D, the impeller and baffles can be modeled with the exact geometry. The challenge then is to integrate the movement of the impeller [20].

2.6.1 Turbulence

All flows become unstable above a certain Reynolds number. In this regime, one say the flow is turbulent. The flow is fluctuating and disordered, and the velocity and pressure fluctuates in all three dimensions [35]. A number of dimensionless parameters have been developed for the study of fluid dynamics. These are used to categorize different flow

regimes. One of the most common parameters, is the Reynolds number. This is defined as the ratio of inertial forces to frictional forces. Another way to look at it, is the ratio of the forces that give rise to the motion versus the forces that slow the motion down. The most common version of the Reynolds number is for pipe flow given by equation 2.38.

$$Re = \frac{\rho u d}{\mu} \tag{2.38}$$

Here ρ is the density, u the axial velocity, d the pipe diameter, and μ the dynamic viscosity of the fluid. For a stirring tank, this equation will be modified, as shown in equation 2.39.

$$Re = \frac{N D^2 \rho}{\mu} \tag{2.39}$$

Here N is the impeller speed (rev/sec) and D is the diameter of the impeller. As mentioned above, the value of this number may decide whether the flow will fall into the turbulent or laminar regime. The transition between laminar and turbulent regime in pipe flow is around Re=2000. For a mixing vessel it is somewhere between Re=50 and Re=5000, but usually lower than for pipe flow [20].

Turbulent flow consist of rotational flow structures, called turbulent eddies, with a wide range of length scales. Initially separated particles of fluid, even though those separated by long distance, can be brought together by the motions of the eddies. A consequence of this is that heat, mass and momentum are exchanged [35]. The effect of fluctuation of the mean velocity and other variables need to be integrated into a CFD model in order to get valid results. This can be done by using a turbulence model [20].

Several methods are available that includes turbulence in the Navier-Stokes equations. Based on the turbulence flow, the desired accuracy and what you are looking for, a model can be chosen. The methods can be divided into three categories [35]:

- RANS - Reynolds Averaged Navier-Stokes.
- LES - Large Eddy Simulation.
- DNS - Direct Numerical Simulation.

For most engineering problems, it is not necessary to know all details about the turbulent fluctuations. Often, average bulk motion is the most important information, and the time-averaged flow properties will therefore be sufficient. When turbulence is included, the transported quantity is assumed to be the sum of an equilibrium and a fluctuating component, $u_i + u_i^{'}$. After time-averaging over many cycles of the fluctuation, terms containing factors of the fluctuating component average to zero. The RANS-equations are obtain and this is given in equation 2.40.

$$\rho \frac{DU_i}{Dt} + \frac{\partial}{\partial x_j}(\rho \overline{u_i^{'} u_j^{'}}) = -\nabla p + \mu \nabla^2 U_i \tag{2.40}$$

Here U_i is the average velocity in the x_i direction, p is the mean pressure and ∇^2 the laplacian. The term $(\rho\overline{u_i^{'}u_j^{'}})$ involving the turbulent shear stress, makes the number of unknowns larger than the number of equations. In order to compute turbulence flows with RANS, additional turbulence modeling is necessary. Which turbulence model to choose depends on the solution accuracy and type of flow. The different models are categorized based on the additional number of transport equations that need to be solved along with the RANS equation. For a turbulence model to be useful, it must be both accurate, simple and economical to run [35]. The most common turbulence models to use is listed below.

- Mixing length model: 0 extra transport equations
- Spalart-Allmaras model: 1 extra transport equation
- $k-\epsilon$ model: 2 extra transport equations
- $k-\omega$ model: 2 extra transport equations
- Algebraic stress model: 2 extra transport equations
- Reynolds stress model (RSM): 7 extra transport equations

All the turbulence models, except the RSM, are based on the Boussinesq approximation given in equation 2.41. This relates the stresses to the mean rate of deformation, and introduces the turbulent (eddy) viscosity μ_t.

$$-\rho\overline{u_i^{'}u_j^{'}} = \mu_t\Big(\frac{\partial U_i}{\partial x_j} + \frac{\partial U_j}{\partial x_i}\Big) - \frac{2}{3}\rho k\delta_{ij} \tag{2.41}$$

k is the turbulent kinetic energy per unit mass, given in equation 2.42.

$$k = \frac{1}{2}(\overline{u'^2} + \overline{v'^2} + \overline{w'^2}) \tag{2.42}$$

In engineering applications, the most widely used turbulence model is the $k-\epsilon$ model. It is robust and economical [20]. The model is computed by solving two extra transport equation along with the RANS flow equation. One equation is for the kinetic energy k given in equation 2.42, and the other for the dissipation of kinetic energy ϵ given in equation 2.43:

$$\epsilon = 2\nu\overline{s_{ij}^{'}s_{ij}^{'}} \tag{2.43}$$

where $s_{ij}^{'}$ is the fluctuating deformation rate.

The $k-\epsilon$ model is not suited for swirling flow and therefore a few modified models exist. The $k-\epsilon$ model has also weak performances near walls compared to other models. One model with better near wall performance is the $k-\omega$ model. Menter [21] transformed the $k-\epsilon$ model into a SST $k-\omega$ model in the near wall region and a standard

$k-\epsilon$ model in the fully turbulent region far from the wall. The SST $k-\omega$ mode will be used in this thesis.

The SST $k-\omega$ model

The $k-\omega$ model is computed by solving two additional transport equations. One equation for the kinetic energy k and the other for the specific dissipation ω. Two versions of the model have been proposed, a standard model and a shear stress transport (SST) model. The SST $k-\omega$ model changes automatically to $k-\epsilon$ behavior in the free stream area. One avoid the sensitivity problems with the $k-\omega$ model in free shear turbulence. The SST $k-\omega$ model combines the standard $k-\omega$ model and the $k-\epsilon$ model, and is therefore a popular turbulence model to use. The SST $k-\omega$ model is often choosen for its good behaviour in adverse pressure gradients and separating flow [35]. The model is given in equation 2.44.

$$\frac{\partial(\rho k)}{\partial t}+\frac{\partial(\rho u_j k)}{\partial x_j}=P-\beta^*\rho\omega k+\frac{\partial}{\partial x_j}\Big[(\mu+\sigma_k\mu_t)\frac{\partial k}{\partial x_j}\Big] \tag{2.44}$$

The ϵ-equation is transformed into an ω-equation, by substituting $\epsilon=k\omega$. The equation for the SST $k-\omega$ model consist of an extra source term on the right side compared to the standard $k-\omega$ model. This is a cross-diffusion term, which arises during the $\epsilon=k\omega$ transformation of the diffusion term in the ϵ-equation [35].

2.6.2 Meshing

To be able to solve the equations numerically, the whole process need to be discretized. The area where the fluid flows will be described by a series of connected control volumes, or computational cells. Advancement in time and space are described by small, finite steps. This process is referred to as discretization. One use a grid or a mesh to break the domain into a set of sub-domains. The mesh is important in terms of convergence, accuracy and computational time. It is important to have a good mesh in order to obtain an acceptable solution The elements in the grid can be in many sizes and shapes. When simulating in two dimensions, the elements are usually either quadrilaterals or triangles. In three dimensions, the elements can be tetrahedral, prisms, pyramids, or hexahedra [20]. The most common grids for a 3D simulation are hexahedra elements in a structured form or an unstructured tetrahedra grid for more complex geometries. A tetrahedra grid has typically 6-7 times more elements than an equal hexahedra [1].

The density of cells in a computational mesh should be fine enough to capture the details of the flow, but not so fine that the overall number of cells in the domain is excessively large. A large numbers of cells require more time to solve [20]. Numerical diffusion is the error that occur when the discretized equations behave different than the differential equations. The size of the mesh influences the numerical diffusion, and is therefore important in order to obtain a accurate solution. The goal is to have a resolution that captures all relevant flow features, such as the boundary layer [28].

It is also desirable to have the cell size changes as smooth as possible. A large difference in the neighboring cell size can result in truncation errors [4].

The skewness represent how near a cell or a face is to the ideal form [4]. The skewness is a number between zero and one, where one is the ideal. What the number should be, is dependent on what cell geometry that is chosen. When solving the equations, an assumption is that the cells are close to ideal. High skewness is therefore not acceptable [28].

2.6.3 Solution methods for stirring tanks

As mentioned above, a stirring tank normally consist of impellers mounted on a shaft, and optionally internals and baffles. If it is necessary to model the geometry of the impeller exactly, it must be done in 3D. Several methods are available to describe the motion of the impeller. The grid used must be able to adapt to the solver approached employed. The most common models to use today are discussed below [20].

Rotating frame model

For problems where all the moving parts are rotating at a prescribed angular velocity, and the stationary walls are surfaces of revolution with respect to the axis of rotation, the entire domain can be referred to as a single rotating frame of reference. In this case the rotating frame model can be used [4]. This model solves the momentum equation for the whole domain in a rotating frame. Problems solved with this model typically use the angular velocity of the rotating component as the angular velocity of the frame [20]. In a stirred tank problem, the impeller is this component and the frame is therefore assumed to rotate together with the impeller. When defining this one choose the impeller to be at rest inside the frame. This is a simple steady state model. If the tank consist of baffles, they need to be given a motion through or into the fluid, which this model can not do. This approach can therefore only be used when simulating tanks with no baffles and internals [20].

Multiple reference frames model

The multiple reference frames model, or MRF model, is a modification of the rotating frame model. This model can be used when one need to use more than one reference frame in the simulation, which can be both rotating or non-rotating frames. This model allows for baffles and other complex internals when simulating a stirring tank.

This method involved separating the volume into two, a stationary outer zone and a moving inner zone. The rotating frame consist of the impeller which is at rest inside the frame. The stationary frame consist of the tank walls and the baffles [20]. The MRF method is suitable when the flow near the boundary between the outer and inner zone is close to uniform [31]. This model is powerful in that multiple rotating reference frames can be included in a single domain. The resulting flow field is representative of a snapshot of the transient flow field in which the rotating parts are moving. However, in many cases the interface can be chosen in such a way that the flow field at this location is independent of the orientation of the moving parts. That is, if an interface can be drawn on which there is little or no angular dependence, the model can be a reliable tool for simulating time-averaged flow fields. It is therefore very useful in complicated

situations where one or more rotating parts are present [4].

Sliding mesh model

This approach is a time-depending model where the grid around the rotating components physically moves during the simulation. The velocity of the component inside the moving mesh, such as the impeller and the shaft, is zero. The mesh surrounding the impeller moves with an noncontinuous motion, consisting of small discrete steps. After each step, the set of conservation equations is solved iterative until convergence is reached. Then the next step happens, and convergence is once again obtained. During each of these calculations, information passes through the interface from the rotating to the stationary regions and back again [20].

In order to rotate one mesh relative to another, the boundaries between the meshes needs to be a surface of revolution. Initially, the boundary grid must have two superimposed surfaces. This is because during the solution, one will remain with the rotating mesh region, and the other will remain with the stationary mesh region [20].

The sliding mesh model is the most informative method for mixing tanks. By using this model for transient simulations, one can capture low frequency oscillations in the flow field. In order to rotate one mesh relative to another, the boundary between the meshes needs to be a surface of revolution [20]. The sliding mesh model is computationally more expensive than the steady state methods.

Chapter 3

Numerical simulation of mixing performance

When mixing two liquids, it is important that the fluids are homogenized in order to get a dispersion layer to observe. Numerical simulation is used to evaluate the mixing performance. The droplet size after the mixing is an indicator of whether the agitation is sufficient or not. By evaluating the mixing performance before doing the experiment, testing in the laboratory can be optimized.

This chapter presents the numerical setup for mixing in a batch test. The effect of rotational speed and presence of static baffles will be investigated. Calculation of the theoretical droplet size after the mixing will be done and discussed.

The simulations settings are chosen based on Fluent theory guide and Cameron's experience.

3.1 Simulation cases

The mixing will be affected by several factors. Simulations are therefore performed to evaluate how much the rotational speed and the presence of baffles affects the mixing, and if the mixing in the used test setup will be sufficient. To investigate the effect of these factors, six study cases will be simulated. These cases will simulate the flow in the bottle with three different rotational speeds, with and without the presence of baffles. The simulation will investigate the rotational moment each velocity yields, and this value will be used to find the energy added to the fluids. With this energy, the theoretical droplet size can be estimated. The droplet size is an indication of how stable an emulsion is, and if the fluids are homogenized.

As a simplification, the simulation will be performed as a one-phase fluid, with water properties.

3.1.1 Geometry

ANSYS Design Modeler was used to design the geometry shown in figure 3.1. The geometry is based on the batch setup which is discussed in chapter 4, with equal dimension. These dimensions are given in table 3.1.

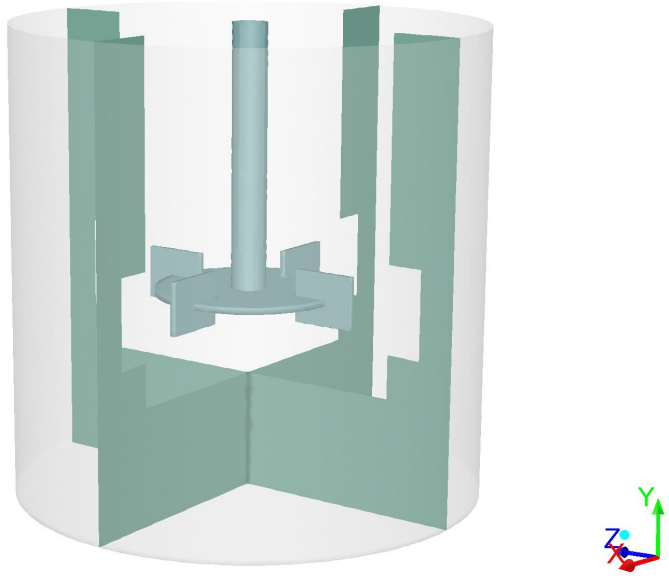

Figure 3.1: Geometry used in simulation. Showing baffles and impeller

Geometry	*Dimension [mm]*
Beaker diameter	80
Liquid level height	80
Width of baffles	12
Height of baffles in bottom of beaker	20
Diameter of impeller	42
Height of impeller blade	9
Diameter of shaft	7

Table 3.1: Geometry dimensions in the simulations

In order to apply the rotational movement, an inner zone surrounding the impeller was created. This is shown in figure 3.2. The inner fluid zone will be used to specify the rotational motion, and must be separated from the stationary domain. The simulated geometry consist of two body parts, an inner body containing the rotating impeller and a stationary outer body containing the walls of the beaker and the static baffles. This separation of the fluid domain will allow the impeller to rotate in the simulation.

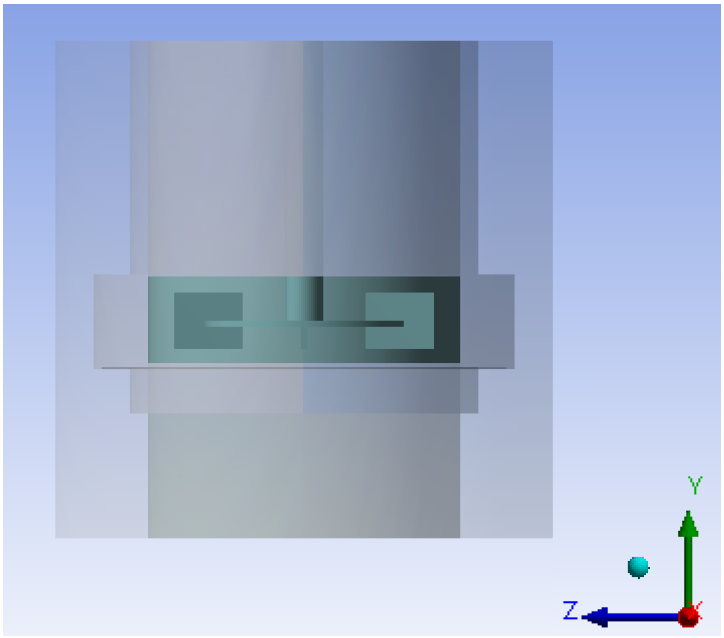

Figure 3.2: Fluid domain divided in two parts, fluid-inner and fluid-outer. Inner fluid zone marked with green

Static baffles are constructed in the stationary fluid domain. When simulating without baffles, these are chosen to be interior faces by a setting in the program. Only the boundary condition and the cell zone condition need to be changes between the cases with and the cases without static baffles. This also ensure that the mesh is identical for the two assemblies.

3.1.2 Mesh

Mesh generation was done with ANSYS Meshing. The shape of the elements was chosen to be tetrahedral due to the complexity of the impeller. The chosen grids are therefore unstructured and has higher numerical error compared to structured grids.

It is important to obtain a grid size independent solution. An independency test was therefore used to determine the minimum grid resolution that achieves a solution independent of the mesh quantities. Four different grid sizes were tested, and these are presented in table 3.2. It was chosen to simulate these tests without baffles, and with an angular velocity of 2000 rpm. A grid independency test involves evaluating the physics of the flow, and observe that the solution is equal as when using an increased amount of grid cells. It is desirable to use a grid with few elements to reduce the computational expenses, but it is important that the physics is independent of the grid size.

Case	*Element size [mm]*	*Grid*
1	2.0	$0.436 \cdot 10^6$ cells
2	1.5	$0.966 \cdot 10^6$ cells
3	1.0	$3.22 \cdot 10^6$ cells
4	0.75	$7.5 \cdot 10^6$ cells

Table 3.2: Grid cases

Numerical convergence is monitored through the residuals of the continuity equation, turbulent kinetic energy equation and dissipation rate equation. Fluent uses the value of 10^{-3} as default for the convergence criteria. Once the residuals drop below this, the solution is regarded converged. This value can be adjusted. Numerical convergence will only indicate that the solution has reached a stationary solution. Convergence of the physical properties is also important. A monitor was set up for the mass weighted average tangential velocity. The area considered was chosen to be 25 mm from the origin. Then, the value is measured outside the rotational impeller zone. Mass-weighted averaged can be used to find the average value on a surface in the flow, while area-weighted average can be used to find the average value on a solid surface. Numerical iterations were performed on the four grid cases until the tangential velocity was stabilized.

Figure 3.3a shows the convergence history for the tangential velocity. The four grid cases are presented. The mass-weighted average tangential velocity is plotted against the number of iterations. As can be seen, a high number of iteration is necessary for the solution to converge. The solutions can now be regarded as converged and steady state has been reached.

A mesh independent solution is obtained when the solution provides the same result for different grid sizes. The result of the independency test is shown in Figure 3.3b. The stabilized tangential velocity is plotted against the number of cells. As can be seen, the solution is stabilized in case 3 and 4. This indicate that for a grid with 3.22 millions cells and more, the simulations provide the same result. The simulation is then independent of grid size.

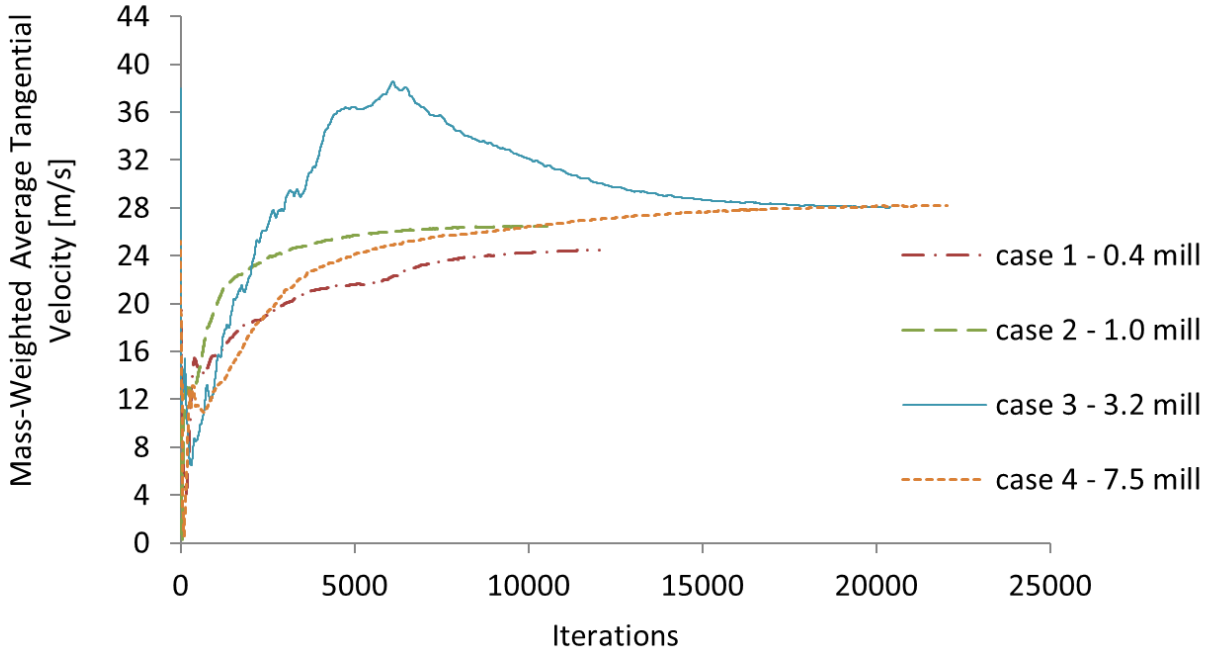

(a) Convergence history of Tangential Velocity on radial-coordinate-25mm

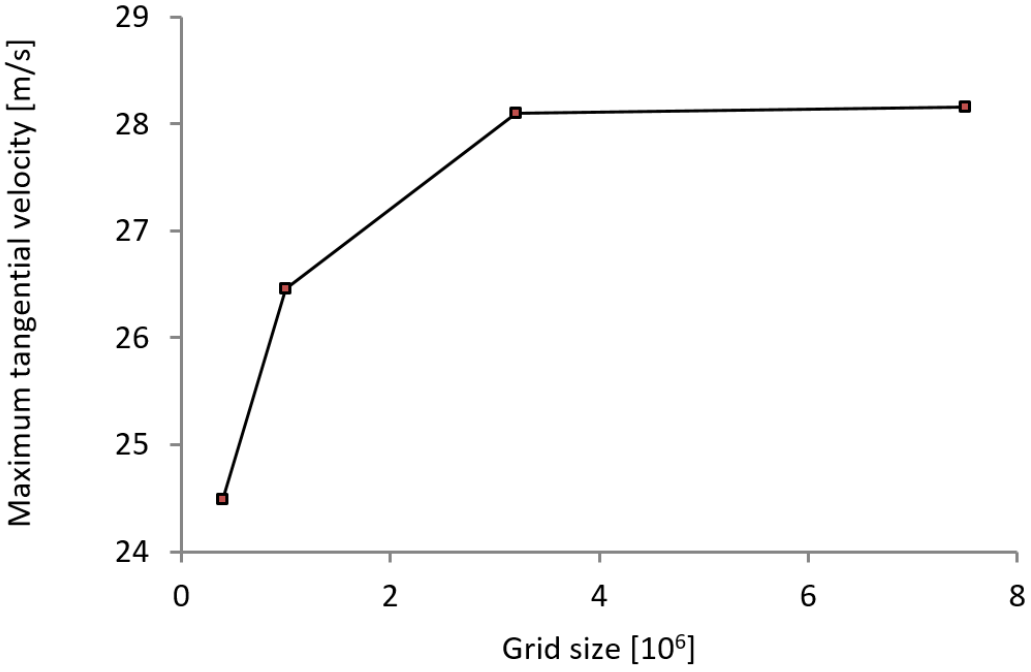

(b) Tangential velocity when physical convergence is reached

Figure 3.3: Investigation of mesh independency

It is preferable to use a mesh with few elements due to computational expenses. Meshing with element sizes of 1 mm and $3.22 \cdot 10^6$ cells is therefore chosen. With this mesh one obtain a valid solution with the least number of cells as possible. The mesh metrics are shown in Table 3.3. The values are within the recommended values for acceptable mesh quality [34]. With a reasonable simulation setup, the mesh should therefore reduce numerical errors and avoid convergence.

Elements 3.22M		
Orthogonal quality	min	0.266
	max	0.998
	avg	0.865
Skeweness	min	0.951
	max	0.999
	avg	0.214
Aspect ratio	min	1.158
	max	332.87
	avg	1.830

Table 3.3: Mesh quality

3.2 Simulation setup

The simulations were performed with ANSYS Fluent, and solved for steady-state, using three-dimensional grid. The Moving Reference Frame (MRF) approach, described in section 2.6.3 was used to account for the relative movement between impeller and baffles. This model is the simplest model that can be used in cases with both moving and stationary parts [2].

3.2.1 Turbulence model

The simulation must use a laminar or a turbulent model, where the correct model to use is dependent on the flow regime. A turbulent model is more computationally expensive, but will be used since the flow is turbulent. Fluent provides several turbulence models, where k-epsilon, k-omega and RSM are the ones typically used for industrial flows. The choose of turbulence model is based on flow characteristics and regime, geometry and computational time. For this simulation, the turbulent model SST k-omega is chosen. This model is chosen because it is a simple model that performs well with complex geometries. The model also behaves well in near wall areas. Bakker [7] investigated agitation of fluids by impellers, and stated that the shear stress transport (SST) k-omega model is the preferred model when simulating turbulent mixing.

Which turbulence model that is the best choice for this simulation have not been closely looked into. Another alternative to the SST k-omega model is the RSM model, which provides good results for swirling flows [4]. This is a more complex and computationally expensive model and is therefore not chosen for this simulation.

3.2.2 Discretization schemes

Discretization methods approximates the differential equations by a system of algebraic equations that is solved by the computer [28]. To numerically obtain solution for the governing equation, discretization methods need to be implemented. The accuracy of the solution is dependent on the discretization.

Fluent requires one to choose a discretization scheme for each governing equation, and different methods can be used. The first and second order upwind schemes are the recommended schemes. The practical difference between these is the truncation error, which is the difference between the exact equations and the discretized equations. The truncation error is reduced in a second order scheme because more cell faces are taken into interpolation. The accuracy is therefore higher for a second order scheme than for a first order scheme, which also may introduce a high level of diffusion [28].

For this simulation, the discretization of momentum, turbulent energy and turbulent dissipation was done using the second order upwind method, which is the default method. The volume fraction equation was discretized with the first order scheme.

Under-relaxation of the equations is used to control the update of computed variables at each iteration [4]. This will help stabilizing the convergence. These under-relaxation values can be changes under unstable behavior, but are kept as default here.

3.2.3 Cell zone condition and boundary condition

In Ansys Fluent, the boundary conditions for the two fluid domains, fluid-outer and fluid-inner are specified. Fluid-inner is the rotational reference frame, and frame motion is therefore selected to activate the MRF model. The desire rotational velocity is specified. Motion of the parts is then accounted for, even in a steady state solver. By specifying the rotation of the core, all the grid cells are given an additional source term to account for the local acceleration [4]. The outer fluid zone is stationary and therefore no further boundary conditions is set.

With the fluid-inner set to a rotating reference frame, the impeller becomes a stationary wall inside this frame. The velocity of the impeller relative to the adjacent cell zone is zero, and the impeller will rotate with the same velocity as the frame.

The boundary conditions for the baffles will switch between being a stationary wall or an interior wall. The top of the outer fluid domain is chosen to be a slip condition, with zero shear stresses.

3.3 Simulation result and discussion

The aim for the simulation work is to study the effect of rotational speed and stationary baffles. By doing this the batch setup can be evaluated and optimized. Baffles are suppose to prevent the fluid from flowing in large circulation loops around the vessel. To illustrate the effect of inserting static baffles, pathlines for 2000 rpm is presented, with

and without baffles. The pathlines are colored by velocity magnitude (m/s). This is shown in figure 3.4.

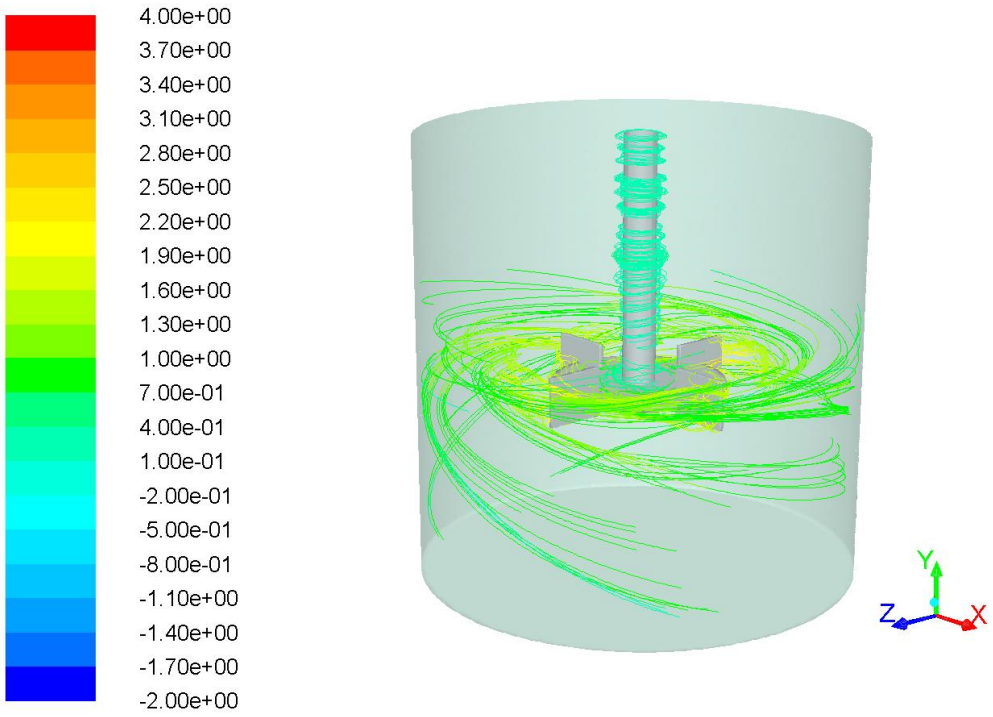

(a) Mixing without static baffles and 2000 rpm

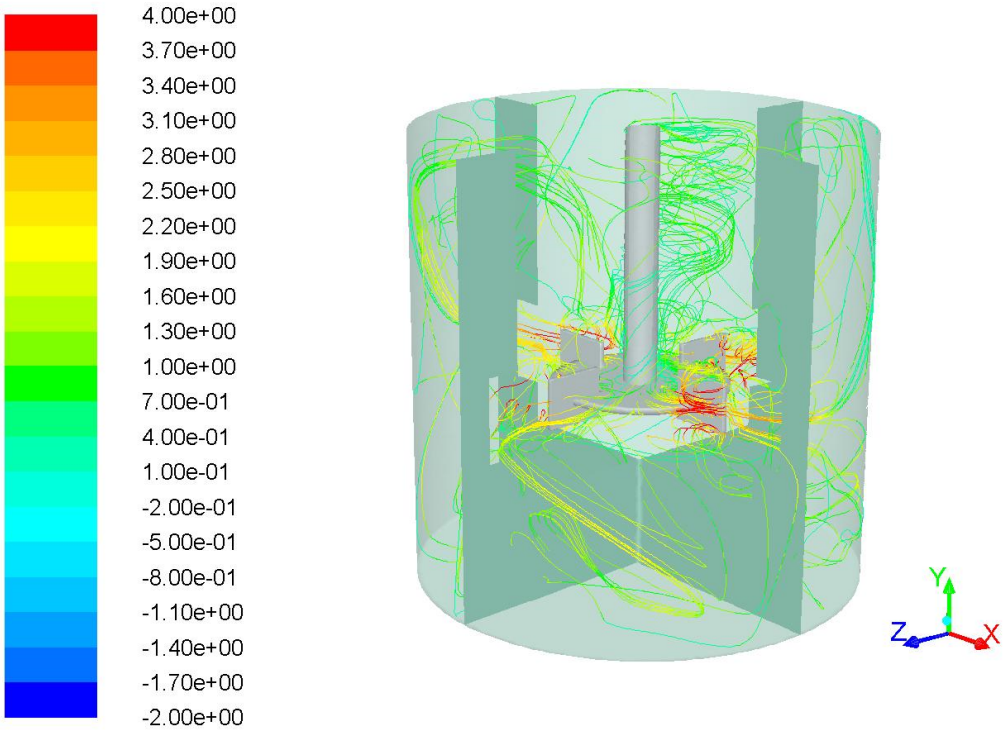

(b) Mixing with static baffles and 2000 rpm

Figure 3.4: Pathlines colored by velocity magnitude (m/s). Showing the difference between simulating with and without static baffles

As can be seen in figure 3.4a the pathlines are circulating in large loops around the vessel. The pathline velocities are relatively constant, which mean there is low rates of acceleration. This indicates that little energy is added to the fluid, and low presence of turbulence. Figure 3.4b show that the static baffles interact the swirling motion of the flow, and causes a more complex turbulent flow. Different velocity is present in the flow field, which mean the fluid is accelerating. More energy is therefore added to the fluid, and this mean the agitation is improved.

It is important to investigate if the mixing is sufficient to homogenized the fluids. This is done by finding the energy added to the fluids by the mixer, and calculating the droplet size this yields. The droplet size is an indication of the stability of the emulsion. From the simulations, the torque moment can be extracted. Table 3.4 lists the three torque moments found for each rotational velocity.

Rotation [rpm]	*Moment without baffles [Nm]*	Moment with baffles [Nm]
500	0.0028	0.0080
1000	0.0076	0.0332
2000	0.0280	0.1319

Table 3.4: Torque moment yield by rotations

By multiplying the torque moment with the angular velocity ω $[rad/s]$, the power input to the fluids are found. This is shown in equation 3.1.

$$P = T \cdot \omega \tag{3.1}$$

P represent the power given in watt, T the torque moment and $\omega = rpm * 2\pi/60$ the angular velocity. This yields table 3.5, which shows the calculated power for each velocity.

Rotation [rpm]	*Power without baffles [W]*	Power with baffles [W]
500	0.147	0.419
1000	0.796	3.477
2000	5.864	27.625

Table 3.5: Power yield by rotations

These values are plotted against rotational speed in figure 3.5.

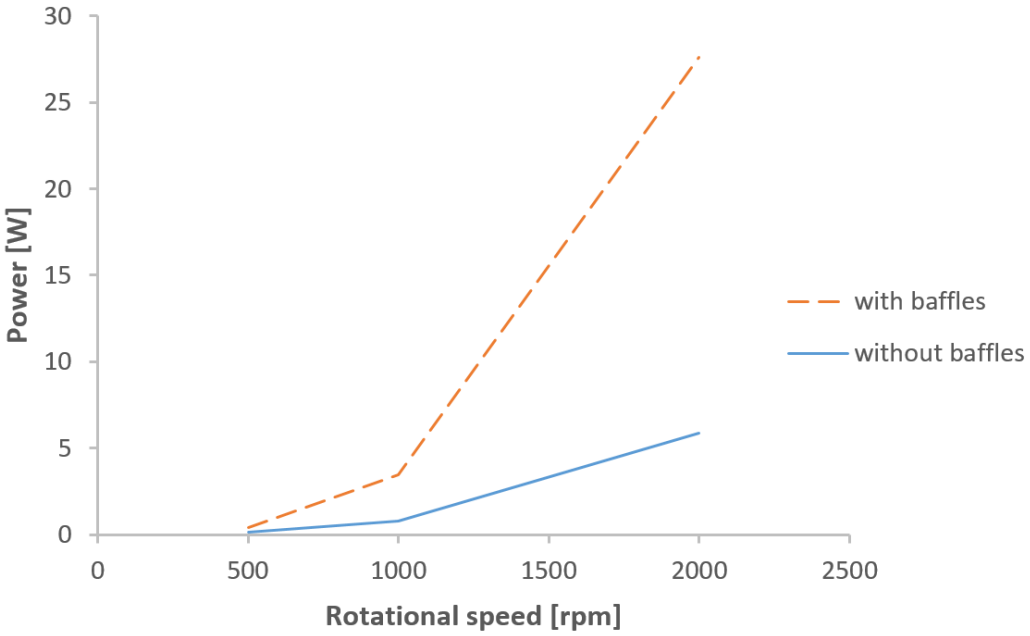

Figure 3.5: Watt plotted against rpm

As can be seen, both the rotational speed and the present of baffles gives significant effect on the power input to the fluid. This effect increases with higher rotational speed. According to these results, mixing with baffles is proved to be more efficient than mixing without. The effect is given in figure 3.6. Here the power ratio between mixing with baffles and without baffles is plotted. This plot show that even for the lowest rotation speed, the effect of baffles is 2.9 times the result without baffles.

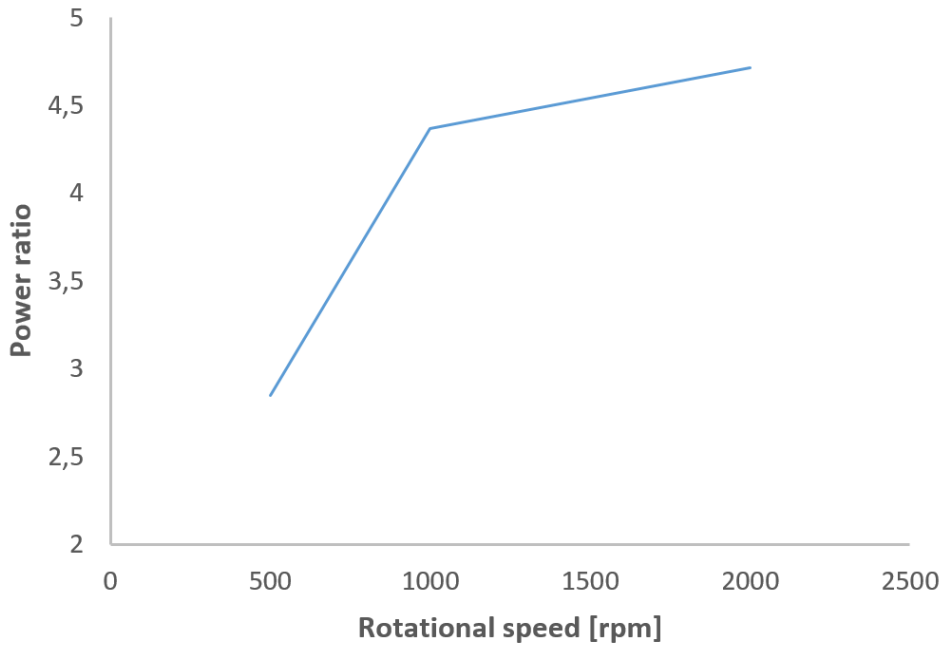

Figure 3.6: Effect of baffles given by the power ratio between mixing with and without baffles

The theoretical droplet sizes can now be calculated. This is shown in the following section.

3.3.1 Calculation of droplet size in mixer

A rule of thumb is that the droplets should be 1000 micron or smaller after the mixing to be representative for a gravity separator [6]. This indicates that the two liquid have formed a homogenized emulsion, and that the mixing is therefore sufficient. The droplet size can be calculated when knowing the work done by the impellers on the fluid.

In section 2.3.3 droplet break up due to turbulence was discussed, and a formula for calculating the droplet size was presented. A simplified way of estimating the droplet size is given in equation 3.2. This formula is proposed by DAVIES [9], and based on the isotropic turbulence law for low-viscosity liquids. This formula will is used to calculate the droplet size after the mixing.

$$d_{max} = c \cdot \left(\frac{\sigma}{\rho_c}\right)^{0.6} \cdot P_M^{-0.4} \tag{3.2}$$

Equation 3.2 gives the maximum droplet size that will survive the turbulence. Several assumptions needs to be taken. The coefficient c should be in the range from 0.5 to 1.0. Based on this, the mid value 0.75 is chosen for this case. σ is the interfacial tension between water and Exxsol D60. This is approximately $0.030 N/m$. For ρ, the density of water $1000 kg/m^3$ is used. The final parameter P_M represent the mean power input per

unit mass within the effective region where the drop dispersion occurred. It is assumed that the effective region is the whole bottle volume, which is 400 ml. P_M is found by dividing the power input P with this volume, shown in equation 3.3.

$$P_M = \frac{P}{mass} = \left[\frac{W}{kg}\right] \tag{3.3}$$

Inserting equation 3.3 in 3.2 yields:

$$d_{max} = 0.75 \cdot \left(\frac{0.030}{1000}\right)^{0.6} \cdot \frac{P}{0.4}^{-0.4}$$

By inserting P for different rotations, the droplet sizes are obtained. This is given in table 3.6.

Rotation [rpm]	*Droplet size without baffles [µm]*	*Droplet size with baffles [µm]*
500	2164	1423
1000	1101	610
2000	495	266

Table 3.6: Result of droplet size calculation for each simulation case

This result show that for 2000 rpm, both with and without static baffles provide a result below the thumb rule requirement. This also implies for the case with 1000 rpm and static baffles. The case without static baffles and 1000 rpm, gives a result slightly over the thumb rule, which may be good enough. For 500 rpm, both with and without static baffles provide a result over the thumb rule requirement. This means that by this thumb rule requirement, mixing with 1000 rpm or more, and the presence of baffles will be sufficient to homogenize the fluids.

3.4 Summary

In this chapter, the purpose was to see what effect rotational speed and the presence of static baffles have on mixing performance in a stirring vessel. By doing this, the setup for the laboratory batch testing can be optimized. It was important to evaluate if the mixer was sufficiently good to homogenize the fluids.

The result showed that both rotational speed and the presence of static baffles influences the mixing significantly. The power ratio for the cases with and without baffles was always 2.9 or more for the cases tested. Inserting static baffles in the beaker during batch testing will therefore increase the mixing with a factor of 2.9 or more.

The droplet size is estimated based on the energy added to the fluids when stirring. As a rule of thumb, the droplets should be smaller than 1000 μm for the fluids to be homogenized. The results showed values below this, and indicates that the mixing will be sufficient.

Chapter 4

Experimental study - Batch settling experiment

This chapter present batch settling experiments. The purpose is to test different fluid system consisting of model oil and salinity water, and find out what affects the stability the most. Another goal is to use the batch data to predict the behavior in a separation vessel by applying one of the separation models discussed in chapter 2.

Batch testing is often considered a suitable first option when testing oil and water emulsions in a laboratory. This is due to simple and repeatable experiments. However, batch tests are less representative than testing with continuous pilot settlers, and these tests are therefore often used in the next phase of the design process. In the following sections, separation will be observed and evaluated with batch tests. The test equipment, test matrix and choice of fluid will be presented. The result will be discussed and connected to a continuous experiment.

4.1 Background

At Cameron's test facility at Sintef Coastal and Harbour laboratory in Trondheim, continuous settling experiments with model oil and water have been carried out earlier. The experiments was unable to provide good results. The two phases were separating instantly, failing in creating a dispersion band to observe. By changing the fluid system, the goal is to form a more stable dispersion providing a dispersion band where the decay can be recorded. Testing different fluid system in the continuous test rig would be both expensive and time assuming. Performing batch test are therefore considered an attractive alternative.

When performing batch settling test it is important that the fluids are homogenized. If not, the different fluids will separate immediately into two clear phases, and no dispersion band will be created. In order to get a homogenized mixture, the agitation must be sufficient. From the optimization study in chapter 3, theoretical calculations indicates that the selected mixer should be good enough to homogenize the fluids. Also, the simulations showed significant effect of the present of baffles.

If the batch experiment is successful and a dispersion band is created, then this information will be transferred to a continuous system with one of the separation models discussed in chapter 2. By doing this, validation of the model can also be done.

4.2 Experimental setup

The presented experiments are performed in 600 mL cylindrical glass beakers, with diameter of 80mm. Mixing of the fluids is done by a stirrer. A four bladed steal impeller (width=11mm, height=8mm) is used as the mixing tool. The mixer has three gears and an adjustable velocity from 25 to 2000 rpm. Both the mixer and the beaker is borrowed from the Chemistry department at NTNU.

The tests are carried out with a total volume of 400 mL, and the propeller height is fixed at 40 mm from the bottom of the beaker. Monitoring is done by visual observation and recording of the decay of the interface.

4.2.1 Mixing performance

As discussed earlier, it is important that the fluids are homogenized after the mixing. Large liquid-circulation loops developed in stirred vessels make mixing performance poor. Mixing efficiency is easily enhanced by the use of rectangular boards called "baffles". Typically, four baffles are symmetrically installed and mounted vertically on the wall in an agitated vessel. Baffles not only enhance mixing performance, but also prevent the deformation of liquid free surface and the entrainment of air bubble [14].

The simulations in chapter 3 showed significant effect of static baffles. It is therefore chosen to do batch experiments with the presence of baffles. Based on the dimensions of the glass beaker and the impellers, four baffles are designed in Solid Edge and manufactured. Solid Edge is a 3D CAD software used for design and design documentation. The baffles has a width of 12mm. To make the test system as simple as possible, the baffles are designed as two parts. This way, they can easily be installed and removed from the beaker.

A lid was also designed in Solid Edge and manufactured. The purpose was to enhances the mixing efficiency further by minimizing the amount of air added to the fluids. Another advantage is that the lid is designed to fit together with the baffles inside the beaker. This makes the baffles more stable and the mixing more secure. With a handle, the lid can easily be moved up and down to adjust the height. During the mixing, the lid was held just below the surface. Figure 4.1 shows the drawing of the lid and the baffles.

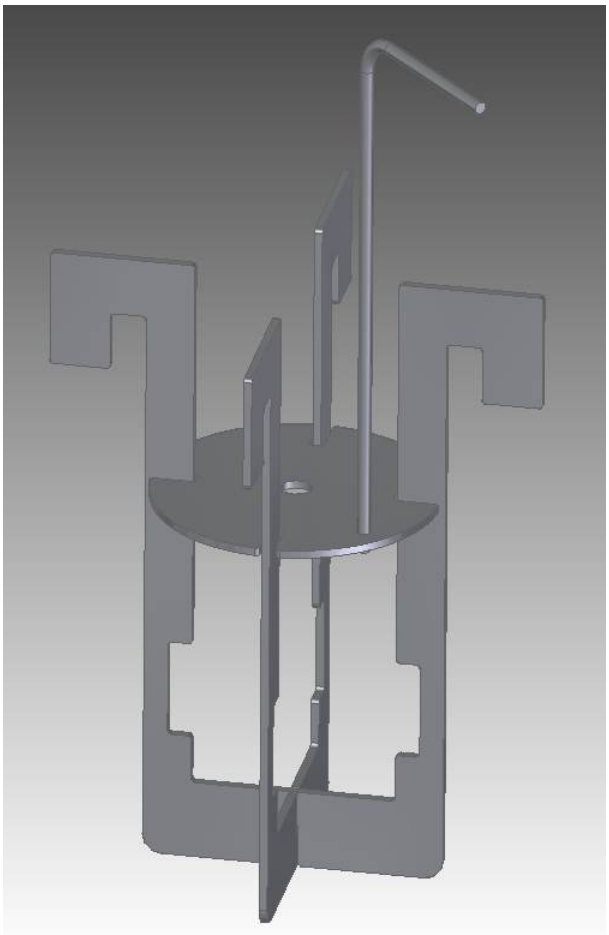

Figure 4.1: Vanes and lid modeled in Solid Edge

Figure 4.2 and 4.3 shows the actual test setup in the laboratory.

Figure 4.2: Batch test setup

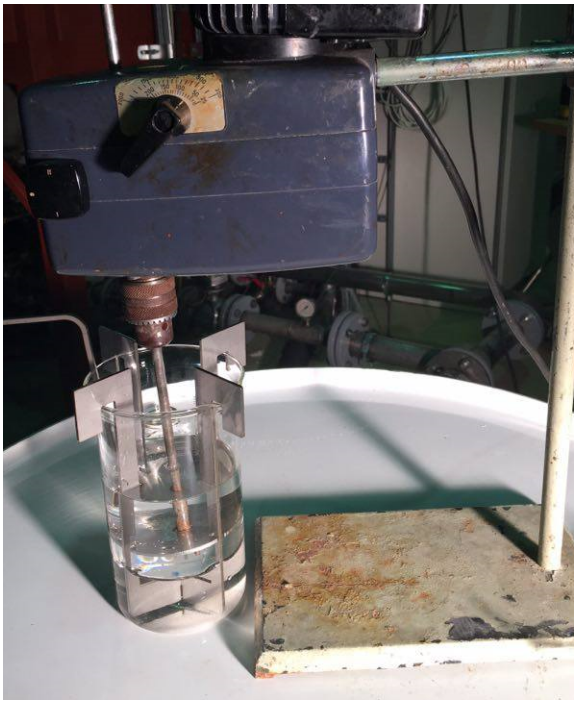

Figure 4.3: Batch test setup

4.2.2 Fluid system

The fluid system in the experiments will be Exxsol D60 and salinity water. There are several reasons for using a model oil instead of crude oil. Crude oils are more expensive and also has environmental and safety issues to consider. Model oils are transparent, and monitoring of the interfaces therefore becomes easier. A crude oil dispersion may become an emulsion unable to separate due to small loop size [3]. Crude oil also has an ageing effect, and this makes it difficult to reproduce [25]. Based on these reasons, testing of liquid-liquid dispersions is performed with model oil. It is important to choose a model system with similar behaviors as crude oil.

When doing separation experiments at atmospheric pressure, Exxsol D60 and tap water with 2.5-3 wt% NaCl are the most used fluid system [5]. Exxsol are dearomatized hydrocarbon fluids with chain lengths from c10h22 to c13H28. It contains no additives, have representative specifications and is not dangerous for health and environment. At ambient temperature, the viscosity is close to a light/medium crude oil [5].

There are some differences between model oil system and crude oil system:

- The coalescence is generally faster than observed in real crude system [10]
- Model oils have lower inversion point, in the region of 30-40% [3]
- The separation time of the model oil dispersion increase with water cut. This is opposite from a crude oil system [25]
- A pure model oil system will fail to create a dispersion band without using large flow rates [3].

Pure model oil (Exxsol D60) and water will separate immediately unless higher flow rates than the rate region of interest is used [3]. Alternatively can surfactants be added to stabilize the model oil, as discussed in section 2.5.8. The challenge with surfactants is that it can result in a milky color, making the observation of the interfaces more difficult. Span 80 is an emulsifying agent with surface active characteristics. It was decided to use this as surfactant in the following batch tests, and see if Span 80 can be used as stabilizer for model oil and salinity water.

4.3 Test matrix

When performing experiments it is desirable to test different concentrations of the surfactant, and see how this affect the stability of the fluids. Therefore, Span 80 is added to the fluids with 0.05 %, 0.1 % and 0.2 % of the total volume. These concentrations are based on literature and pre-testing in the lab. Experiments with Span 80 as emulsifying agent have been carried out by others earlier. Then concentrations from 0.1 % to 5.0 % were used, both based on total volume and based on volume of oil. The concentrations in the following tests are therefore chosen based on these experiments, where the lowest concentration is set based on the smallest amount possible to measure in the lab.

Steward [30] stated that sufficient agitation is important for an emulsion to exist. The effect of different rotational speeds will be tested. The rotational speed that will be tested are based on the simulations, 500 rpm, 1000 rpm and 2000 rpm. Even though the simulations indicated that 500 rpm is not sufficient to homogenize the fluids, this rotation is included in the test matrix. In order to verify the effect of water cut in the mixture, all the cases will be carried out with different water cuts (20 %, 30 % and 40 %).

It is desirable to compare the settling with cases without any surfactants. Nine tests will be performed with different rotational speeds and water cuts, and zero concentrations of Span 80 added. This yield in total 36 cases presented in table 4.1.

Case	*Water cut [%]*	*Span 80 concentration [vol.%]*	*Rotation [rpm]*
1	20	0.00	500
2	20	0.00	1000
3	20	0.00	2000
4	30	0.00	500
5	30	0.00	1000
6	30	0.00	2000
7	40	0.00	500
8	40	0.00	1000
9	40	0.00	2000
10	20	0.05	500
11	20	0.05	1000
12	20	0.05	2000
13	30	0.05	500
14	30	0.05	1000
15	30	0.05	2000
16	40	0.05	500
17	40	0.05	1000
18	40	0.05	2000
19	20	0.10	500
20	20	0.10	1000
21	20	0.10	2000
22	30	0.10	500
23	30	0.10	1000
24	30	0.10	2000
25	40	0.10	500
26	40	0.10	1000
27	40	0.10	2000
28	20	0.20	500
29	20	0.20	1000
30	20	0.20	2000
31	30	0.20	500
32	30	0.20	1000
33	30	0.20	2000
34	40	0.20	500
35	40	0.20	1000
36	40	0.20	2000

Table 4.1: Test matrix for batch settling experiment

4.4 Results and discussion

The first experiments were carried out without any surfactants in order to compare the other experiments with these cases. The result was a very unstable dispersion, that would separate in just a matter of seconds. Recording of the interfaces was therefore difficult. The initial dispersion height and the time needed to separate the phases is used to plot a linear estimated line for the sedimentation height. This decay is shown in figure 4.4.

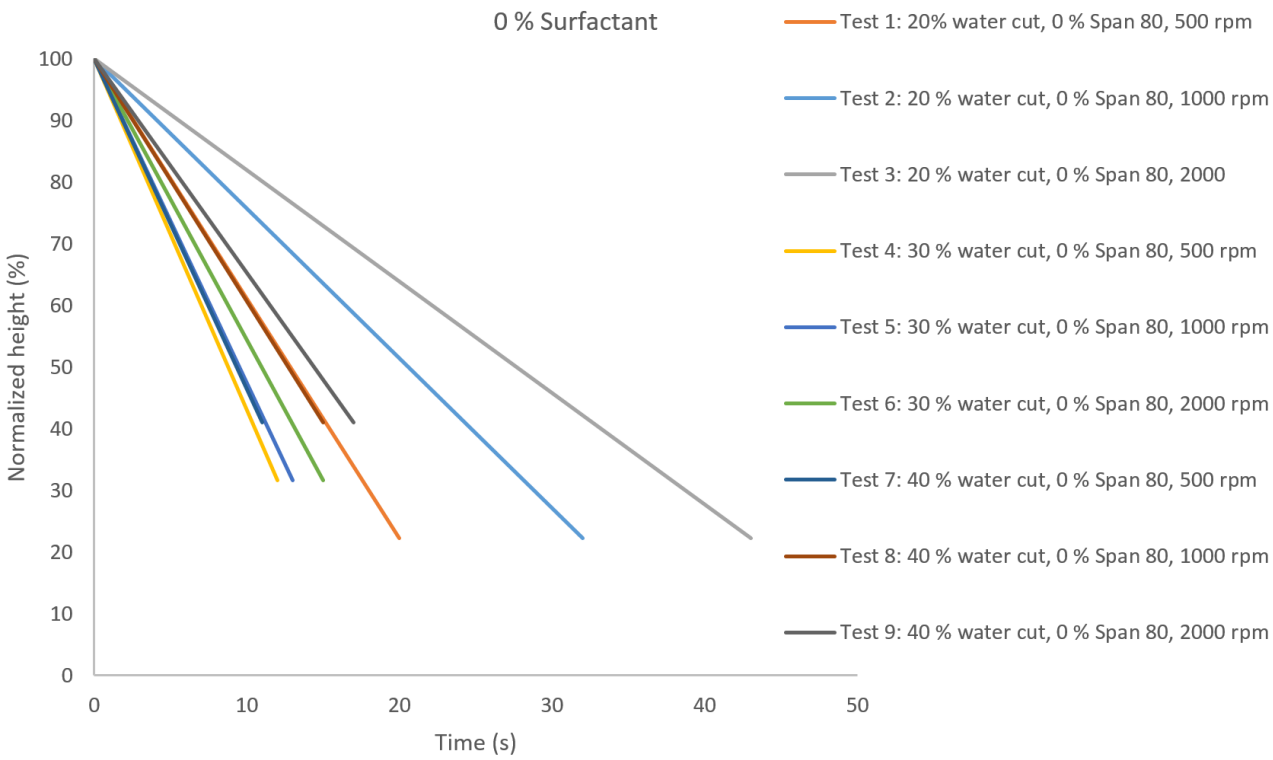

Figure 4.4: Plot of settling vs. time for samples without any surfactants

If the test cases are divided in three groups based on the water cut, one observe that the rotational speed has a significant impact on the separation rate. The effect of the velocity can be observed for all the cases, but is especially easy to observe for the cases with 20 % water cut. This correspond to the theory in section 2.5, where sufficient agitation was set to be a requirement for an emulsion. From these settling curves, the three cases with 20 % water has the longest separation time, while the cases with 30 % and 40 % water cuts separates faster. The six cases with the highest water cut, gives quite similar results. It seems like the cases with 30 % water cut separates the fastest, but there are some uncertainties in the measurements. This is due to the rapid separation, which made it difficult to measure the separation time correct.

Further experiments were carried out with different concentration of Span 80. The result was that the fluid system did become significant more stable. For all the cases, a dispersion band was created, where the decay could be recorded. The rate of the decay was affected of both the rotational speed and the water cut. An interesting observation was that while the oil phase would separate within a few minutes, the water phase was

still occupied in the dispersion for a long time. Even with just a small droplet of Span 80, the water phase would use several hours to separate completely. This means that while the oil was separated out, all of the water was still remaining in the dispersion band. Hence, one effect of Span 80 was that the oil drops remaining in the dispersion band will hinder the water droplets of settling out.

Since this is oil-continuous cases, it was decided to only record the dispersion band while the oil was separated out. This was done by observing the sedimentation interface. The distance y was constant throughout the experiments. The decay of the sedimentation height is plotted against time. All the results are presented below. As can be sees, the separation time is considerably longer than when no Span 80 was added. The effect of Span 80 added to the model oil versus no Span 80 added is significant.

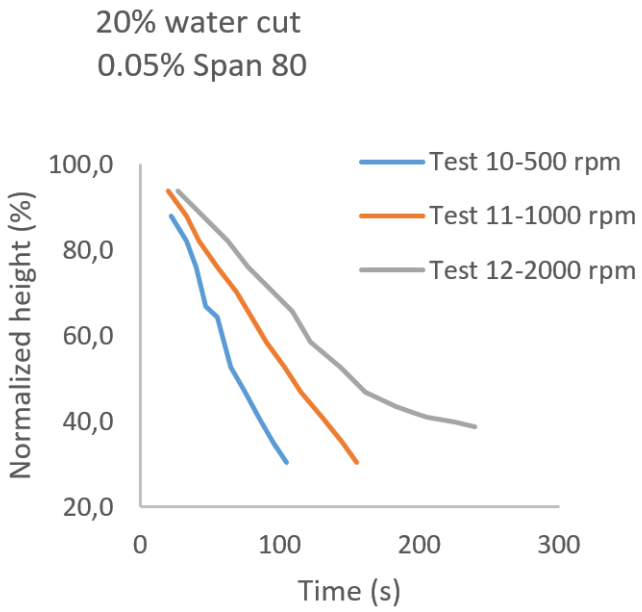

Figure 4.5: 20 % water cut and 0.05 % Span 80

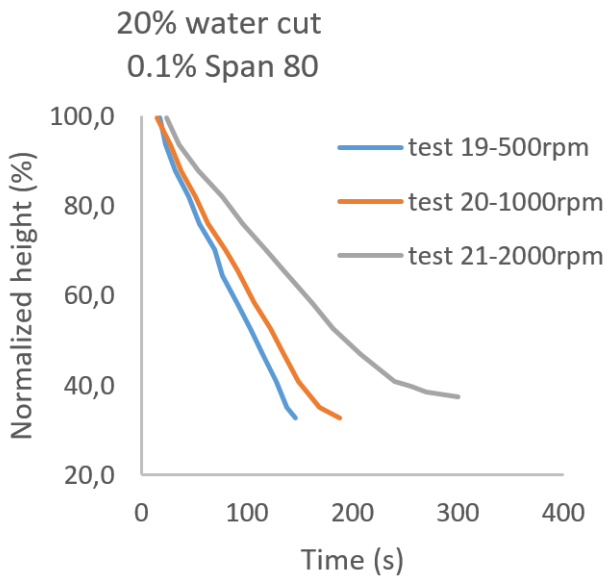

Figure 4.6: 20 % water cut and 0.1 % Span 80

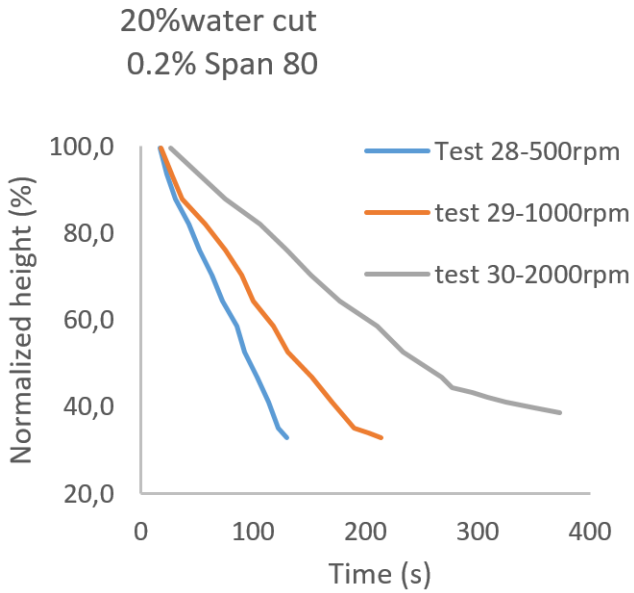

Figure 4.7: 20 % water cut and 0.2 % Span 80

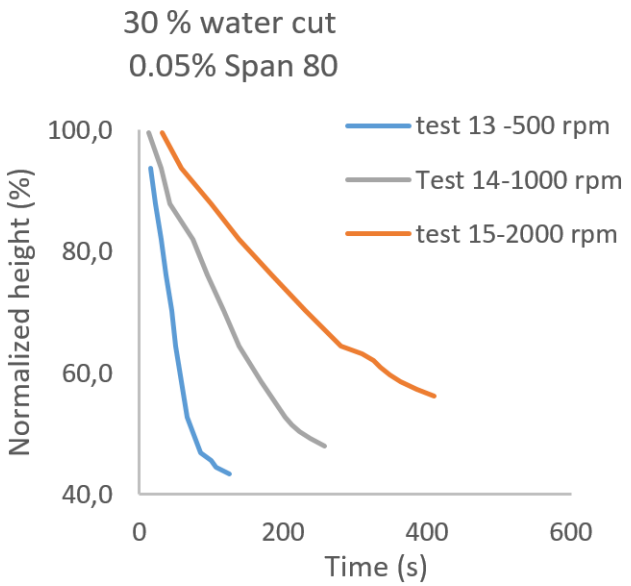

Figure 4.8: 30 % water cut and 0.05 % Span 80

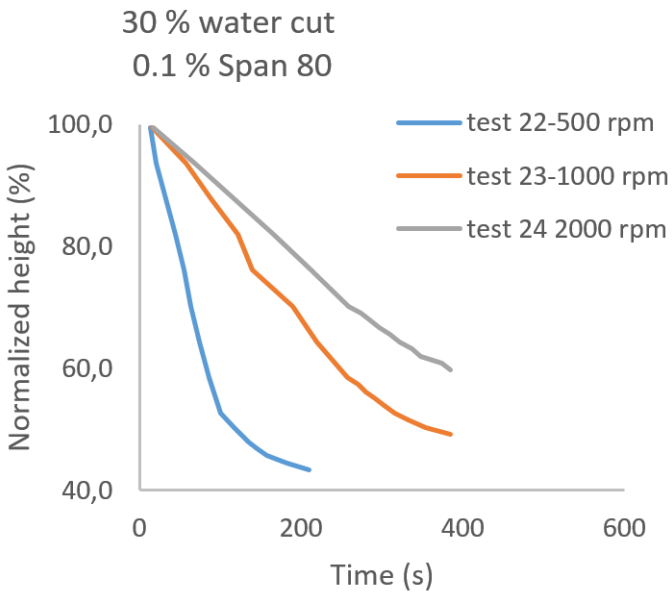

Figure 4.9: 30 % water cut and 0.1 % Span 80

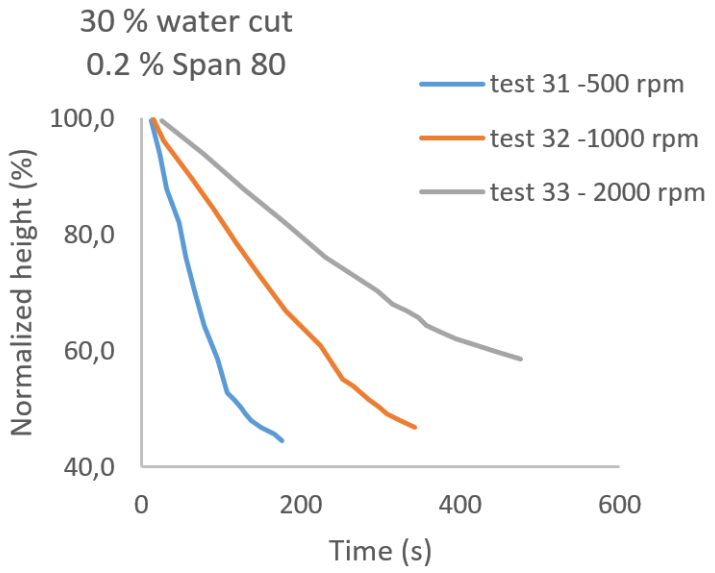

Figure 4.10: 30 % water cut and 0.2 % Span 80

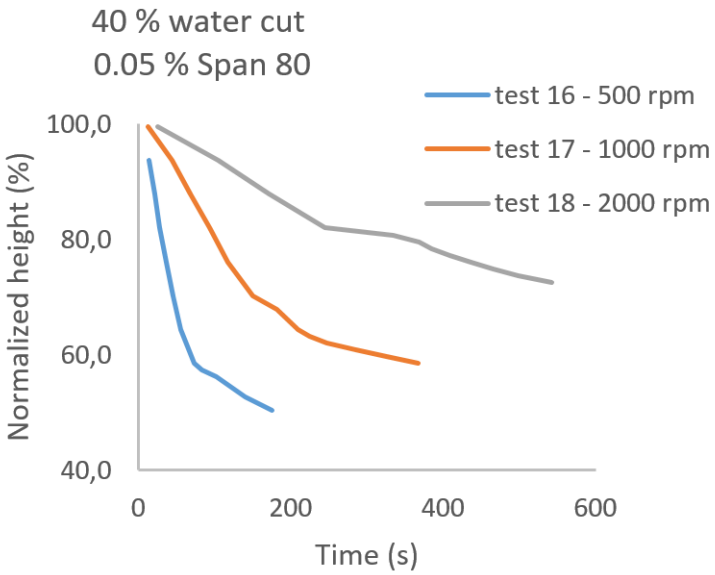

Figure 4.11: 40 % water cut and 0.05 % Span 80

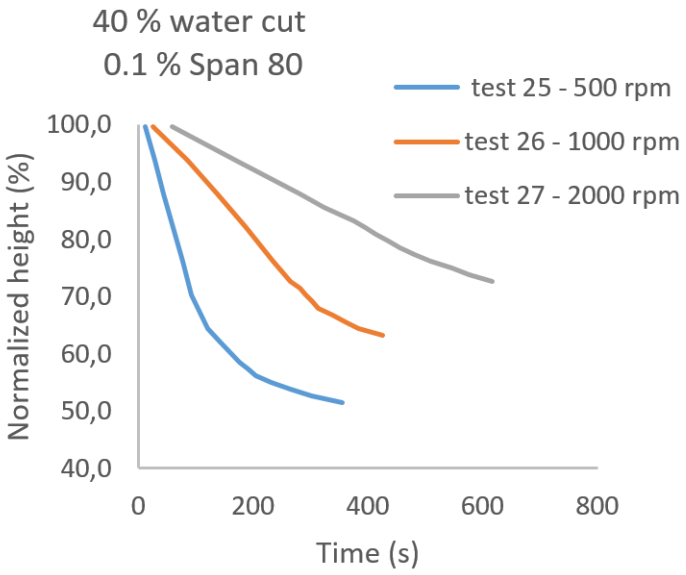

Figure 4.12: 40 % water cut and 0.1 % Span 80

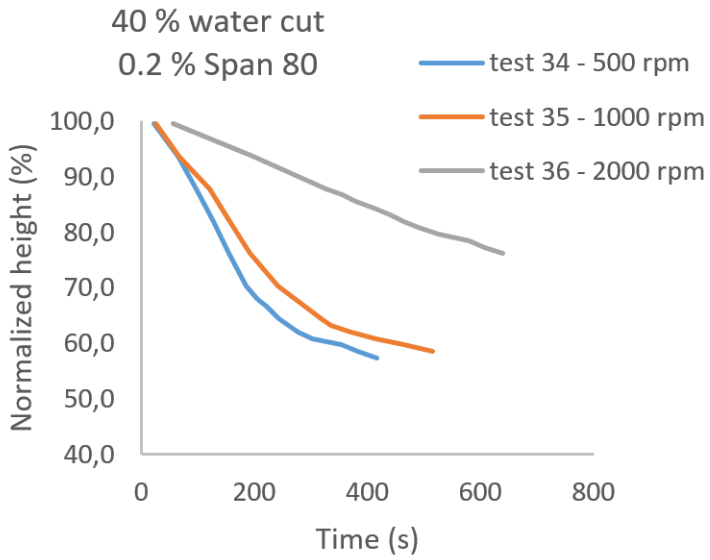

Figure 4.13: 40 % water cut and 0.2 % Span 80

The plotted curves from the settling tests shows an approximately exponential decay. The interfacial coalescence is more rapid than the sedimentation rate, hence no dense-packed layer is created [17]. One of the aims of these experiments is to find out what influences the stability of the dispersion layer the most. This is discussed in the following sections. A lot of the factors that may impact the stability is kept constant, such as the viscosity of the fluids, the density of the fluids, the water salinity and the age of the emulsion. Therefore, the factors investigated here is the effect of agitation, surfactant amount and water cut.

4.4.1 Effect of agitation

From the result curves, it is clear that agitation influences the separation considerably. The separation rate decreases with higher rotational speed. Agitation causes turbulence, which leads to droplet break up. A higher rotational speed result in smaller droplets in the mixture. By comparing the curves, one see that the agitation is more significant for the settling than the Span 80 concentration. This can indicate that for these cases, the droplet size is more important for the stability than the amount of surfactants. The theory discussed in section 2.5 about agitation determining the stability [30] correspond to this result.

To illustrate the effect of the agitation, a simplification is made. By assuming an linear decay of the dispersion height, the separation rate becomes constant. Figure 4.14, 4.15 and 4.16 shows the changes in separation rate for different rotational speeds. All the separation rates are given in cm/s.

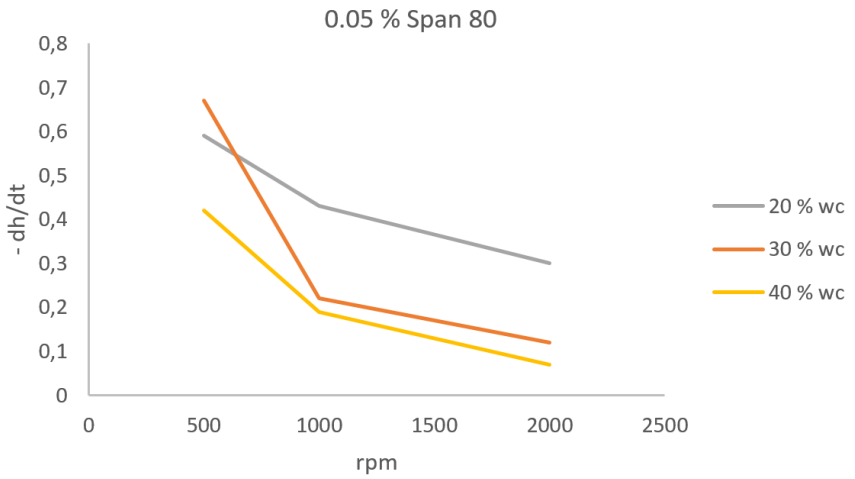

Figure 4.14: Separation rate for different rpm with Span 80 concentration 0.05%

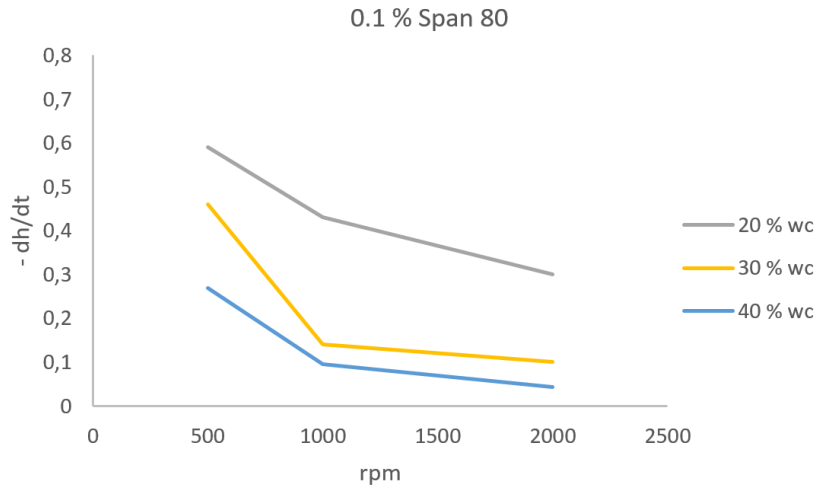

Figure 4.15: Separation rate for different rpm with Span 80 concentration 0.1%

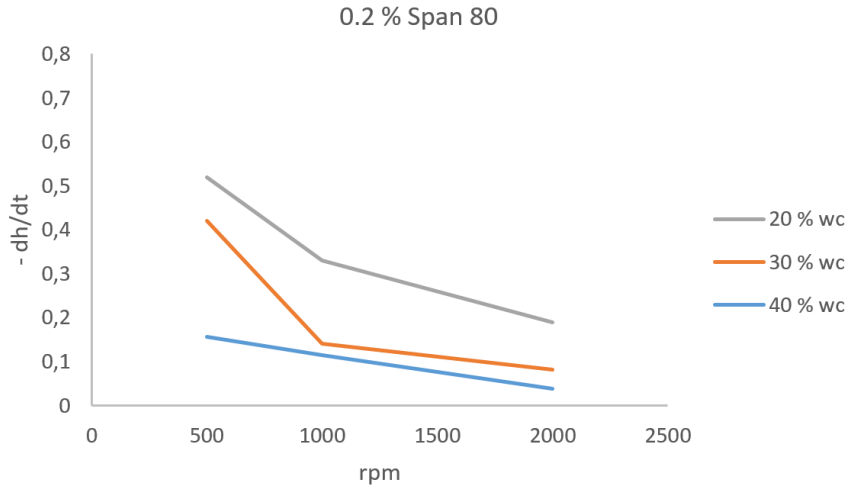

Figure 4.16: Separation rate for different rpm with Span 80 concentration 0.2%

As can be seen, there is a more significant change between 500-1000 rpm than between 1000-2000 rpm. This indicate that after a certain point of agitation, when the fluids are completely homogenized, the effect of increased turbulence is less noticeable. One also observe from these curves that there is a clear effect of water cut. This will be discussed further in the following section.

4.4.2 Effect of water cut

When observing the settling curves, the effect of water cut is obvious. All the cases, except one, provide the same result, the separation rate decreases with higher water cut. The only exception is the case with 500 rpm, 0.05 % Span 80 and 30 % water cut. A higher separation rate for a lower water cut is consistent with the theory of settling. When water drops are falling down, oil must come up. More water in the mixture, means more barriers for the oil, which slows down the settling of the drops. The separation

rate of the oil will therefore decrease. Figure 4.17, 4.18 and 4.19 illustrates the changes in separation rate for different water cuts. From the figure, one can observe that the effect of water cut decreases when the rotational speed increases. This indicates that the effect of turbulence dominates the stability of the emulsion when the agitation is over a certain level.

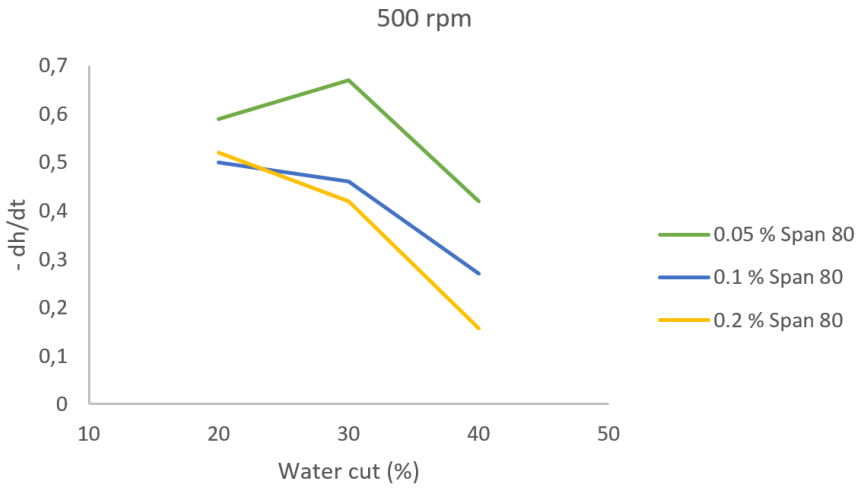

Figure 4.17: Separation rate for different water cuts with 500 rpm

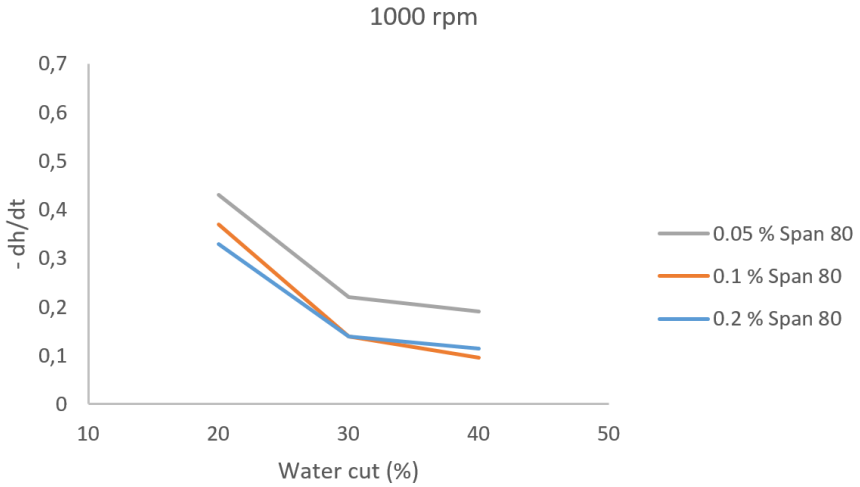

Figure 4.18: Separation rate for different water cuts with 1000 rpm

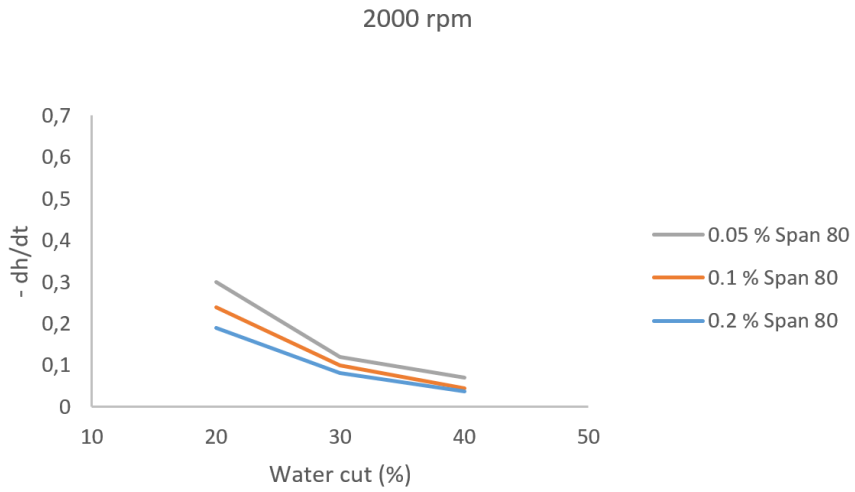

Figure 4.19: Separation rate for different water cuts with 2000 rpm

4.4.3 Effect of surfactant

The effect of surfactant is also evaluated. Arnold and Steward [30] stated that the agitation and the degree of emulsifying agents (surfactants) determines the degree of stability. A high degree of surface-active chemicals will prevent the droplets from coalescing, and slow down the separation. The results from these tests shows that when the turbulence is high, the effect of surfactant is small. The impact of agitation is much more significant. However, when compared to the tests without any surfactants, it is clear that some Span 80 is necessary to form an emulsion. This indicates that adding surfactants will make the fluids more stable, but at a certain amount of Span 80 further increase will not affect the stability. The reason for this may be that with the smallest concentration tested here (0.05 %), the droplet surface is fully covered with Span 80. Increasing in the concentration will then not affect the droplets ability to coalesce. Figure 4.20, 4.21 and 4.22 shows the changes in separation rate for Span 80 concentration. These curves shows that the changes in Span 80 concentration influences the separation rate less than the rotational speed, especially when the turbulence is high.

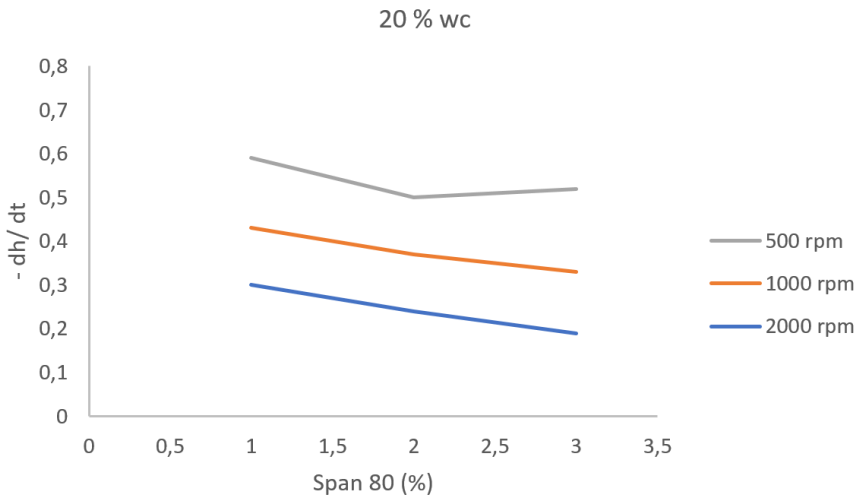

Figure 4.20: Separation rate for different Span 80 concentration with 20% water cut

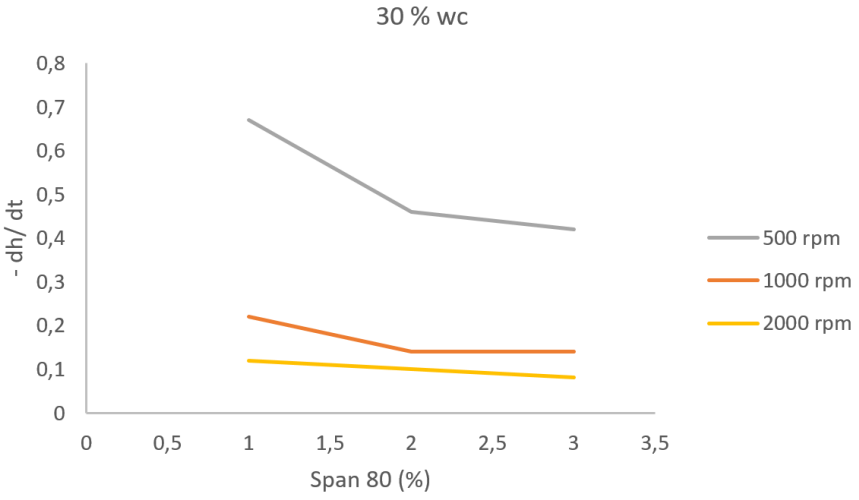

Figure 4.21: Separation rate for different Span 80 concentration with 30% water cut

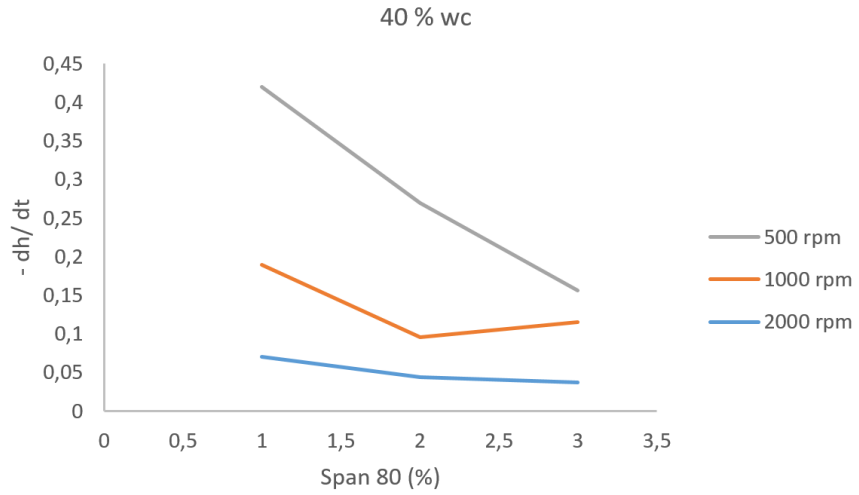

Figure 4.22: Separation rate for different Span 80 concentration with 40% water cut

4.5 Transfer from batch to continuous settling

Continuous test settlers are considered to be more representative than batch experiments. Continuous settler experiments are often performed after batch experiment, as a final step in the testing. Continuous setting tests with the same fluid system as the batch tests will be carried out in this thesis. It is necessary to transfer the information from the batch setup to the continuous test rig.

From the results, it may look like the degree of turbulence affects the separation rate the most. Turbulence is dependent on the rotational speed and how much energy that is added to the fluids by the mixer. This energy is calculated from the simulation results in chapter 3. By multiplying the tangential moment $[Nm]$ with the rotational velocity ω, the power is determined. The power divided by the batch volume, yields the watt per kg, shown in equation 4.1

$$P = \varepsilon = \frac{power}{volume}\,[\frac{W}{kg}] \tag{4.1}$$

Since all the energy into the batch is lost, the dissipation is set equal to the energy added to the mixture.

Table 4.2 shows the energy dissipation for the three rotational speeds.

Rotation [rpm]	ε *[W/kg]*
500	1.05
1000	8.69
2000	69.05

Table 4.2: Energy dissipation rates

In oil-production systems, there will be valves upstream the settler. All valves have in common that fluid flow is forced through a restriction where energy is dissipated and a pressure drop occurs [32]. The pressure drop determines the initial drop size distribution, as explained in section 2.3. Therefore the pressure drop across the valve upstream a continuous settler must be determined before testing. In order to relate the batch data with a continuous settler, a relationship between the pressure drop in the choke valve and the and the energy dissipation rate from the mixer can be found.

Chapter 2.3.3 discusses the energy dissipation rate through a valve. From this theory, equation 4.2 can be expressed. This equation is one way of connecting the batch setup with the continuous test rig.

$$\Delta P \cdot Q = \varepsilon \cdot \rho_{tot} \cdot V \tag{4.2}$$

Here ΔP is the pressure drop through the valve, Q is the volume flow rate in the inlet and ϵ is the energy dissipation. In stead of using the energy dissipation through the valve, the energy dissipation from the batch mixing will be used. ρ_c is the total density of the fluids and V is the volume of the zone of intense turbulence. According to Van der Zande [33], L is equal to $2.5 \cdot D_p$, where D_p is the pipe diameter. In this case, the diameter is 2 inches and the volume then becomes $2.57 \cdot 10^{-5} mm^2$. The total density is found by equation 4.3.

$$\rho_{tot} = \frac{\rho_{oil} \cdot Q_{oil} + \rho w \cdot Q_w}{Q_{tot}} \tag{4.3}$$

By inserting the energy dissipation rate for the mixer, the total density of the fluid and the volume in equation 4.2, one obtain a connection between the batch test and the continuous test rig. The parameters on the left side can then be varied to archive a desired result.

4.6 Separation models

Different ways of predicting the steady state dispersion height from batch settling tests is discussed in section 2.4.1. The idea behind the different models is that based on the decay of the dispersion layer, one can predict the steady state dispersion height in a continuous settler. In the following section, Hartland and Polderman's separation models will be used to transfer the batch data to a flowing rig. By doing this, a validation of the separation model is also done. Both the models assumed the viscosity to be the only variable affecting the relationship between the dispersion height and the flux. Other authors have later come up with new models, which take additional factor into consideration.

The results from these batch tests shows an exponential decay of the dispersion layer. This means that the sedimentation rate is slower than the interfacial coalescence rate. Hence, each droplet has coalesced with the homogeneous interface before the next droplet arrives, and no dense-packed layer is created. For an exponential decay, Hartland and Polderman's models are identical. This is shown by rearranging Hartland's equation 2.23 for a continuous settler, with $a = 1/k_1$ and $b = 1/k_2$.

$$\frac{Q}{A} = \frac{H_d}{\frac{1}{k_{c1}} + \frac{H_d}{k_{c2}}}$$

In section 2.4.3, a and b was defined as functions of viscosity. Hence, k_{c1} and k_{c2} can be expresses as in equations 4.4 and 4.5.

$$\frac{1}{k_{c1}} = k\mu^l \tag{4.4}$$

$$\frac{1}{k_{c2}} = m\mu^n \tag{4.5}$$

k_{c1} and k_{c2} are constants for the continuous system. In order to find these, the constants k_{b1} and k_{b2} for the batch system need to be determined. The relationship between the batch constants and the continuous system constants are given in equation 4.6 and 4.7.

$$k_{c1} = k_{b1}\frac{\bar{\bar{\epsilon}}}{\epsilon_F} \tag{4.6}$$

$$k_{c2} = k_{b2}\frac{\bar{\bar{\epsilon}}}{\epsilon_F} \tag{4.7}$$

Where ϵ_F is the hold-up in the feed dispersion, and $\bar{\bar{\epsilon}}$ is the average dispersed phase hold up fraction. $\bar{\epsilon}$ is given by y/h, and $\bar{\bar{\epsilon}}$ is the average throughout the settling. Since these bath tests only gave a separation of the oil phase, y is constant. The formula for $\bar{\epsilon}$ can therefore not be used. By assuming that none of the water has been separated, the average dispersion phase hold up can still be calculated. This is done by diving the volume of water with the remaining dispersion volume. This means that the average phase hold up of water increases as oil is separated out of the dispersion. ϵ_F is the original water cut in the batch sample.

For a dispersion layer only consisting of a sedimentation zone, a rule is that $\bar{\bar{\epsilon}} < 0.75$ [17]. This yields the average phase up of water and feed hold up in table 4.3.

Water cut [%]	ϵ_F	$\bar{\bar{\epsilon}}$
20	0.2	0.48
30	0.3	0.53
40	0.4	0.58

Table 4.3: Feed hold up and average hold up of water in dispersion

How to find k_{b1} and k_{b2} is given in section 2.4.2, and this is shown and discussed in the following section.

4.6.1 Calculation of batch constants

The batch results were plotted according to Hartland and Polderman's approach. When plotting $1/(-dh/dt)$ with respect to $1/h$, this is supposed to yields a straight line with slope $1/k_{1b}$ and intercept $1/k_{2b}$.

Figure 4.23 show the result for test 13, while the rest of the plots are given in Appendix A. As can be seen, they are not providing a straight line. However, the tendency of a line is obtained by using the least square method. It appears like the plotted points differs more and more from this linear line as h decreases. Polderman and Hartland's models only takes the viscosity into account when finding a relation between flux and dispersion height. The results of these tests indicates that their models may not be fully valid, especially not for low dispersion heights. As h decreases, factors in addition to the viscosity may affect the separation significant.

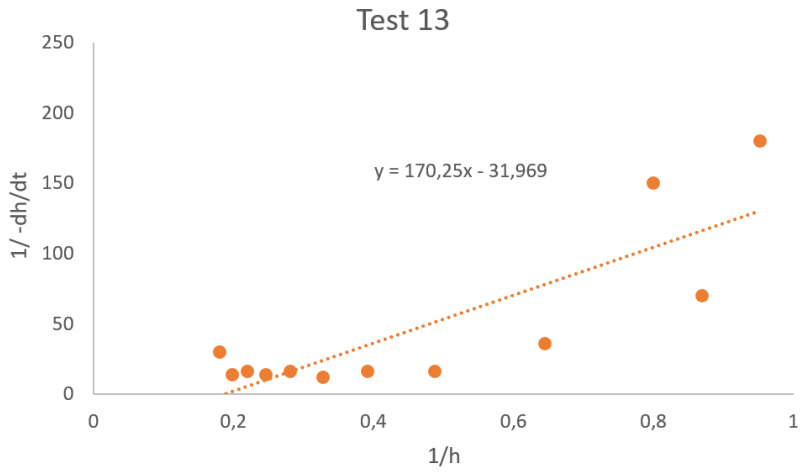

Figure 4.23: $1/(-dh/dt)$ plotted against 1/h for test 13

From these plots one observe that some tests provide better results than others. Some of the plots matches a linear fit well, while others differs a lot. It looks like the tests

provide better results in the beginning, when the dispersion height h is high. One must also take into account the uncertainties when measuring the dispersion height.

Validation of batch constants

The linear fit was found by using the least square method, and thus represent some uncertainties. A validation of the obtained k_b values has been done. This were done using the constants and calculating backward to obtain the settling curves these constant gives. These curves are compared to the measured settling curves, and an indication of how accurate the obtained constants are. The test of the result is given in Appendix B. As can be seen, the calculated settling decay is fairly close to the experimental decay. Settling time was considered the most important factor when validating the constants. As long as the settling time is correct, the constants is regarded acceptable. This applies to all of the cases, except test 10, 20 and 23.

4.6.2 Correction of batch constants

Although the validation of the batch constants gave reasonably results, the separation model shows weaknesses. It seems like low values of $1/h$ fits well with a linear fit, while high values of $1/h$ differs from the fit. High values of $1/h$, means low dispersion heights. One can suspect the uncertainties in the measuring to affect this result, since it is difficult to measure the exact dispersion height. However, if this was the source of the error, the plotted points are expected to be more randomly placed. It is reason to believe there are physical reasons for the points to differ from the linear fit.

One reason for what happens can be that the fluid concentration is changing. The measurement is based on the sedimentation interface, but what happens in the dispersion band below this interface is unknown. What is believed to be the main reason for this behavior with low dispersion heights, is that the remaining dispersion consist of the hardest drops to separate. This can be because the smallest droplets are left in the dispersion, or due to accumulation of Span 80.

The result indicates that Polderman's model is not valid for thin dispersion layers. This is not a problem for a steady state separator, where the fluids flow through the vessel and the dispersion band is constant. This problem regarding Polderman's model is therefore special for a batch case. As a correction, the low dispersion heights are removed from the plots. Since Polderman's model does not need to take low dispersion heights into account for a continuous settler, this correction is justified.

The values kept are the ones that seems to provide a linear fit, roughly the ones where $1/h$ is below 0.5. This yields a new linear fit, with positive k values (except case 18). Hence, all the calculated fluxes are now positive. The results of this correction is given in Appendix C, but to illustrate the effect of the correction, figure 4.24 show the result for test 13.

Even with the correction, one see that the plotted points not always yields a good

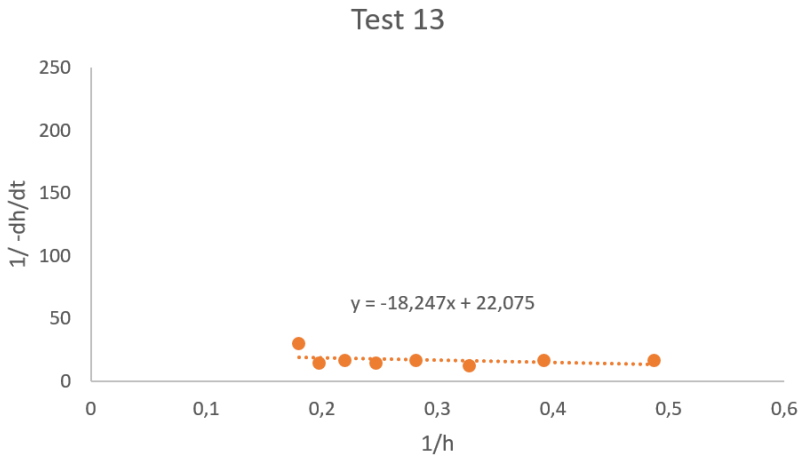

Figure 4.24: Plotting of batch constants with correction

linear fit. However, the k values are positive, and will therefore be used. When k_{b1} and k_{b2} are determined, k_{c1} and k_{c2} can be calculated using equations 4.6 and 4.7 together with table 4.3. In the next section, these constants will be used to calculate the allowable flux according to Polderman's model.

4.6.3 Calculation of allowable flux according to Polderman's model

Polderman's model for calculating the allowable flux is applicable for a dispersion height H_d of 0.4 m. Inserting this height into equation 4.8 together with the calculated constants yields the fluxes.

$$\frac{Q}{A} = \frac{H_d}{\frac{1}{kc1} + \frac{1}{k_{c2}} H_d} \tag{4.8}$$

This flux will show where in figure 2.9 a system with this model oil is compared to the crude oil systems Polderman used. For Exxsol D60, the viscosity is 1.68 [cS]. The result is shown in figure 4.25.

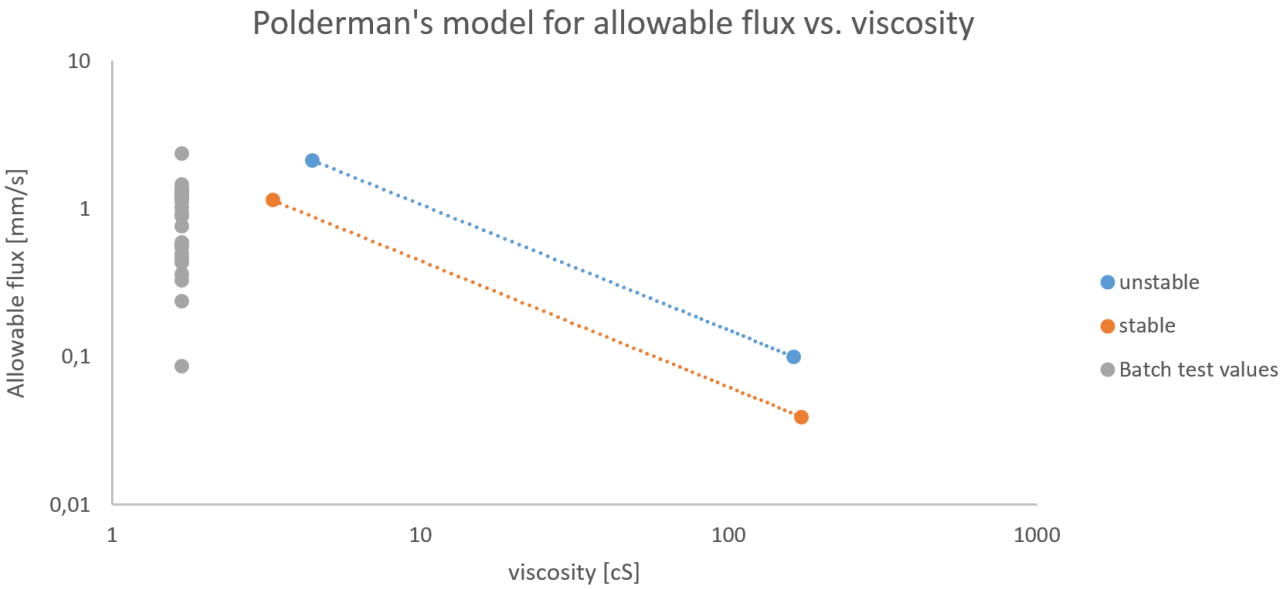

Figure 4.25: Allowable flux according to Polderman's model in a continuous settler based on batch test results and correction

As can be seen, the plotted values are mainly located below the line for stable emulsions, and the location varies considerably. The goal for this thesis is to simulate crude oil behavior using model oil. By drawing lines from the plotted fluxes to the line for unstable emulsions, one find the corresponding crude oil viscosities. The viscosities interesting to simulate are the ones between 3-20 cS. Crude oil with higher viscosity than this is difficult to separate. Figure 4.26 illustrate this area. As can be seen, several of the plotted fluxes are located in this ares. This indicates that batch test with the tested fluid systems are able to simulate crude oils in the interesting viscosity range.

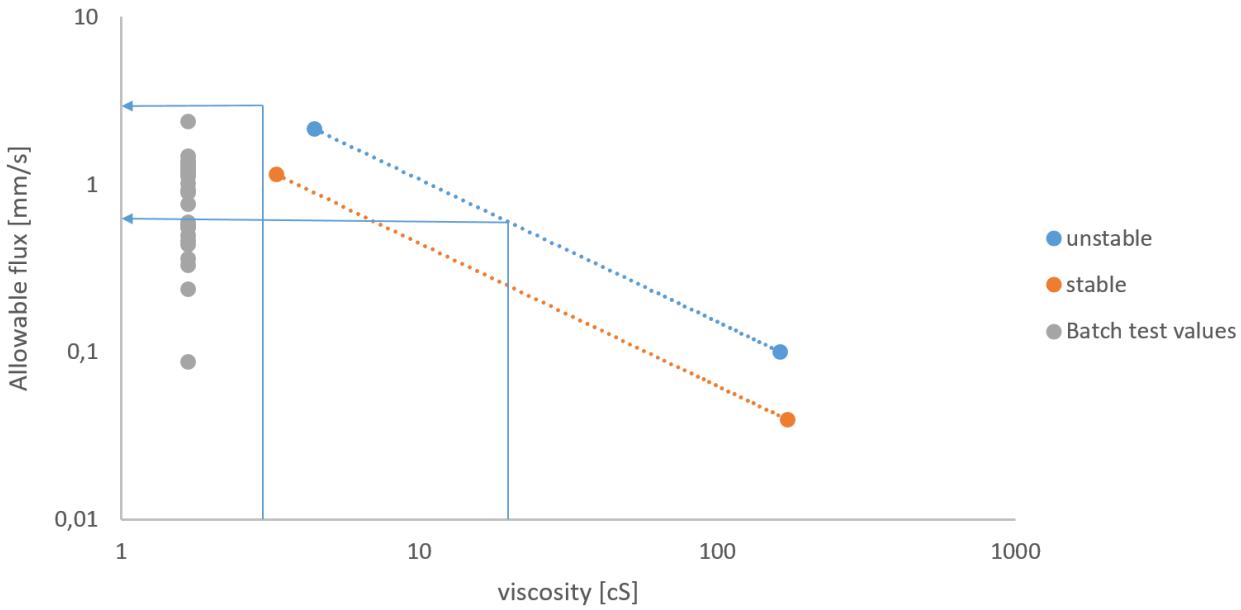

Figure 4.26: Allowable flux according to Polderman's model showing the viscosity area interesting to simulate for crude oils

Flux plotted against rotation and Span 80 concentration

In order to see the effect the amount of surfactant and the rotation have on the allowable flux, concentration of Span 80 and rpm are plotted against flux. This is given in figure 4.27 and 4.28.

From these plots one observe that there are small changes for Span concentrations from 0.1 % - 0.2 % for all rotations. It is therefore difficult to say anything about the effect of Span 80 here. The difference in flux is higher from 0.05 % - 0.1 % concentrations. While the change in flux is relatively small for all Span 80 concentrations, one observe an increased change from 0.05 % - 0.1 % for a low speed and a high water concentration (500 rpm, 40 % wc).

Span 80 will work as an emulsifying agent when added to the model oil and water. It forms a coating on the droplets, which hinders them from coalescing into larger droplets when they collide. The total surface to cover will increase with increased water cut and mixing. An increased water cut means more droplets to cover. Increased mixing will break up droplets into smaller droplets, which gives a larger total surface to cover.

Different rotations show a more distinct change in flux values. For most of the cases, an increase in speed means a lower allowable flux to obtain the desired dispersion height. When the rotation increases, the result is smaller droplets due to break up, which take longer to coalescence. The dispersion is then more stable, and the flux needs to be decreased in order to obtain the desired dispersion height. The observation that higher rotations yields lower fluxes corresponds to theory, and is expected. However, it contradicts with Polderman's model, which state that only viscosity affects the separation.

With high rotation and water cut, the Span 80 concentration should influence the stability more than for lower rotations and water cut. This is because the total surface to cover is increased. One expected therefore that an increase in Span 80 concentration for high water cut and high rotation would give a more stable dispersion, and therefore a lower flux. For these results, the different concentrations only gives minor changes. This may be because too much Span 80 is added. If the concentration is high, the surfactant will continue to cover all droplets even with high rotation and water cut.

In these tests, Span 80 concentration is with respect to total volume. But Span 80 dissolves in oil, which mean that the concentration increases in oil with increasing water cut. 0.05 % Span 80 with respect to total volume is 0.2 mL. When calculating Span 80 with respect to oil, this gives variation of 0.04 mL from 20 % wc to 40 %. This means that it is difficult to evaluate the effect of Span 80 concentration when the effect also varies with water cut. In retrospect, one can therefore argue that Span 80 concentration should be with respect to oil volume.

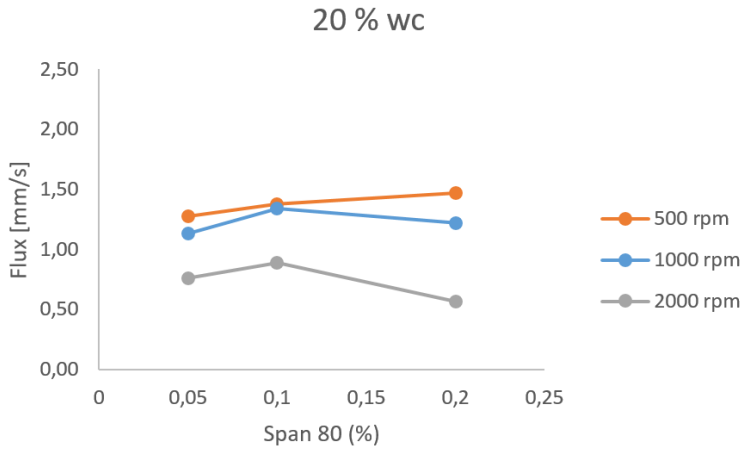

(a) 20 % water cut

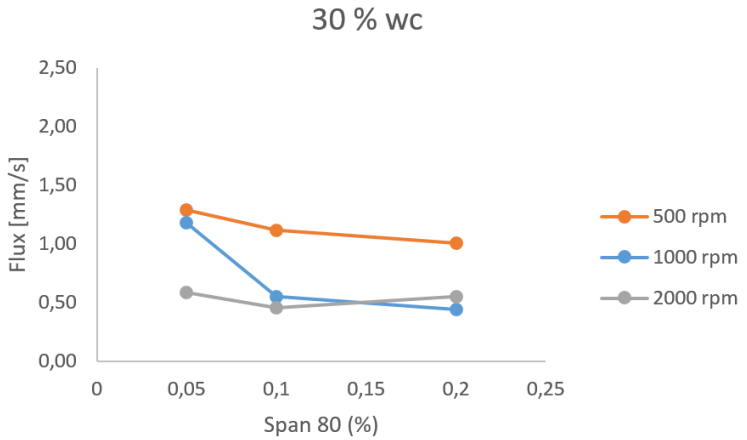

(b) 30 % water cut

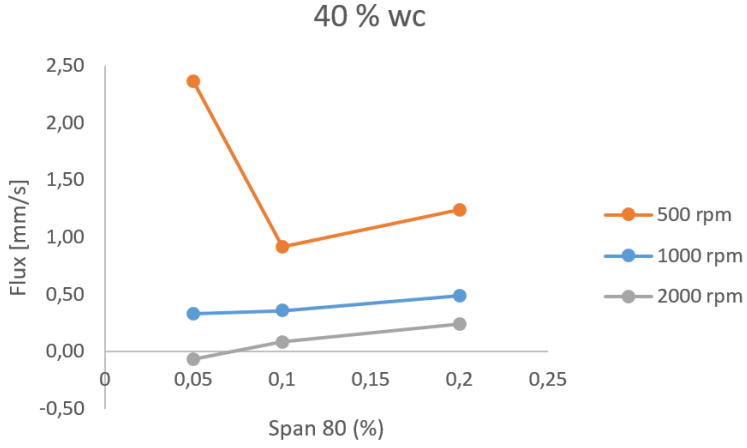

(c) 40 % water cut

Figure 4.27: Allowable flux plotted against Span 80 concentrations for different water cuts

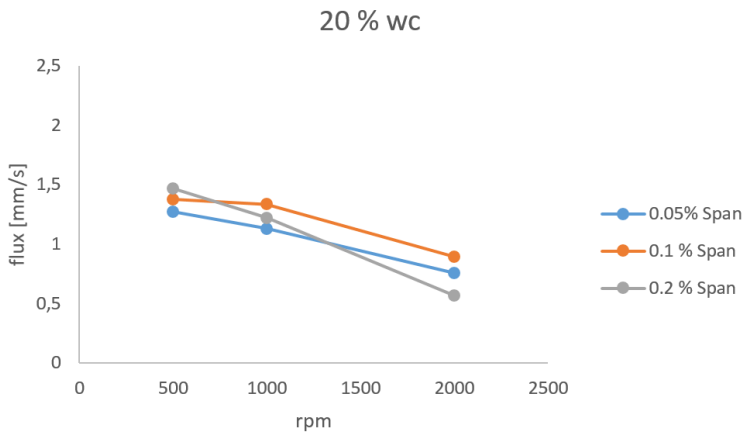

(a) 20 % water cut

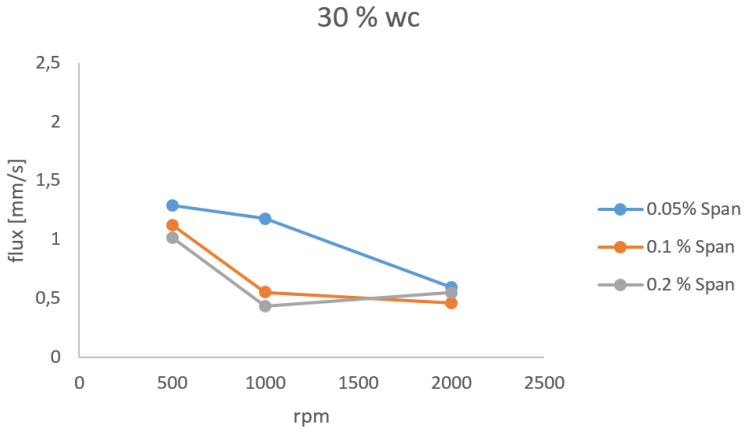

(b) 30 % water cut

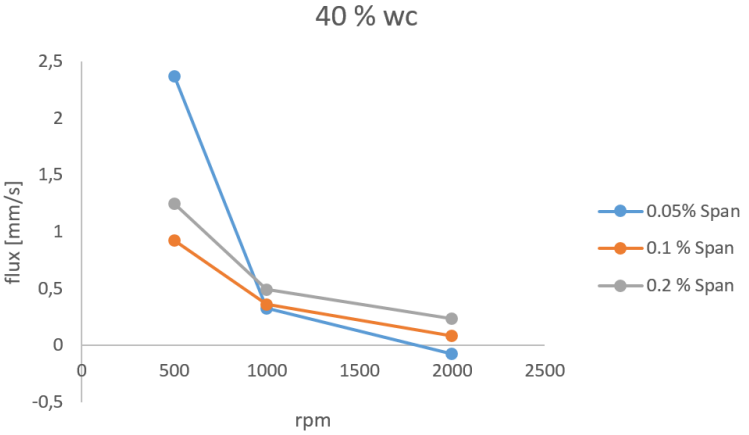

(c) 40 % water cut

Figure 4.28: Allowable flux plotted against rpm for different water cuts

4.7 Summary

In this chapter batch tests were carried out with model oil, salt water and different concentrations of Span 80. The goal was to investigate if model oil can be used to simulate crude oil. Span 80 is a surfactant with surface active behavior. The purpose was to decrease the droplets ability to coalescence with each other, and see if Span 80 can be used as a stabilizer for model oil. Investigation of how different factors affect the stability was also done.

When comparing the separation of the fluids for the cases with and without Span 80, it is clear that the present of Span 80 affects the stability significant. Model oil and water is separating instantly, while fluid systems with Span 80 is much more stable.

The factors tested was agitation, surfactant amount and water cut. Agitation proved to have the greatest effect on the stability. While the effect of Span compared to no Span is significant, the effect of the tested concentrations is small. This may be because the concentration of Span 80 is too high. If all the water droplets are covered in surfactant, an increase will not affect the stability further.

By using Polderman's model, the batch data was connected to a flowing system. For a steady state dispersion height of 0.4 m, the separation model gave different allowable fluxes. The tested concentrations of Span 80 provided small changes in flux values. An increase in rotation resulted in lower available fluxes. This contradict with Polderman's model, which only account for the effect of viscosity.

The crude oil viscosities that is interesting to simulate is between 3-20 cS. The result provided fluxes in this area, which means that batch testing showed very promising result regarding simulating crude oil behavior using model oil.

Chapter 5

Experimental study - Continuous settling experiment

In chapter 4, Span 80 was tested as stabilizer for model oil and water with good results. In this chapter, flowing settling tests have been carried out. The purpose is to see if these tests provides the same stability result as the batch tests.

Polderman's model is used to transfer the batch data to the continuous separator setup. The allowable flux is calculated based on a specific steady state dispersion height. When testing for the different fluxes, this is the dispersion height to expect. Validation of the separation model is then done.

This chapter presents the test rig, setup and test matrix. In addition, the result will be presented and validation of Polderman's models will be discussed.

5.1 Test Rig

The continuous test separator is installed at Cameron's laboratory. The test facility has one high pressure gas rig, and one liquid rig which operates at atmospheric pressure. For these experiments, the test separator will be combined with the liquid rig. The special geometry of the test separator makes the rig more flexible and gives a higher liquid capacity [28].

5.1.1 Test separator

The test separator is designed to emulate a large horizontal gravity separator in the small test flow loop available. It is designed with rectangular shape and open top. One advantage with the rectangular shape is that the cross section area is constant. This means the cross section area is independent of the liquid level in the tank. A thin rectangular tank will also provide a thicker dispersion layer than a cylindrical separator with the same volume. This separator can reproduce a lager scale separator at smaller fluid volumes and lower flow rates. The shape of the separator, and the fact that the sides are made of acrylic glass, makes it possible to observe the separation process. A detailed description can be found in Sørbø[28]. Figure 5.1 shows a picture of the test separator, located on top of the feed separator.

Figure 5.1: Overview of the rectangular test separator on top of the grey feed separator [28]

Assuming the phase velocities are equal, investigation shows that the expected separation performance and flow characteristics are similar to a cylindrical vessel with equal length, NIL and NLL [28].

Oil and water enters the inlet nozzle at high momentum. A perforated plate is installed close to the inlet to redistribute the dispersion and water phase. At the exit, a weir plate is placed to divide the phases.

The separator dimensions are given in table 5.1

Parameters	*Dimensions [m]*
Length	5.0
Height	1.25
Width	0.2
Weir	0.5

Table 5.1: Test separator dimensions

The design of the test separator is based on a cylindrical 3-phase separator. The NLL (normal liquid level) and NIL (normal interface level) levels are determined based on this reference separator, where typically values of NLL and NIL are 60% and 40% of the diameter. The interfacial heights used in the test separator are given in table 5.2. These levels will be controlled during the tests [28].

Level setting in test unit	Height [m]
NLL	0.75
NIL	0.30

Table 5.2: Interfacial heights

5.1.2 Instrumentation

The choice and location of instruments is important. In order to validate the results and the separation model, the information from the experiments needs to be reliable. The dispersion height will be measured at four locations along the flow direction. Table 5.3 shows the different measurement locations. The dispersion height calculated with Polderman's model is based on the height just before the weir, which is represented by Z_4.

Measurement	*Location [mm]*
Z_1	920
Z_2	2270
Z_3	3580
Z_4	4570

Table 5.3: Location of dispersion height measurement

To make sure that the NIL and NLL levels remains constant the valve openings will be adjusted by differential pressure transmitters.

The total flow rate is measured by a Coriolis flow meter. An electromagnetic flow meter will be used to determine the water flow rate. The oil flow rate can then be found by subtracting the water flow rate from the total flow rate.

5.1.3 Inlet system

The pressure drop across the shear valve influence the drop size distribution. A manually controlled gate valve will be used to create the dispersion. Measurement of the pressure drop will be done with a differential pressure transmitter, and correct measurement is necessary in order to determine the drop size distribution. The pipe taps are placed 2.5 pipe diameters upstream and 8 pipe diameter downstream the valve, which is by theory the place of maximum pressure recovery. This placement is important in order to measure the correct pressure loss.

5.1.4 Feed separator

The feed separator is a cylindrical vessel with diameter 0.98 m. Its purpose is to fully separate the incoming water and oil from the test separator. The feed separator operates the same way as the test separator, where the fluids are separated by gravity, and the phases are divided by a weir. It is important that the feed separator separates the fluids completely in order to achieve reliable information from the test separator. Using sufficient water volume in the feed separator, one ensures the oil to flow over the weir.

The water level needs to be lower than the weir to avoid carry over of water into the oil pump.

5.2 Test matrix

The aim of this chapter is to test the same fluid system as in the batch tests, and see if one obtain the same settling result. If we do, this indicates that batch tests can be used to test separation in fluid systems.

Test 13, with 30 % water cut, 0.05 % Span 80 and 500 rpm is chosen as base for the continuous experiments. This case yields an allowable flux of 1.4 mm/s, which is regarded reasonable for the test rig. This flux is also in the interesting viscosity range based on Polderman's model, shown Figure 4.26. The total flow rate, Q is then calculated by equation 5.1.

$$Q = q \cdot A \tag{5.1}$$

Here Q is given in m^3/h, q is the flux in m/h and A is the intersection area in m. The result is Q = 5.0 m^3/h. This value yields different flow rates for the oil and water phase, depending on the water cut.

All the cases will be carried out with this total flow rate, while the pressure drop across the choke valve and the water cut will be varied. This flux is found from Polderman's model, and is therefore based on a dispersion height of 0.4 m. If the model if fully valid this is the dispersion height to expect. When the water cut is varied, the dispersion height is expected to change.

The pressure drop across the choke valve will be varied. This is since it determines the initial drop size distribution. In chapter 4, equation 4.2 presented a relationship between the dissipation energy and the pressure drop. By using this equation together with the energy dissipation rate for 500 rpm and the total density for 30 % water cut, this yields $\Delta P = 0.045$ bar. The energy dissipation rate is given in table 4.2, and the total density is calculated with equation 4.3. ΔP is close to zero, which corresponds to Polderman's theory. His model assumes that the dispersion height is independent of the drop size distribution. The first pressure drop that will be tested is 0 bar. Pressure drops of 0.5 bar and 1.0 bar will also be tested. This gives the test matrix in table 5.4.

Water cut [%]	Q_{oil} $[m^3/h]$	Q_w $[m^3/h]$	ΔP_1 *[bar]*	ΔP_2 *[bar]*	ΔP_3 *[bar]*
20	4.0	1.0	0	0.5	1.0
30	3.5	1.5	0	0.5	1.0
40	3.0	2.0	0	0.5	1.0

Table 5.4: Test matrix for experiments in continuous settler rig

It is important to obtain a steady state situation in order for the tests to be valid. This is ensured by running the loop several times. When performing the tests, NIL and NLL should be at constant fixed values. During the experiments, the parameters in table 5.5 will be held constant. Each test will be done three time

Parameters	*Value*
Temperature	298 [K]
Pressure	1.0 [bara]
Viscosity	1.33 [cP]
ρ_{oil}	793 [kg/m^3]
ρ_{water}	998 [kg/m^3]

Table 5.5: Constant parameters for continuous settling experiment

5.3 Results

The test showed indications of too little oil in the system. This made it impossible to achieve the planned NIL and NLL levels. The solution was to decrease both levels until NLL was at the same height as the weir. The dispersion band should not be affected by this, so an assumption was made that this change can be done without consequences. When having NLL equal to weir, only one valve need to be continuously controlled to keep the liquid levels constant.

Before Span 80 was added, tests with just Exxsol D60 and salinity water were performed. Cameron's experience is that this results in an instant separation. The tests done provided the same result. No dispersion band was created, and the two phases separated instantly. In order to test separation with model oil, the oil needs to be stabilized to represent real crudes.

0.05 % Span 80 was added to the fluids. This had significant effect, and resulted in a stable emulsion. The goal was to create an emulsion similar to the batch test, where the separation was possible to observe. This emulsion proved to be too stable. The oil and water that were mixed, formed an emulsion that took hours to break. The emulsion was flowing though the system, not separating in the feed separator.

To investigate the stability, the throughput was stopped, and the test separator was used as a large batch test. The decay of the dispersion layer should now resemble the decay in chapter 4, but the phases were barely separating. As a test of how stable the emulsion was, the height was measured with a time interval of 10 minutes. The result was a dispersion height decrease of 12 mm. This is shown in figure 5.2.

(a) Dispersion layer at t=0

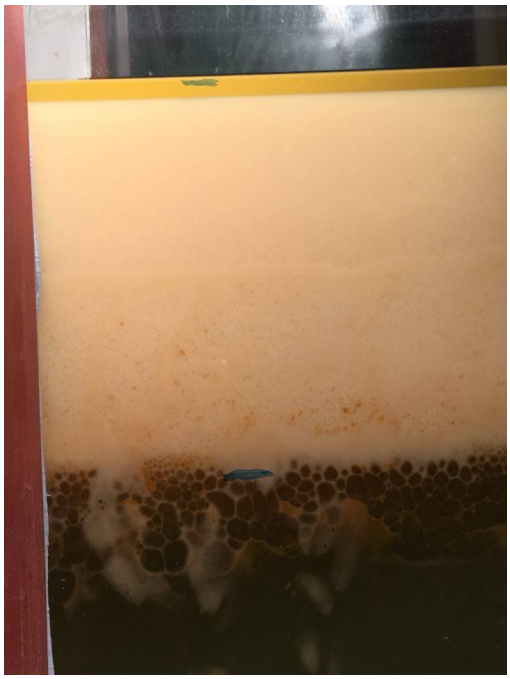

(b) Dispersion layer at t=10.

Figure 5.2: Decay of dispersion layer with $\Delta t = 10$ min

Large oil droplets were observed at the interface between the dispersion layer and the water phase. Figure 5.3 shows a close up of this interface. These droplets indicates that there are strong surface active agents present, which prevents the droplets from coalescing.

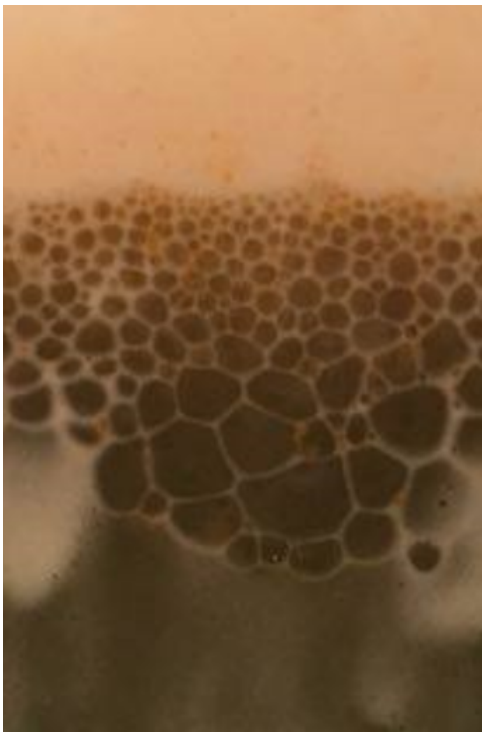

Figure 5.3: The coalescing interface, where water droplets are prevented from coalescing

The stable emulsion made further testing impossible. There are several factors that may have affected why these test behaved so differently from the batch tests. Before the testing started, there were a severe presence of microbes bacteria in the oil. A filtering process was performed for two weeks, which was time assuming, and also failed to remove all of the substance. The microbes clanged to the liquid interfaces and gathered together close to the weir. A bacteria killer (biocide) was added as an attempt to remove the microbes. This did not show any distinct effects. Both microbes and biocide was therefore occupied in the oil when testing. This makes it a different fluid system than the one testes with batch tests, which were clean.

The low volume of oil may also have affected the stability. When adding Span 80, it was impossible to achieve the desired water cut, even with the decreased liquid levels. Span 80 dissolves in oil, so if the volume of oil is lower than anticipated, the relationship between Span 80 and oil is different than for the batch tests. The lowest water cut possible to achieve now was 60 %. Long delivery time on new oil prevented further testing with more oil.

Other explanations for why the fluid system became more stable now than when batch testing is the obvious difference in mixing. The effect of rotation was transferred using equation 4.2, which may not be precise enough. In this flowing rig, the smallest droplets

in the stable emulsion are circulating around in the system without separating.

5.4 Summary

In chapter 4, separation of different fluid systems were tested with batch tests. The goal was to see if batch tests can be used to predict crude oil behavior, and the result showed promising result. In this chapter, the same fluid system was tested in a continuous settler rig. The purpose was to investigate if these experiments provided similar settling results. Exxsol D60, salt water and Span 80 was used as fluid system.

Polderman's model was used to transfer the batch data to the continuous system. This model present a relationship between the steady state dispersion height and the allowable flux. The flux was calculated based on a dispersion height of 0.4 m. If the model is valid, this is the dispersion height to expect.

When only testing model oil and salt water, it resulted in a complete separation as expected. Span 80 with a concentration of 0.05 vol.% of the total volume was added to the fluids. This resulted in a very stable emulsion, which prevented further testing. The stability of the emulsion was different than when batch testing. Span 80 dissolves in oil, and this may be the reason for the stable emulsion. The desired water cut was impossible to achieve, so the amount of oil compared to water was different from the batch tests. In retrospect, one suspect that the Span 80 concentrations should be lower than first expected, and with respect to oil volume instead of total volume. The oil also contained a significant amount of bacteria, which may have affected the result.

Chapter 6

Conclusion

This work has focused on examining oil-water separation in batch separation tests. The ultimate goal was to find out if model oil can be used to simulate crude oil behavior. Batch tests are less time assuming and less expensive than continuous settler tests. If batch tests can be used to test fluid systems, this is more efficient.

Different fluid systems involving model oil, salt water and surfactant have been tested. The batch separation results were analyzed and transferred to a flowing system using Polderman's model. Relevant literature on oil-water separation, batch settling tests, and numerical modeling of mixing is presented.

Numerical simulations of mixing in a batch test were performed as an optimization study before testing. This was done to investigate mixing performance based on rotation and the presence of static baffles. It is important that the fluids are homogenized after the mixing to be representable for a batch separation test. Both higher rotation and the presence of baffles proved to have significant effect on the mixing performance. The power input to the fluid was measured for all the cases. The simulated power ratio was 2.9 or more for the cases with and without static baffles. Estimation of droplet size indicated that the mixing would be sufficient.

Batch tests were carried out with different rotations, different surfactant concentrations and different water cuts. It is known that model oil and water separates instantly. The goal was to stabilize the fluid system by adding a surfactant. Span 80 was added and proved to have successful result. Investigation of what affects the stability the most was done. Higher rotation gave the greatest effect on stability. This indicates that droplet size determines the separation rate. The tested concentrations of Span 80 gave small changes on the result. This may be because the concentrations tested were too high. If 0.05 % Span 80 covers all the droplets, a higher concentration will not affect the droplets ability to coalescence.

The batch separation result was transferred to a flowing system. Polderman's separation model was used to predict allowable flux for each case for a chosen steady state dispersion height. This approach showed to have weaknesses for low dispersion heights. Polderman's model only take viscosity into account when predicting separation in flowing systems. The weaknesses indicates that other factors affect the separation in addition

to viscosity, and should also be accounted for. The model provided relatively good fits for high dispersions height, which is the case in continuous separators. It was therefore decided to remove the low dispersion heights for this work.

The desired viscosity area to simulate within is between 3-20 cS. Crude oils with higher viscosities than this are difficult to separate. The plotted batch result provided fluxes in this are. This is a promising result, and indicates that batch tests can be used to simulate crude oil.

Experiment in a continuous separator rig was performed with an equal fluid system as when batch testing. The purpose was to investigate if these tests provided the same stability result as batch tests. The result was a much more stable emulsion, which prevented further testing. It is suspected that the test rig had a too low oil volume. As discussed, this may be the reason for the stable emulsion. Span 80 dissolves in oil, which mean the amount of Span 80 compared to oil became different than in the batch tests. Microbes and biocide was also occupied in the oil, which made this a different fluid system than the clean model oil used for batch testing. This may also have affected the stability.

Chapter 7

Further work

Simulating crude oil with a model fluid system in batch tests showed promising results. However, flowing systems needs to be further tested. In this chapter a discussion of what actions that should or could be done for further work is presented.

The numerical modeling of mixing was performed as a one-phase fluid to save time. Two-phase simulations with water and Exxsol D60 properties can be done to provide more authentic results for the intended fluid system. The effect of water cut can then be investigated by CFD.

In further work, a deeper investigation of model oils and surfactant characteristics should be done. This may help when analysing the result. Additional model oils and surfactants can also be tested. By testing model oils with different viscosities, this may provide different stability behavior. Validation of the effect viscosity has on dispersion layer thickness can then be done. It is beneficial to have several test results when comparing with crude oil. An empirical separation model can be derived when having results from different viscosities.

When testing with Span 80 in batch tests, this provided an emulsion where oil was separated out faster than water. The reason for this should be investigated. Testing with other surfactants may influence the stability differently.

Further work with Polderman's model can be done. Different ways to correct the result can be looked into, and a validation after removing the low dispersion heights should be done. Due to time issues, validation was only done before this correction. Additional separation models can be investigated and tested. Polderman's model proved to have some weaknesses, so other models can be more valid. Polderman's model only takes viscosity into consideration, which may not be sufficient. Also, by testing different models, comparison of separation models can be done. Further testing in flowing system should try to validate or improve existing models.

The flowing separation experiments resulted in a stable emulsion that took hours to break. This may be because of a too high concentration of Span 80. Span 80 dissolves in oil, but is estimated based on total volume in this work. Further testing should investigate smaller concentrations of Span 80 and estimation should be based on oil volume.

This way water cut will not affect the effect of surfactant concentration.

The model oil used for the flowing tests were already presence in the system from previous testing. This model oil proved to have a severe presence of microbes bacteria, which was difficult to remove. The bacterias can have affected the result. A recommendation for further testing is therefore to use new model oil. This way one ensure that the fluid system is equal to the one tested with batch tests. One should also ensure that there is enough oil and water to achieve the desired water cuts.

Bibliography

[1] Sindre Alvestad and Erik Storaas. Cfd analysis on scaling down of a reversible cyclone and test rig setup for high pressure testing. 2012.

[2] Houari Ameur and Mohamed Bouzit. Power consumption for stirring shear thinning fluids by two-blade impeller. *Energy*, 50:326–332, 2013.

[3] Per Arild Kjølseth Andresen, Richard Arntzen, and Johan Sjøblom. Stability of model emulsions and determination of droplet size distributions in a gravity separator with different inlet characteristics. *Colloids and Surfaces A: Physicochemical and Engineering Aspects*, 170(1):33–44, 2000.

[4] CFX Ansys. Ansys cfx-solver theory guide. *ANSYS CFX Release*, 11:69–118, 2012.

[5] Richard Arntzen. *Gravity separator revamping.* PhD thesis, Norwegian University of Science and Technology Trondheim, Norway, 2001.

[6] Cameron Process Systems AS. personal communication.

[7] Andre Bakker and Julian B Fasano. Time dependent, turbulent mixing and chemical reaction in stirred tanks. In *AIChE Symposium Series*, volume 90, pages 71–77. New York, NY: American Institute of Chemical Engineers, 1971-c2002., 1994.

[8] JP Brill and GA Gregory. *Multiphase Technology: Technology from the Arctic to the Tropics (BHR Group Publication 31).* Number 31. Mechanical Engineering Publications Limited, 1998.

[9] JT Davies. Drop sizes of emulsions related to turbulent energy dissipation rates. *Chemical Engineering Science*, 40(5):839–842, 1985.

[10] Tom Frising, Christine Noïk, and Christine Dalmazzone. The liquid/liquid sedimentation process: from droplet coalescence to technologically enhanced water/oil emulsion gravity separators: a review. *Journal of dispersion science and technology*, 27(7):1035–1057, 2006.

[11] Tom Frising, Christine Noik, Christine Dalmazzone, Yannick Peysson, and Thierry Palermo. Contribution of the sedimentation and coalescence mechanisms to the separation of concentrated water-in-oil emulsions. *Journal of Dispersion Science and Technology*, 29(6):827–834, 2008.

[12] Per Eivind Gramme. Tekna heavy oil technology for offshore applications - chemistry and physics of heavy oil and other dispersions. 2009.

[13] S Hartland and SAK Jeelani. Choice of model for predicting the dispersion height in liquid/liquid gravity settlers from batch settling data. *Chemical engineering science*, 42(8):1927–1938, 1987.

[14] Shunsuke Hashimoto, Kazuya Natami, and Yoshiro Inoue. Mechanism of mixing enhancement with baffles in impeller-agitated vessel, part i: A case study based on cross-sections of streak sheet. *Chemical engineering science*, 66(20):4690–4701, 2011.

[15] SAK Jeelani and S Hartland. Effect of dispersion properties on the separation of batch liquid-liquid dispersions. *Industrial & engineering chemistry research*, 37(2):547–554, 1998.

[16] SAK Jeelani and Stanley Hartland. The continuous separation of liquid/liquid dispersions. *Chemical engineering science*, 48(2):239–254, 1993.

[17] Shaik Abdul Khadar Jeelani and Stanley Hartland. Prediction of steady state dispersion height from batch settling data. *AIChE journal*, 31(5):711–720, 1985.

[18] Sunil Lalchand Kokal et al. Crude oil emulsions: A state-of-the-art review. *SPE Production & facilities*, 20(01):5–13, 2005.

[19] Lloyd Lobo, Ivan Ivanov, and Darsh Wasan. Dispersion coalescence: Kinetic stability of creamed dispersions. *AIChE journal*, 39(2):322–334, 1993.

[20] ELIZABETH MARDEN Marshall and André Bakker. Computational fluid mixing. *Handbook of Industrial Mixing: Science and Practice*, pages 257–343, 2004.

[21] Florian R Menter. Two-equation eddy-viscosity turbulence models for engineering applications. *AIAA journal*, 32(8):1598–1605, 1994.

[22] Andreas L Nenningsland, Bicheng Gao, Sébastien Simon, and Johan Sjöblom. Comparative study of stabilizing agents for water-in-oil emulsions. *Energy & Fuels*, 25(12):5746–5754, 2011.

[23] Stefan T Orszulik. *Environmental technology in the oil industry*. Springer, 2008.

[24] Thierry Palermo, Jean Philippe Lebrun, Benjamin Brocart, Christine Noik, Philippe Pagnier, et al. Liquid-liquid separation in gravitational subsea separators. In *OTC Brasil*. Offshore Technology Conference, 2011.

[25] Konstantin Panoussopoulos. *Separation of crude oil-water emulsions: experimental techniques and models*. PhD thesis, Swiss Federal Institute of Technology Zurich, 1998.

[26] HG Polderman, JS Bouma, H van der Poel, et al. Design rules for dehydration tanks and separator vessels. In *SPE Annual Technical Conference and Exhibition*. Society of Petroleum Engineers, 1997.

[27] Johan Sjoblom. *Emulsions and Emulsion Stability: Surfactant Science Series/61*, volume 132. CRC Press, 2005.

[28] Vegard Sørbø. Experimental and numerical investigation of oil-water separation. 2014.

[29] WJ Souza, KMC Santos, AA Cruz, E Franceschi, C Dariva, AF Santos, and CC Santana. Effect of water content, temperature and average droplet size on the settling velocity of water-in-oil emulsions. *Brazilian Journal of Chemical Engineering*, 32(2):455–464, 2015.

[30] Maurice Stewart and Ken Arnold. *Emulsions and oil treating equipment: selection, sizing and troubleshooting*. Gulf Professional Publishing, 2008.

[31] MH Vakili and M Nasr Esfahany. Cfd analysis of turbulence in a baffled stirred tank, a three-compartment model. *Chemical Engineering Science*, 64(2):351–362, 2009.

[32] Mark J Van der Zande and WMGT Van den Broek. The effect of tubing and choke valve on oil droplet break-up. In *BHR GROUP CONFERENCE SERIES PUBLICATION*, volume 31, pages 89–100. Citeseer, 1998.

[33] MJ Van der Zande, JH Muntinga, WMGT Van den Broek, et al. Emulsification of production fluids in the choke valve. In *SPE Annual Technical Conference and Exhibition*. Society of Petroleum Engineers, 1998.

[34] Gambit Version. 2. gambit 2 user's guide. *Fluent: Lebanon, NH*, 2001.

[35] Henk Kaarle Versteeg and Weeratunge Malalasekera. *An introduction to computational fluid dynamics: the finite volume method*. Pearson Education, 2007.

[36] Truls Chr Vold. Droplet breakup and coalescence in compact wellstream seperation. 2000.

Appendix A

Calculation of batch constants

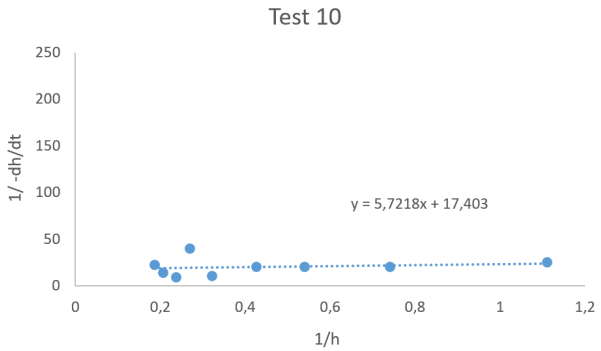

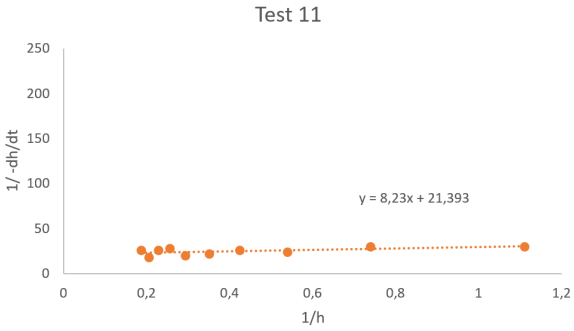

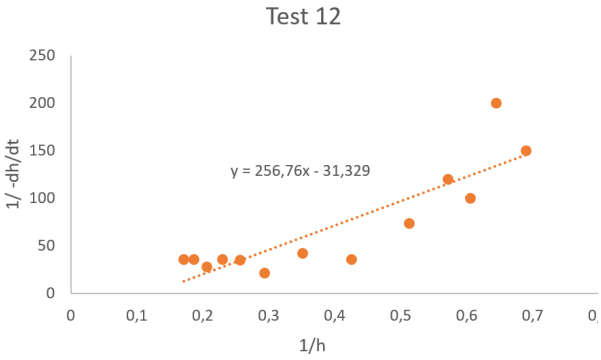

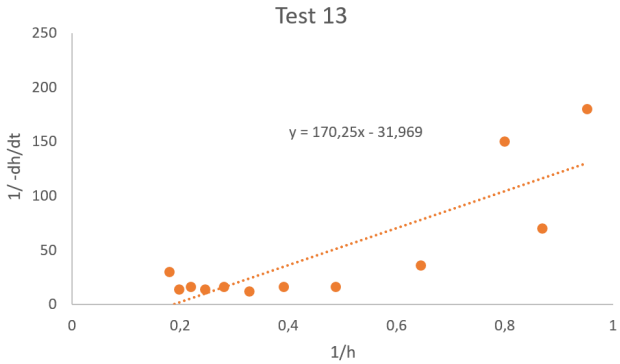

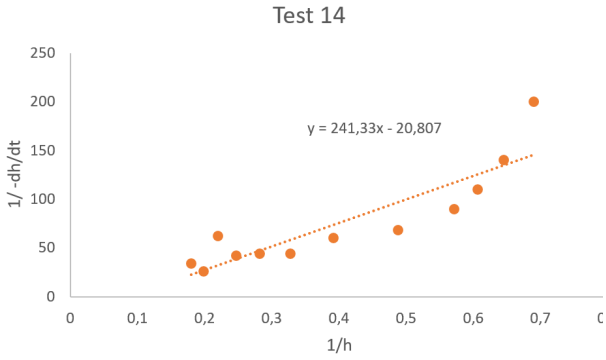

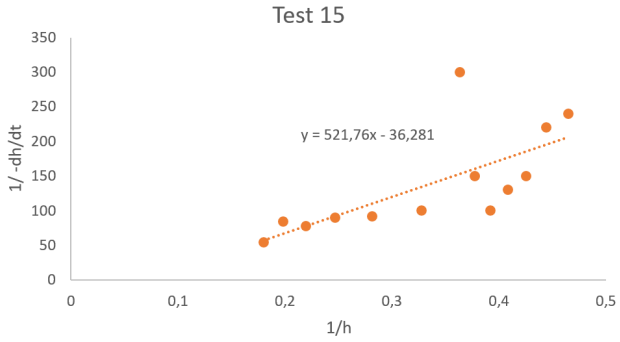

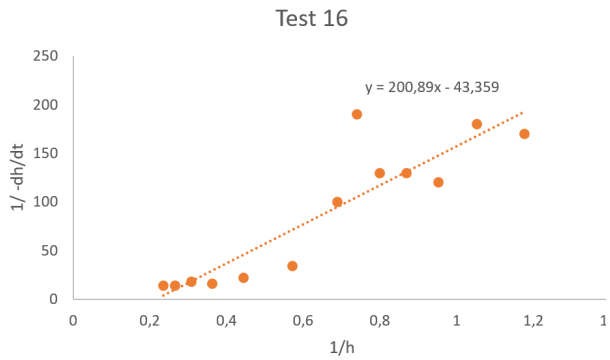
Test 16
y = 200,89x - 43,359
1/ -dh/dt
1/h

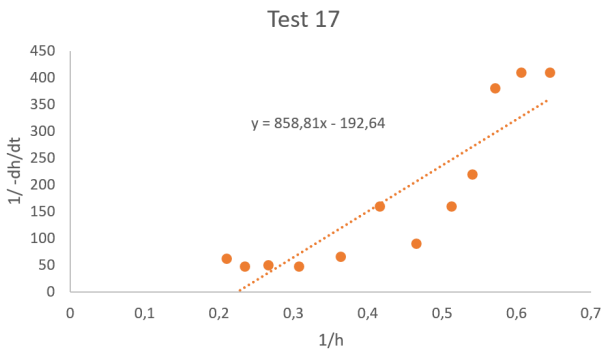
Test 17
y = 858,81x - 192,64
1/ -dh/dt
1/h

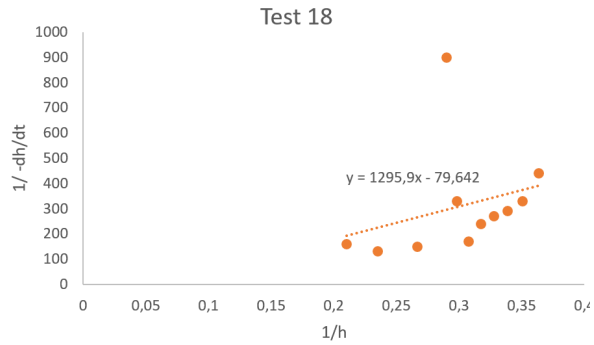
Test 18
y = 1295,9x - 79,642
1/ -dh/dt
1/h

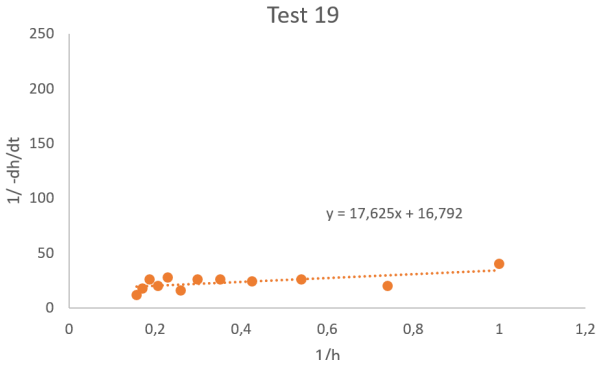
Test 19
y = 17,625x + 16,792
1/ -dh/dt
1/h

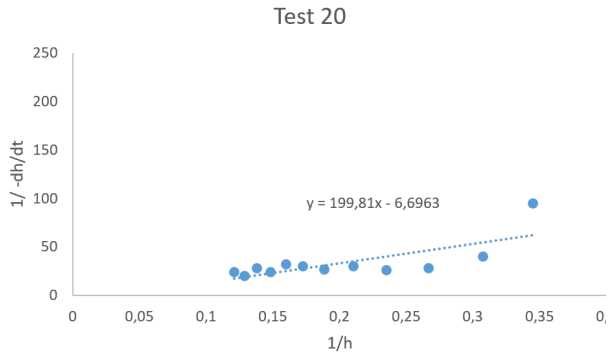
Test 20
y = 199,81x - 6,6963
1/ -dh/dt
1/h

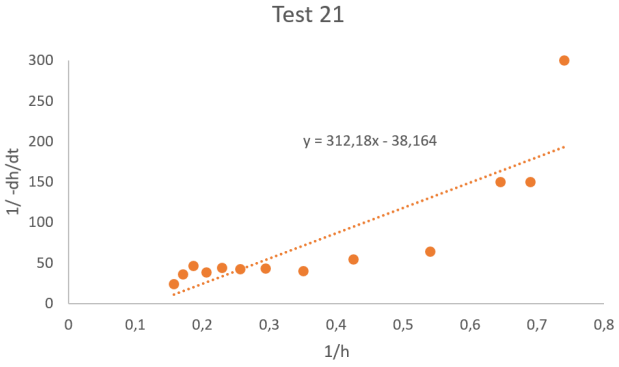
Test 21
y = 312,18x - 38,164
1/ -dh/dt
1/h

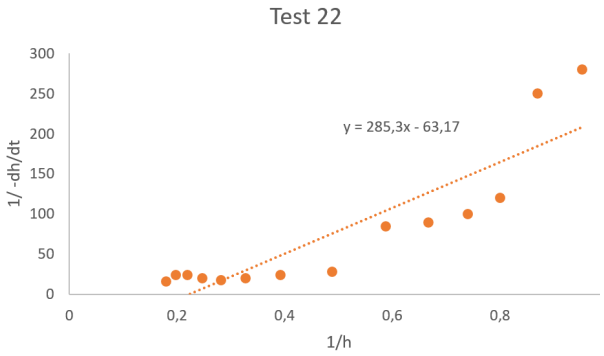
Test 22
y = 285,3x - 63,17
1/ -dh/dt
1/h
300
250
200
150
100
50
0
0
0,2
0,4
0,6
0,8

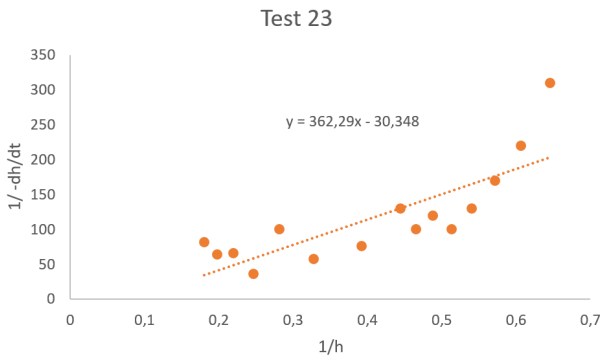
Test 23
y = 362,29x - 30,348
1/ -dh/dt
1/h
350
300
250
200
150
100
50
0
0
0,1
0,2
0,3
0,4
0,5
0,6
0,7

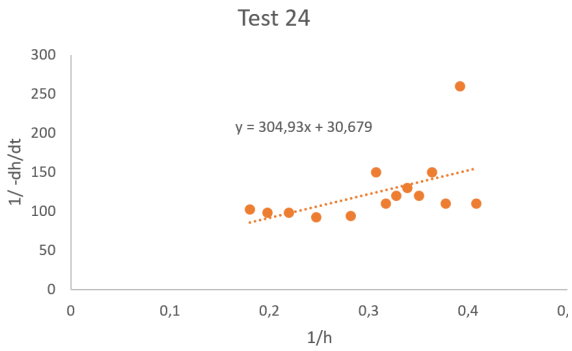
Test 24
y = 304,93x + 30,679
1/ -dh/dt
1/h
300
250
200
150
100
50
0
0
0,1
0,2
0,3
0,4

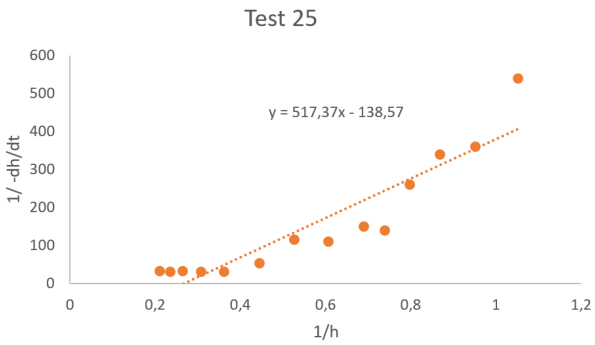
Test 25
y = 517,37x - 138,57
1/ -dh/dt
1/h
600
500
400
300
200
100
0
0
0,2
0,4
0,6
0,8
1
1,2

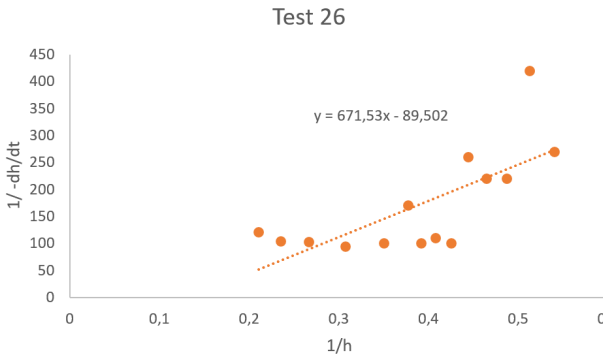
Test 26
y = 671,53x - 89,502
1/ -dh/dt
1/h
450
400
350
300
250
200
150
100
50
0
0
0,1
0,2
0,3
0,4
0,5

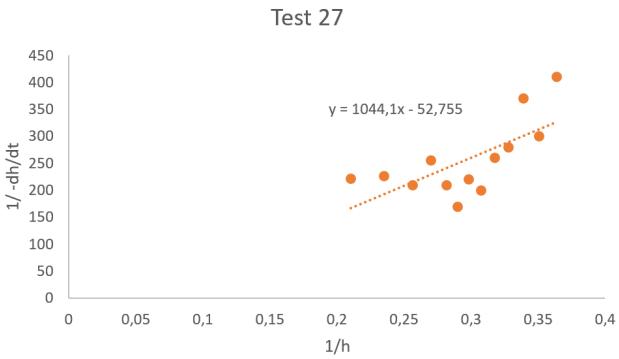
Test 27
y = 1044,1x - 52,755
1/ -dh/dt
1/h
450
400
350
300
250
200
150
100
50
0
0
0,05
0,1
0,15
0,2
0,25
0,3
0,35
0,4

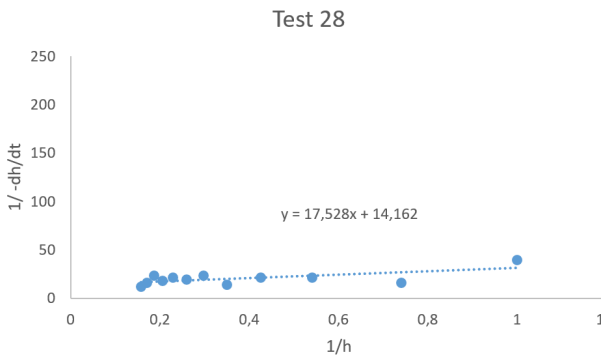
Test 28
y = 17,528x + 14,162
1/ -dh/dt
1/h

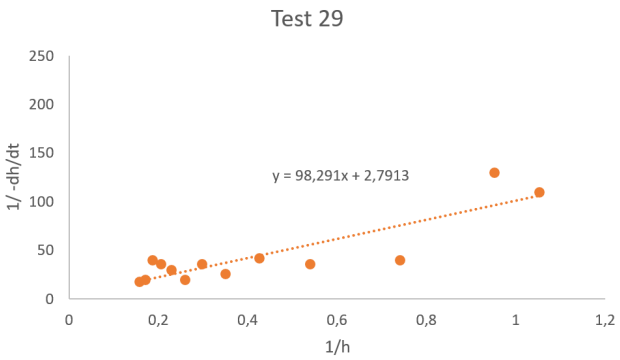
Test 29
y = 98,291x + 2,7913
1/ -dh/dt
1/h

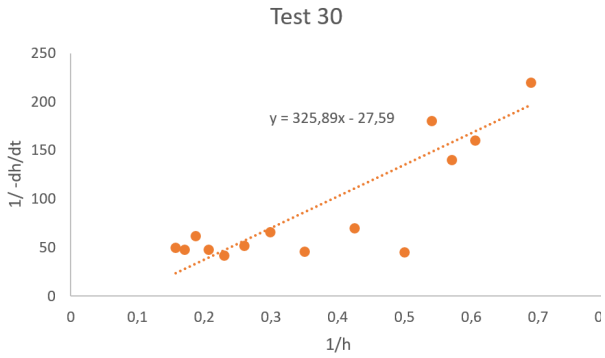
Test 30
y = 325,89x - 27,59
1/ -dh/dt
1/h

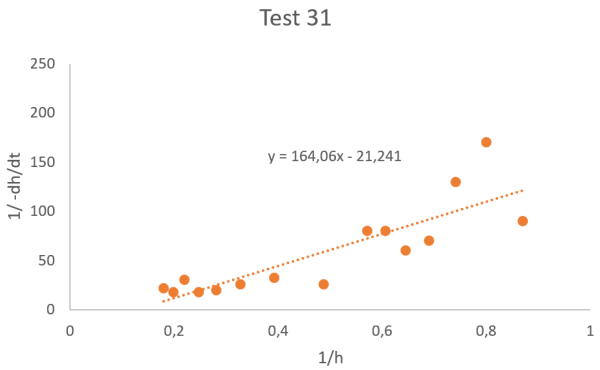
Test 31
y = 164,06x - 21,241
1/ -dh/dt
1/h

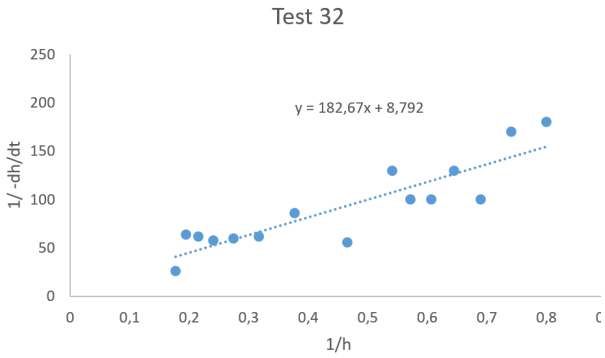
Test 32
y = 182,67x + 8,792
1/ -dh/dt
1/h


Test 33
y = 684,12x - 56,38
1/ -dh/dt
1/h

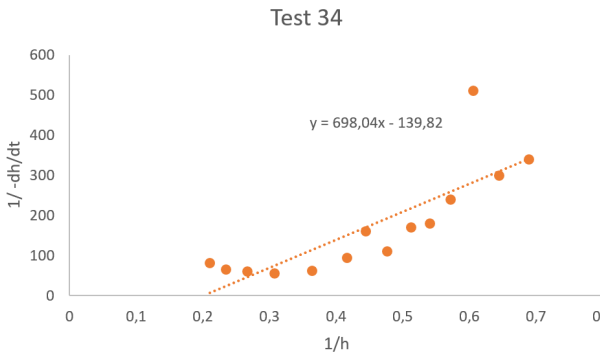
Test 34
y = 698,04x - 139,82
1/ -dh/dt
1/h
600
500
400
300
200
100
0
0
0,1
0,2
0,3
0,4
0,5
0,6
0,7
0

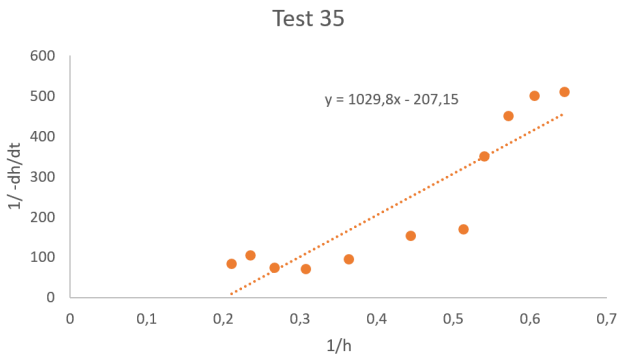
Test 35
y = 1029,8x - 207,15
1/ -dh/dt
1/h
600
500
400
300
200
100
0
0
0,1
0,2
0,3
0,4
0,5
0,6
0,7

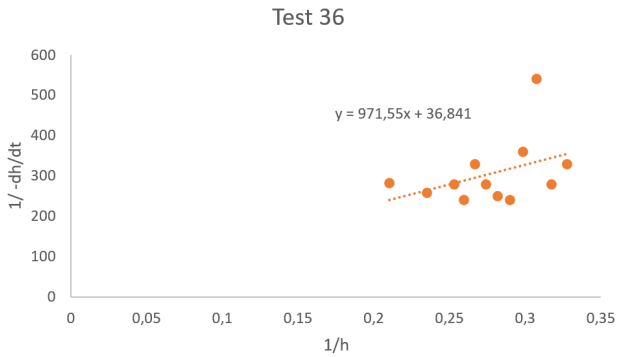
Test 36
y = 971,55x + 36,841
1/ -dh/dt
1/h
600
500
400
300
200
100
0
0
0,05
0,1
0,15
0,2
0,25
0,3
0,35

Appendix B

Validation of batch constants

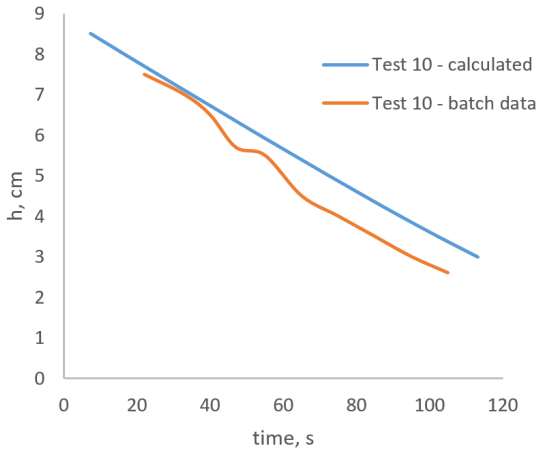

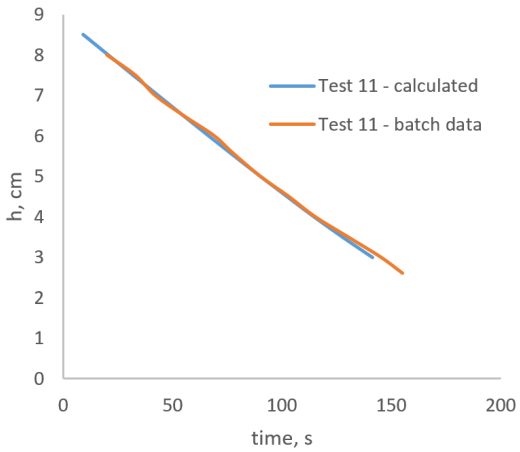

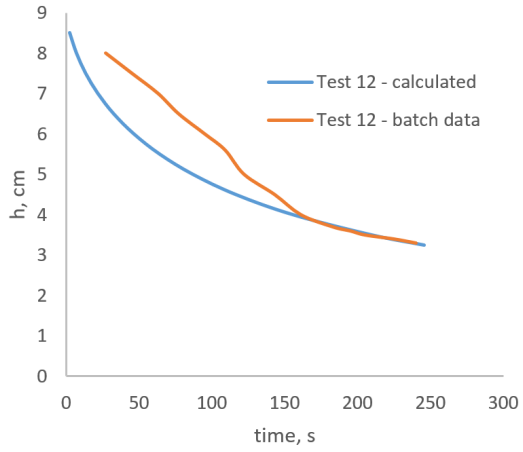

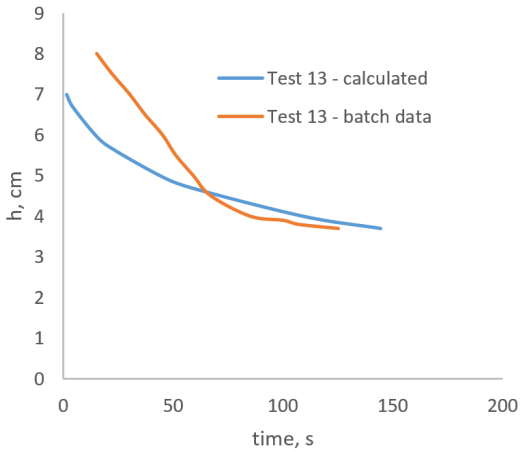

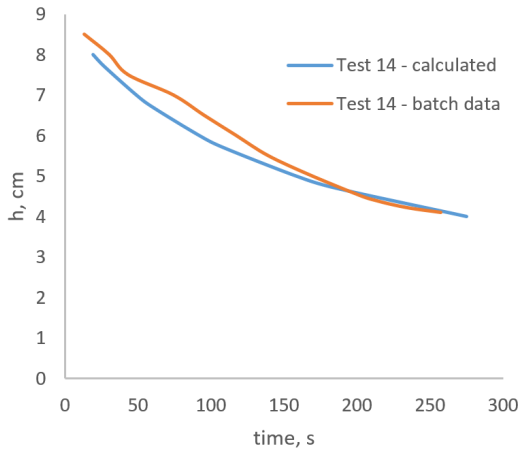
Test 14 - calculated
Test 14 - batch data
h, cm
time, s

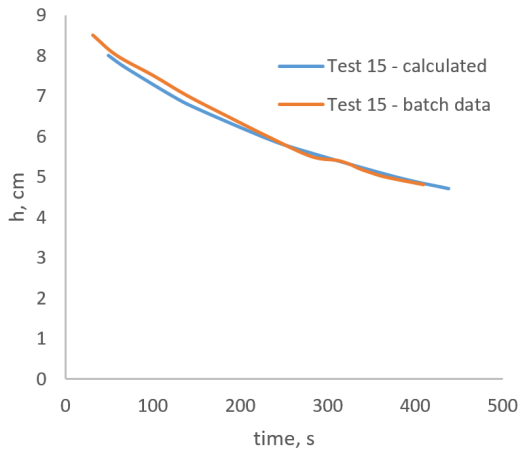
Test 15 - calculated
Test 15 - batch data
h, cm
time, s

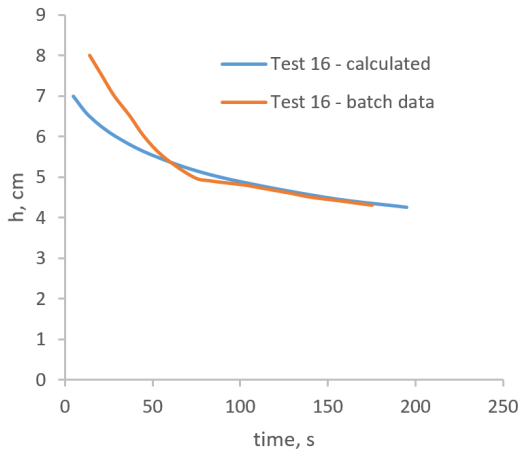
Test 16 - calculated
Test 16 - batch data
h, cm
time, s

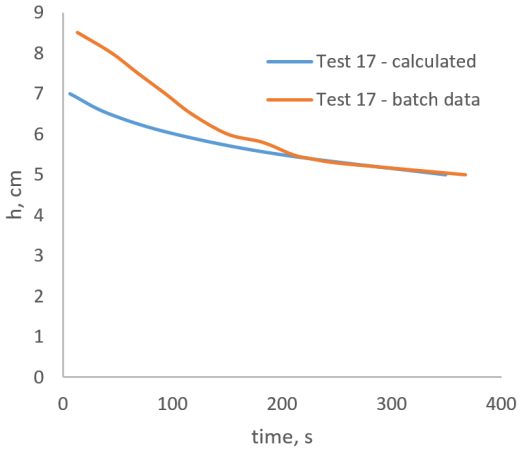
Test 17 - calculated
Test 17 - batch data
h, cm
time, s

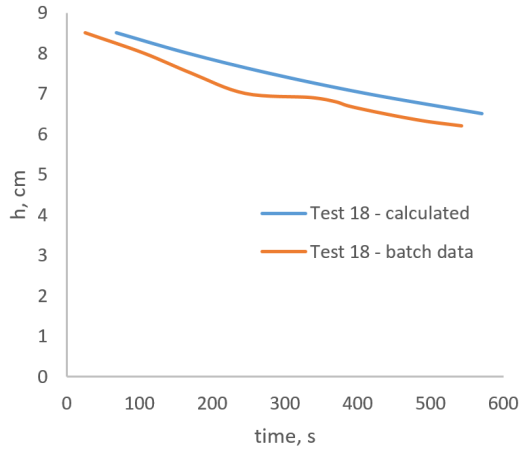
Test 18 - calculated
Test 18 - batch data
h, cm
time, s

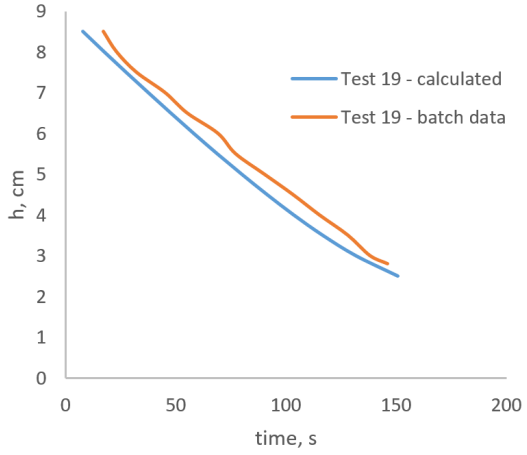
Test 19 - calculated
Test 19 - batch data
h, cm
time, s

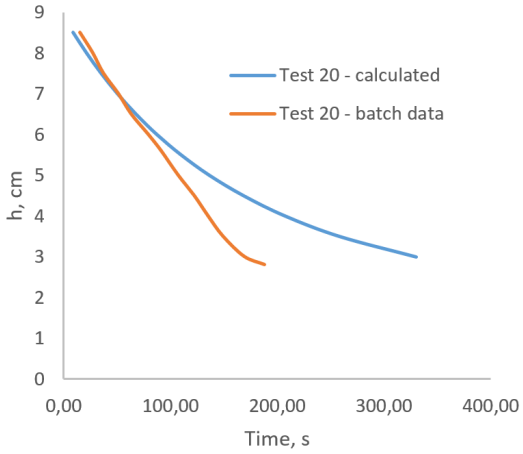
Test 20 - calculated
Test 20 - batch data
h, cm
Time, s
0,00
100,00
200,00
300,00
400,00

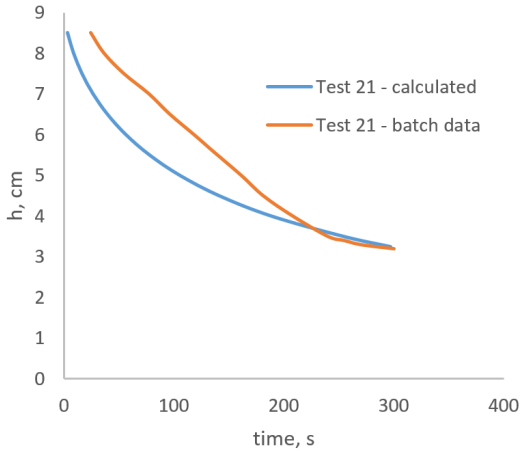
Test 21 - calculated
Test 21 - batch data
h, cm
time, s

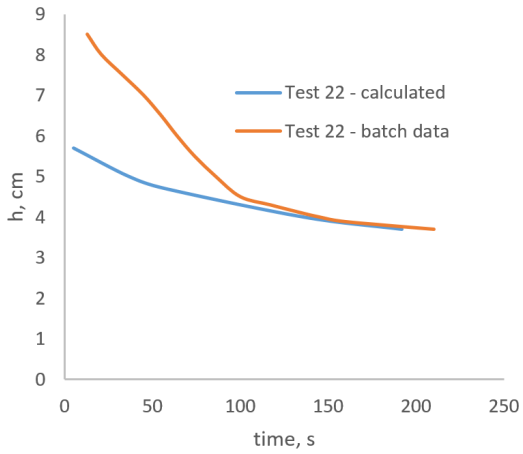
Test 22 - calculated
Test 22 - batch data
h, cm
time, s

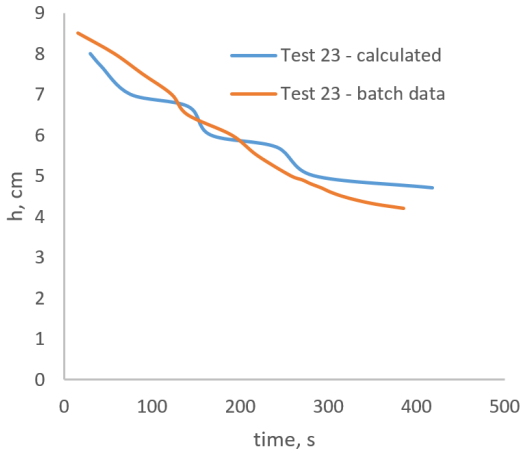
Test 23 - calculated
Test 23 - batch data
h, cm
time, s

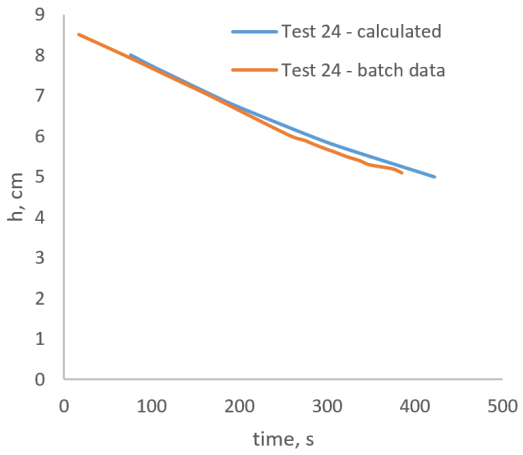
Test 24 - calculated
Test 24 - batch data
h, cm
time, s

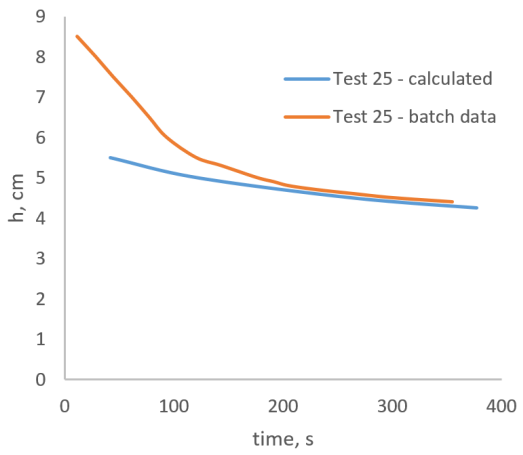
Test 25 - calculated
Test 25 - batch data
h, cm
time, s

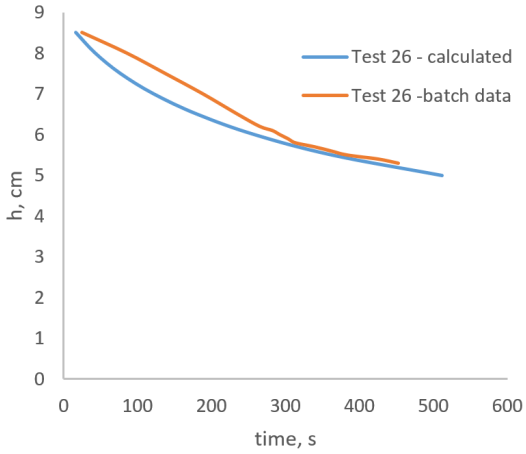
Test 26 - calculated
Test 26 -batch data
h, cm
time, s

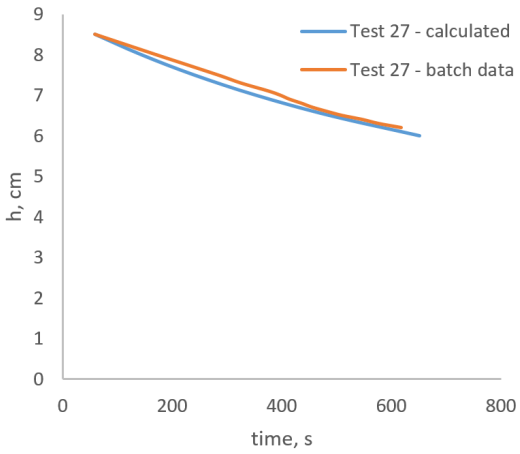
Test 27 - calculated
Test 27 - batch data
h, cm
time, s

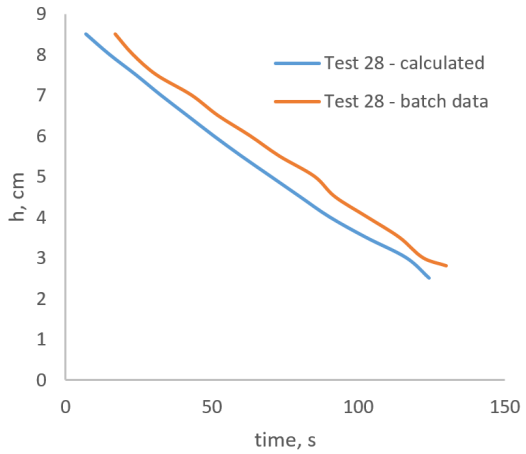
Test 28 - calculated
Test 28 - batch data
h, cm
time, s

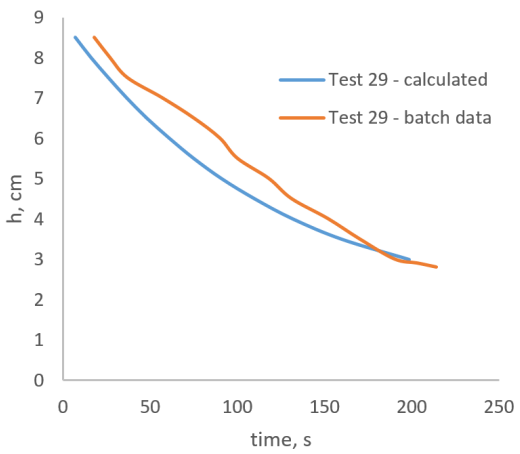
Test 29 - calculated
Test 29 - batch data
h, cm
time, s

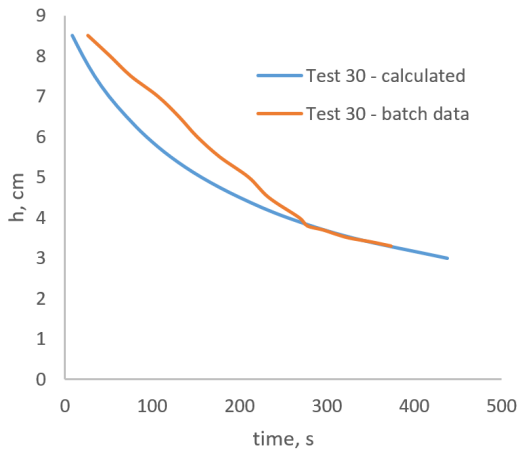
Test 30 - calculated
Test 30 - batch data
h, cm
time, s

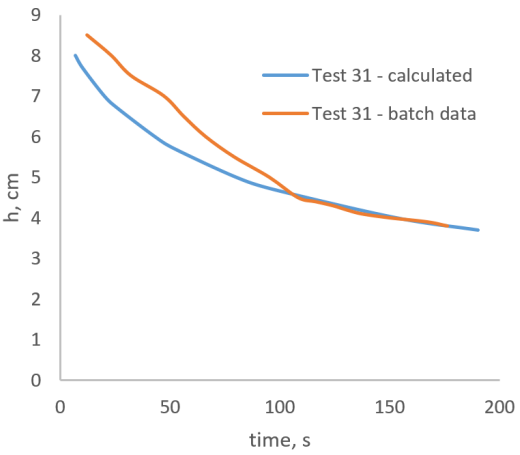
Test 31 - calculated
Test 31 - batch data
h, cm
time, s

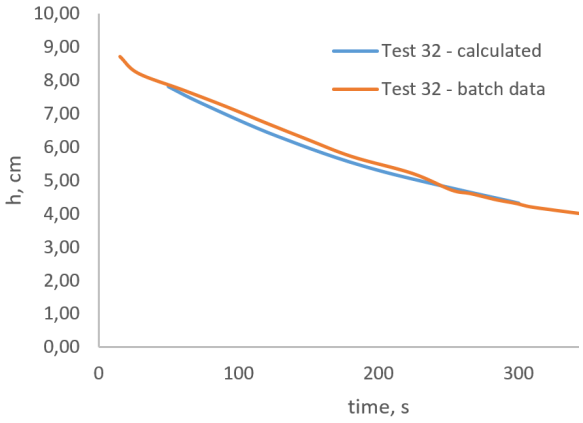
10,00
9,00
8,00
7,00
6,00
5,00
4,00
3,00
2,00
1,00
0,00
h, cm
0
100
200
300
time, s
Test 32 - calculated
Test 32 - batch data

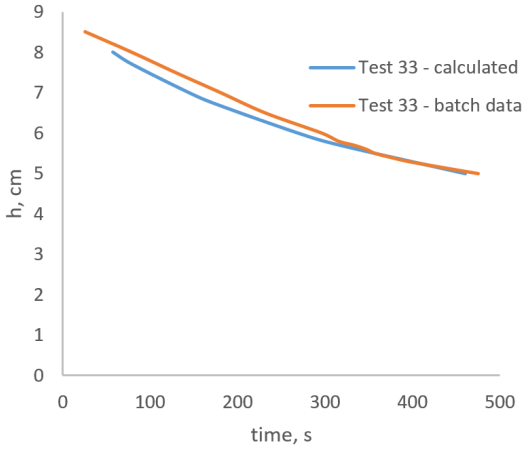
9
8
7
6
5
4
3
2
1
0
h, cm
0
100
200
300
400
500
time, s
Test 33 - calculated
Test 33 - batch data

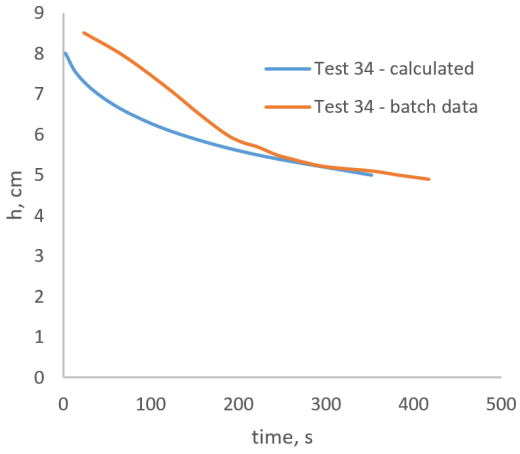
9
8
7
6
5
4
3
2
1
0
h, cm
0
100
200
300
400
500
time, s
Test 34 - calculated
Test 34 - batch data

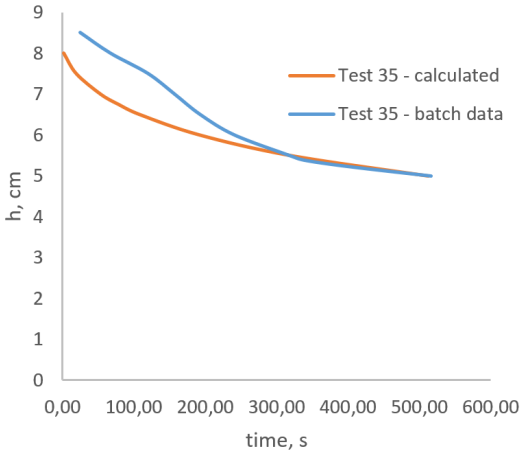
9
8
7
6
5
4
3
2
1
0
h, cm
0,00
100,00
200,00
300,00
400,00
500,00
600,00
time, s
Test 35 - calculated
Test 35 - batch data

Appendix C

Correction of batch constants

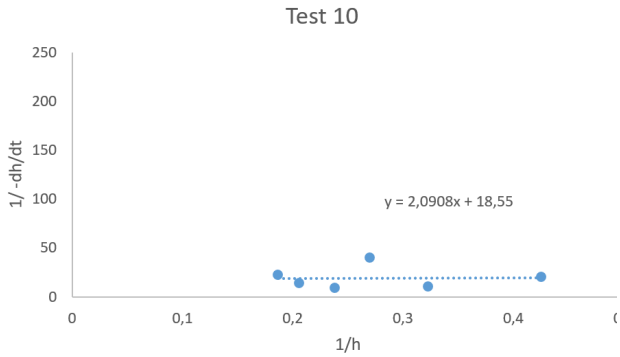

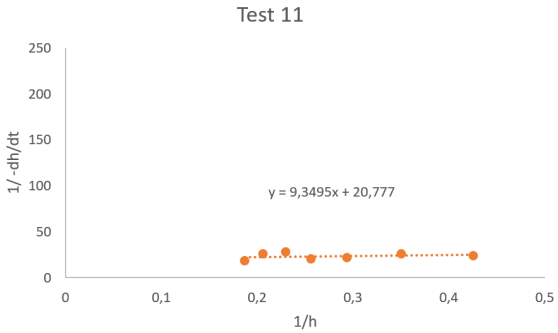

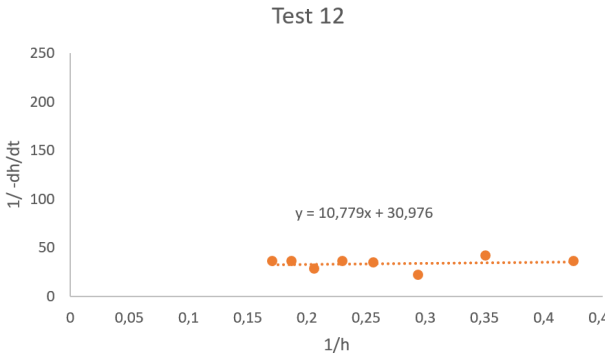

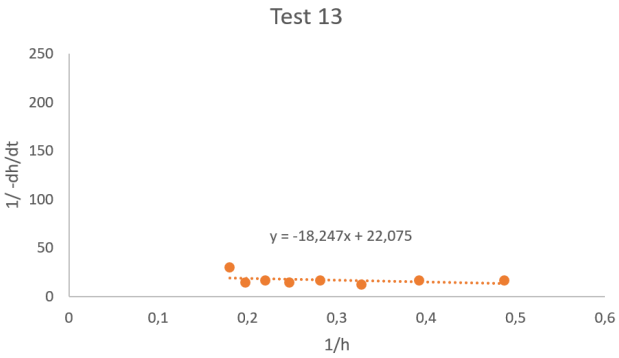

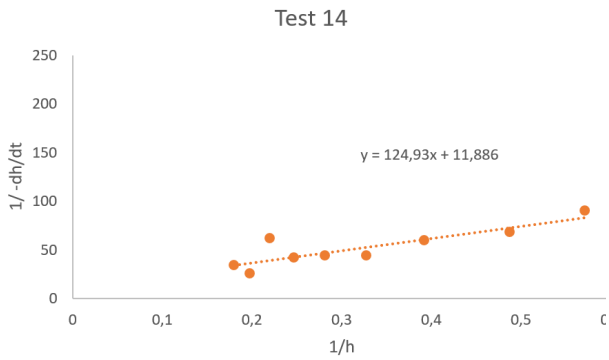
Test 14
y = 124,93x + 11,886
1/ -dh/dt
1/h

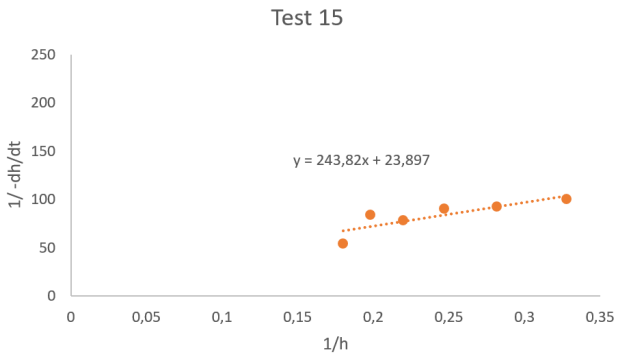
Test 15
y = 243,82x + 23,897
1/ -dh/dt
1/h

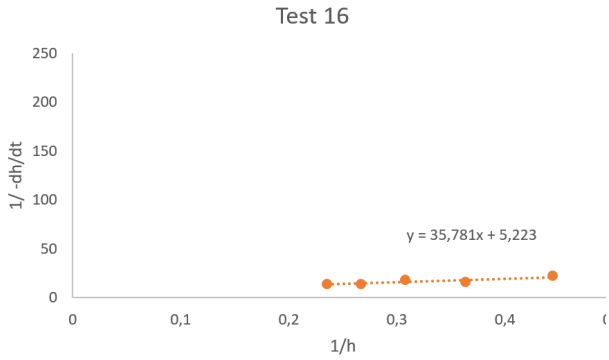
Test 16
y = 35,781x + 5,223
1/ -dh/dt
1/h

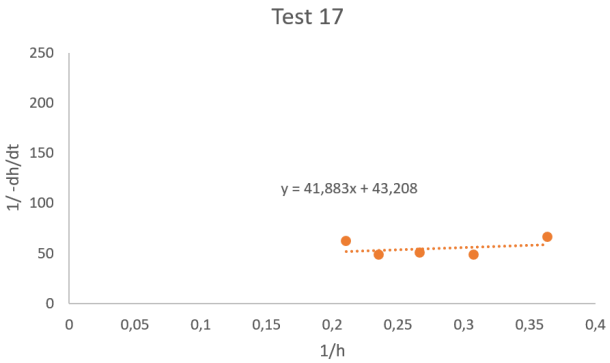
Test 17
y = 41,883x + 43,208
1/ -dh/dt
1/h

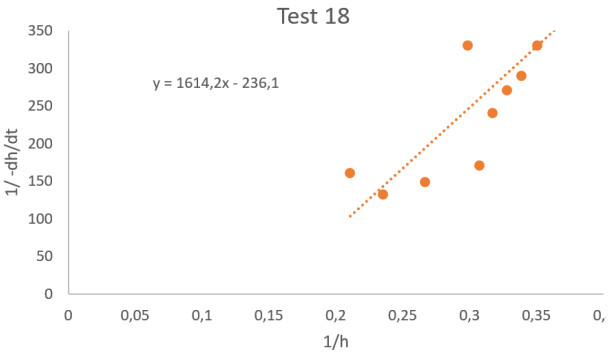
Test 18
y = 1614,2x - 236,1
1/ -dh/dt
1/h

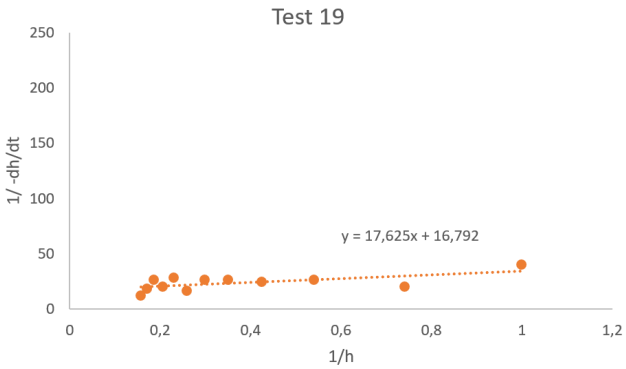
Test 19
y = 17,625x + 16,792
1/ -dh/dt
1/h

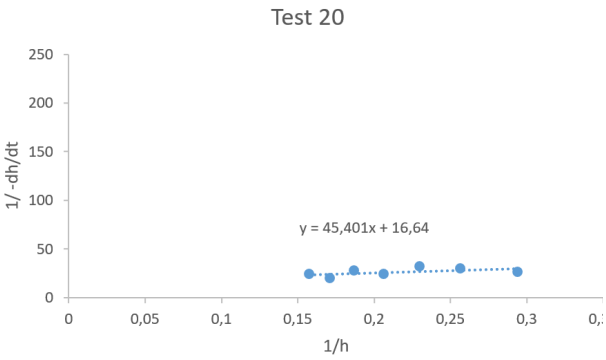
Test 20
y = 45,401x + 16,64
1/ -dh/dt
1/h

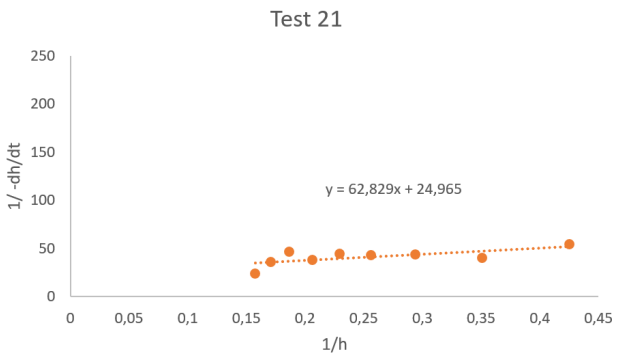
Test 21
y = 62,829x + 24,965
1/ -dh/dt
1/h

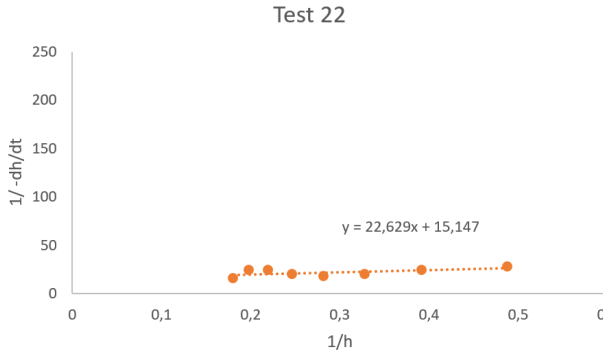
Test 22
y = 22,629x + 15,147
1/ -dh/dt
1/h

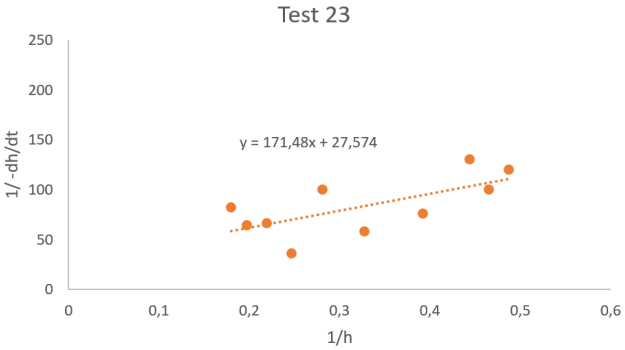
Test 23
y = 171,48x + 27,574
1/ -dh/dt
1/h

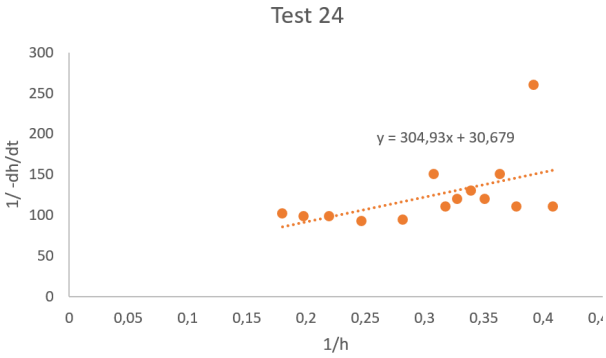
Test 24
y = 304,93x + 30,679
1/ -dh/dt
1/h

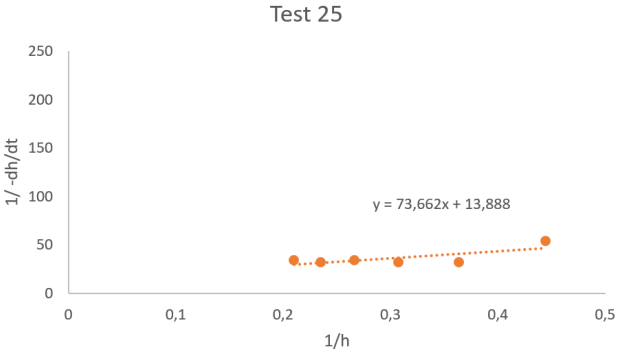
Test 25
y = 73,662x + 13,888
1/ -dh/dt
1/h

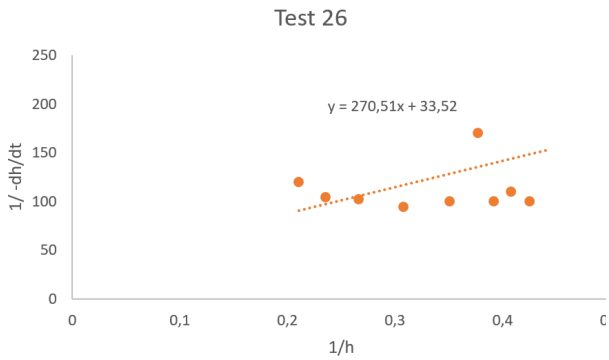
Test 26
y = 270,51x + 33,52
1/ -dh/dt
1/h

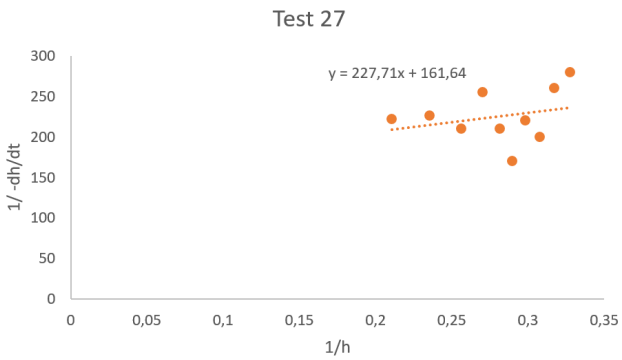
Test 27
y = 227,71x + 161,64
1/ -dh/dt
1/h

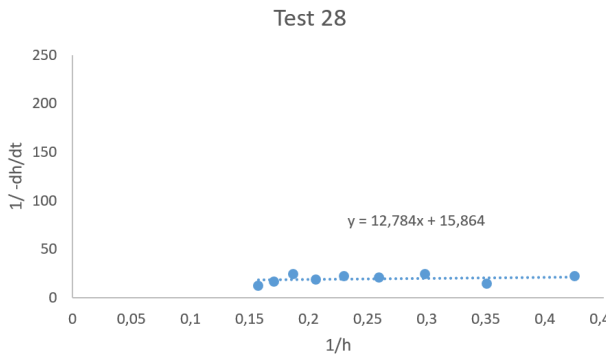
Test 28
y = 12,784x + 15,864
1/ -dh/dt
1/h

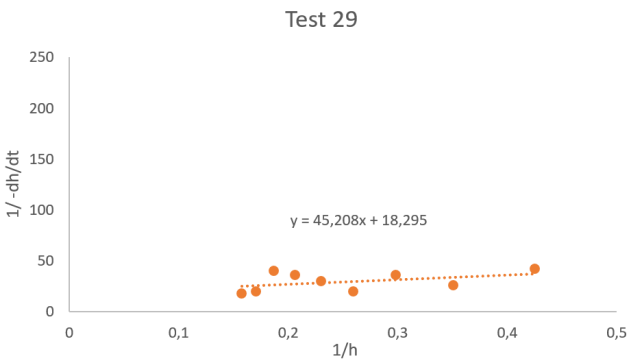
Test 29
y = 45,208x + 18,295
1/ -dh/dt
1/h

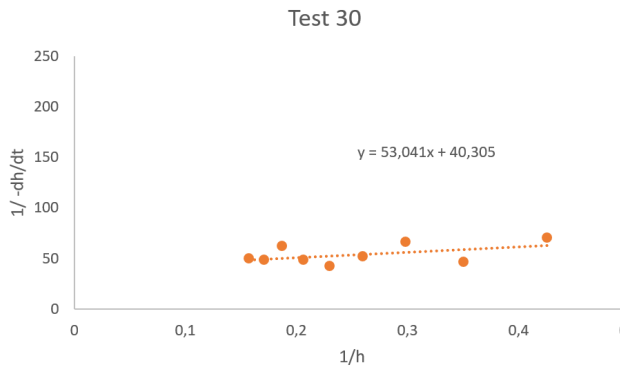
Test 30
y = 53,041x + 40,305
1/ -dh/dt
1/h

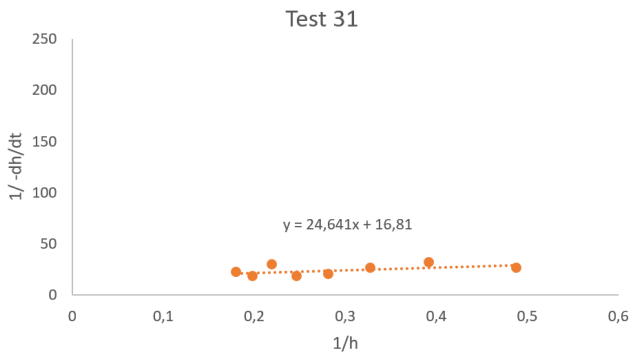
Test 31
y = 24,641x + 16,81
1/ -dh/dt
1/h

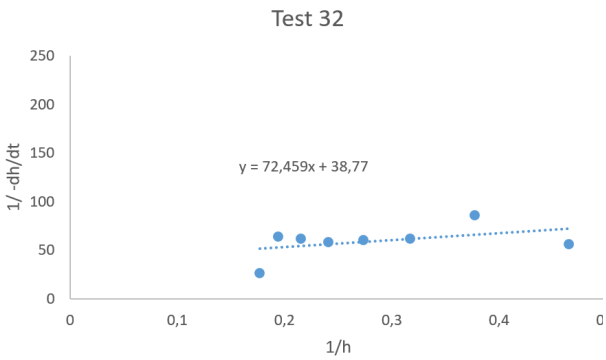
Test 32
y = 72,459x + 38,77
1/ -dh/dt
1/h

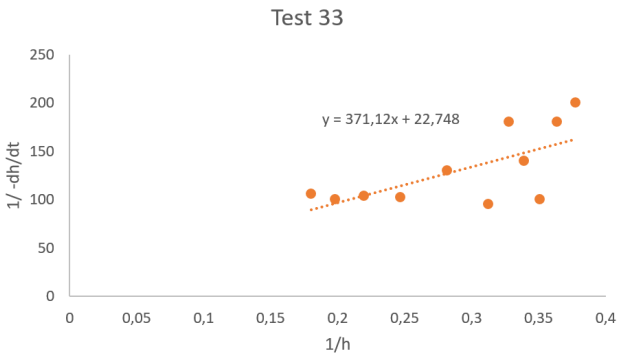
Test 33
y = 371,12x + 22,748
1/ -dh/dt
1/h

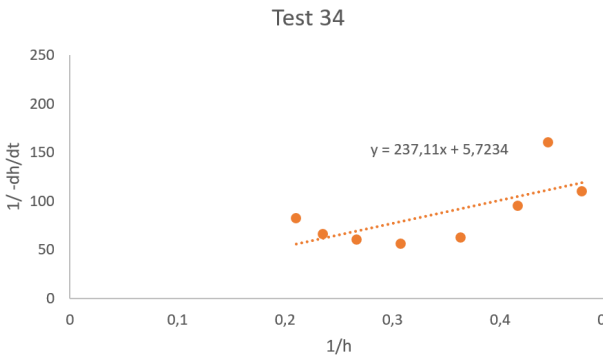
Test 34
y = 237,11x + 5,7234
1/ -dh/dt
1/h

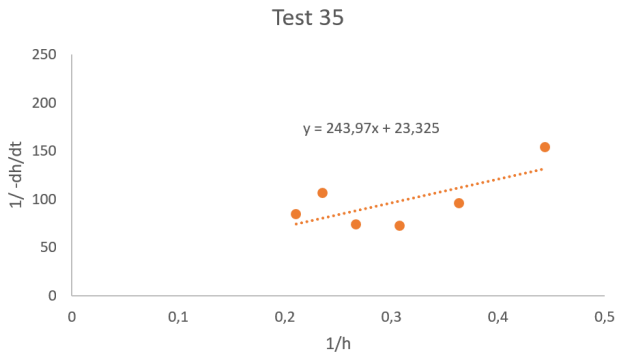
Test 35
y = 243,97x + 23,325
1/ -dh/dt
1/h

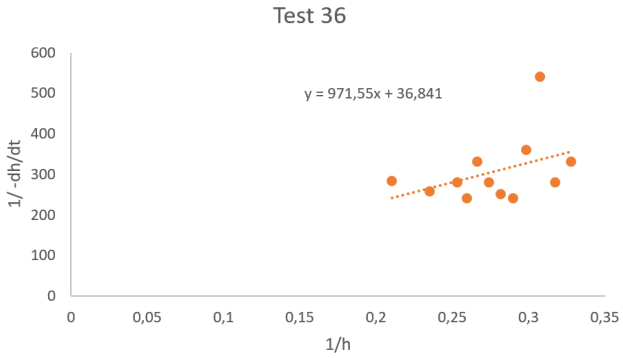
Test 36
y = 971,55x + 36,841
1/ -dh/dt
1/h